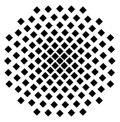

Universität Stuttgart

Few-body quantum physics with strongly interacting Rydberg polaritons

Von der Fakultät Mathematik und Physik der Universität Stuttgart zur Erlangung der Würde eines Doktors der Naturwissenschaften (Dr. rer. nat.) genehmigte Abhandlung.

vorgelegt von

Przemysław Bienias

aus Aleksandrów Łódzki, Polen

Hauptberichter:	Prof. Dr. Hans Peter Büchler
Mitberichterin:	Prof. Dr. Maria Daghofer
Prüfungsvorsitz:	Prof. Dr. Peter Michler
Tag der mündlichen Prüfung:	9. September 2016

Institut für Theoretische Physik III

Universität Stuttgart

2016

List of publications

[1] P. Bienias and H. P. Büchler. "Quantum theory of Kerr nonlinearity with Rydberg slow light polaritons" (2016). arXiv: 1604.05125 (cit. on pp. 6, 10, 23, 49, 95).

[2] P. Bienias. "Few-body quantum physics with strongly interacting Rydberg polaritons". To be published in European Phys. J. Special Top. (EPJ ST) Rydberg Gases (2016). arXiv: 1608.01629 (cit. on pp. 5, 10, 49, 112).

[3] P. Bienias and H. P. Büchler. "Performance of two-photon conditional phase-gate based on Rydberg slow light polaritons". In preparation (2016) (cit. on pp. 6, 10, 49).

[4] K. Jachymski, P. Bienias, and H. P. Büchler. "Three-body interaction of Rydberg slow light polaritons". Phys. Lev. Lett. **117** (2016), 053601. arXiv: 1604.03743 (cit. on pp. 23, 49, 98).

[5] H. Gorniaczyk, C. Tresp, P. Bienias, A. Paris-Mandoki, W. Li, I. Mirgorodskiy, H. P. Büchler, I. Lesanovsky, and S. Hofferberth. "Enhancement of single-photon transistor by Stark-tuned Förster resonances". To be published in Nature Communications (2016). arXiv: 1511.09445 (cit. on pp. 5, 7, 9, 11, 23, 49, 53, 61, 96, 107, 108).

[6] M. F. Maghrebi, M. J. Gullans, P. Bienias, S. Choi, I. Martin, O. Firstenberg, M. D. Lukin, H. P. Büchler, and A. V. Gorshkov. "Coulomb bound states of strongly interacting photons". Phys. Rev. Lett. **115** (2015), 123601. arXiv: 1505.03859 (cit. on pp. 5, 9, 23, 96).

[7] C. Tresp, P. Bienias, S. Weber, H. Gorniaczyk, I. Mirgorodskiy, H. P. Büchler, and S. Hofferberth. "Dipolar Dephasing of Rydberg D -State Polaritons". Phys. Rev. Lett. **115** (2015), 083602. arXiv: 1505.03723 (cit. on pp. 7, 11, 23, 49, 115, 117).

[8] P. Bienias, S. Choi, O. Firstenberg, M. F. Maghrebi, M. Gullans, M. D. Lukin, A. V. Gorshkov, and H. P. Büchler. "Scattering resonances and bound states for strongly interacting Rydberg polaritons". Phys. Rev. A **90** (2014), 053804. arXiv: 1402.7333 (cit. on pp. 6, 10, 23, 49, 59, 67, 84, 86–88, 96–98, 100, 101, 111, 112, 121, 125, 127).

[9] K. Pawłowski, P. Bienias, T. Pfau, and K. Rzążewski. "Correlations of a quasi-two-dimensional dipolar ultracold gas at finite temperatures". Phys. Rev. A **87** (2013), 043620. arXiv: 1304.4792.

[10] P. Bienias, K. Pawłowski, T. Pfau, and K. Rzążewski. "Ground state of a two-component dipolar Fermi gas in a harmonic potential". Phys. Rev. A **88** (2013), 043604. arXiv: 1308.0567.

[11] P. Bienias, K. Pawłowski, M. Gajda, and K. Rzążewski. "Quasicondensation reexamined". J. Phys. Conf. Ser. **414** (2013), 012031. arXiv: 1203.1811v2.

[12] P. Bienias, K. Pawłowski, M. Gajda, and K. Rzążewski. "Statistical properties of one-dimensional attractive Bose gas". Europhys. Lett. **96** (2011), 10011. arXiv: 1103.4017.

[13] T. Karpiuk, P. Deuar, P. Bienias, E. Witkowska, K. Pawłowski, M. Gajda, K. Rzążewski, and M. Brewczyk. "Spontaneous Solitons in the Thermal Equilibrium of a Quasi-1D Bose Gas". Phys. Rev. Lett. **109** (2012), 205302. arXiv: 1205.2363.

[14] P. Bienias, K. Pawłowski, M. Gajda, and K. Rzążewski. "Statistical properties of one-dimensional Bose gas". Phys. Rev. A **83** (2011), 33610. arXiv: 1008.3277.

[15] K. Małek, A. Pollo, T. T. Takeuchi, P. Bienias, M. Shirahata, S. Matsuura, and M. Kawada. "Special feature Star forming galaxies in the AKARI deep field south : identifications and spectral energy distributions". Astron. & Astrophys. **514** (2010). arXiv: 1312.0765.

[16] J. G. T. Jakubczyk, T. Kazimierczuk, A. Golnik, P. Bienias, W. Pacuski, C. Kruse, D. Hommel, Ł. Kłopotowski, T. Wojtowicz. "Optical Study of ZnTe-Based 2D and 0D Photonic Structures Containing CdTe / ZnTe Quantum Dots". Acta Phys. Pol. A **116** (2009), 888.

Summary

In this dissertation, we present research conducted in the field of Rydberg quantum optics. This research would not have been possible without the enormous recent progress in the field of atomic, molecular, and optical (AMO) physics[1], in particular, ultracold atoms and quantum optics [18, 19]. Specifically, Rydberg quantum optics combines the two rapidly developing and still young fields of Rydberg physics and electromagnetically induced transparency (EIT). The long term goal is to incorporate Rydberg-EIT as a building block of quantum simulators [20, 21] and quantum technologies in general [22].

In the last few years, a number of experimental observations [5, 23–31] and theoretical proposals [32–36] were demonstrated in the field of Rydberg-EIT. A variety of applications were shown, such as a deterministic single photon source [24], atom-photon entanglement generation [27], as well as a single-photon switch [29], transistors [5, 30, 31], and an optical π-phase shift created with a stored single-photon pulse [37]. Moreover, the regime of strong interactions between photons has been experimentally demonstrated, leading to a medium transparent only to single photons [25] and to the appearance of bound states for photons [28]. From a theoretical point of view, a full description of the propagation of photons through the medium is limited to extensive numerical simulations and low photon numbers [6, 25, 28, 38–43]. In this dissertation we provide a novel theoretical framework to describe quantum optical nonlinearities in Rydberg-EIT systems and present the application of this framework for two experiments.

Theoretical foundations— In chapter 2, we present the derivation of a microscopic Hamiltonian describing the Rydberg polariton propagation in one dimension [2]. We analyze decoherence processes using a Master equation

[1] A comprehensive overview of the field can be founded in the series of more than 60 volumes of "Advances in Atomic, Molecular, and Optical Physics" published by Elsevier

approach and show for which processes the evolution can be described using the Schrödinger equation with an effective non-Hermitian Hamiltonian. Next, we apply diagrammatic methods to the setup, consisting of a single polariton propagating in an external potential. We solve this setup exactly by a summation of all Feynman diagrams.

Two copropagating polaritons— In chapter 3, we extend our theoretical framework to describe two and more copropagating Rydberg polaritons [8]. In particular, using Feynman diagrams, we analytically derive the scattering properties of two polaritons. We identify new parameter regimes where polariton-polariton interactions are repulsive, giving rise to antibunching of photons. Furthermore, in the regime of attractive interactions, we identify multiple two-polariton bound states, calculate their dispersion relation, and study the resulting scattering resonances. Our method enables us to derive an effective many-body theory for slow light polaritons alone and rigorously justify the previously ad-hoc used adiabatic elimination.

Phase gate— In chapter 4, we analyze the possibility of designing a high fidelity quantum gate between photons using two counter-propagating Rydberg polaritons [3]. Applying our diagrammatic technique, we analytically derive all leading terms which reduce the phase gate fidelity. This allows us to find optimal parameters for experimental realizations and deepens our understanding of the limitations of the Rydberg-EIT scheme.

Kerr nonlinearity— In chapter 5, we analyze the relationship between the classical Kerr nonlinearity and the interacting quantum many-body setup of Rydberg polaritons in the dispersive regime [1]. We show that such a relationship can be obtained when the mass term in the kinetic energy of polaritons is negligible. Then, the quantum input-output theory of polaritons is exactly solvable for an arbitrary atomic density distribution and an arbitrary incoming photon number. In the classical regime, the theory reduces to the well established description of a Kerr nonlinearity. Our method allows for a solution of the problem with not only two-body but also higher-body interactions between polaritons. Consequently, we demonstrate the possibility to probe the microscopic interaction potential, in particular two and three body interactions, between the Rydberg polaritons within a simple homodyne detection scheme for a coherent input state. Finally, past studies showed that the self-consistent quantum theory for a local Kerr nonlinearity is ill defined, and a non-local response time has been proposed to resolve this issue [44]. Using our microscopic approach, we show that a Rydberg-EIT setup is free of such problems due to

either the long range character of the interactions or the quadratic corrections to the polaritonic dispersion relation.

Förster resonances— In the last two chapters, we present theoretical descriptions of two experiments conducted by the group of Sebastian Hofferberth at the University of Stuttgart. First, in chapter 6, we investigate the application of Stark-tuned Förster resonances to boost the efficiency of Rydberg-mediated single photon transistors and the non-destructive detection of single Rydberg atoms [5]. For the parameters used in the experiment, most of the measurements can be explained by analyzing the propagation of a single S-state Rydberg polariton in the presence of a stored S-state Rydberg excitation. Even though a similar problem of a polariton interacting with an impurity via van der Waals interactions has already been studied, the physics in the presented case is substantially different. For example, the common intuition, that for a vanishing Förster defect the Rydberg blockade should be given by the resonant dipolar-interactions $\sim r^{-3}$, is incorrect. We compare our theoretical description with the experimental measurements, achieving very good agreement.

Dipolar dephasing— In chapter 7, we present the results of the second joint experimental-theoretical project [7]. Namely, we study the effects of the anisotropic Rydberg interaction on D-state slow light Rydberg polaritons. Experimentalists observed an increase of the absorption of the probe photons over time. We attribute this increase to the interaction-induced coupling to degenerate Zeeman sublevels, which leads to polaritons being converted to stationary Rydberg excitations. This, in turn, prevents other polaritons from propagating through the cloud. In order to qualitatively describe the observed effect, we develop a model which combines the propagation of the two-photon wave-function through the system with nonperturbative calculations of the anisotropic Rydberg interaction.

Zusammenfassung

Diese Doktorarbeit behandelt Forschung aus dem Bereich der Rydberg-Quantenoptik. Diese Forschung wäre ohne die großen, jüngst erzielten Fortschritte in der Atom-, Molekular- und optische (AMO)-Physik[2], insbesondere bei ultrakalten Atomen und in der Quantenoptik [18, 19], nicht möglich gewesen. Rydberg-Quantenoptik verbindet die zwei schnell wachsenden und noch jungen Forschungsgebiete der Rydberg-Physik und der elektromagnetisch induzierten Transparenz (EIT). Das langfristige Ziel ist es, Rydberg-EIT als Baustein für Quantensimulatoren [20, 21] und andere Quantentechnologien [22] zu etablieren.

In den letzten Jahren gab es etliche experimentelle Beobachtungen [5, 23–31] und theoretische Vorschläge [32–36] zur Rydberg-EIT. Es wurden verschiedenste Anwendungen gefunden — zum Beispiel eine deterministische Einzelphotonenquelle [24], Verschränkung von Atomen und Photonen [27], sowie Einzelphotonenschalter [29], Transistoren [5, 30, 31] und eine optische π-Phasenverschiebung mittels eines gespeicherten Einzelphotonenpulses [37]. Außerdem wurde experimentell gezeigt, dass im Regime der starken Wechselwirkung zwischen Photonen ein Rydberg-Medium nur für einzelne Photonen transparent ist [25] und gebundene Photonenzustände auftreten [28]. Aus theoretischer Sicht ist eine vollständige Beschreibung der Photonenpropagation durch ein Rydberg-Medium nur mit aufwendigen numerischen Simulationen und nur für kleine Photonenzahlen möglich [6, 25, 28, 38–43]. In dieser Doktorarbeit werden neue theoretische Methoden zur Beschreibung optischer Nichtlinearitäten in Rydberg-EIT Systemen entwickelt. Anhand zweier Experimente wird gezeigt, wie diese Methoden in der Praxis Anwendung finden.

Theoretische Grundlagen— In Kapitel 2 wird ein mikroskopische Hamiltonian

[2] Die vom Elsevier Verlag herausgegebene, 60-bändige Bücherreihe „Advances in Atomic, Molecular, and Optical Physics“ gibt einen umfassenden Überblick über das Forschungsgebiet.

hergeleitet, der die Propagation von Rydberg-Polaritonen in einer Dimension beschreibt [2]. Mit einem Mastergleichungsansatz analysieren wir Dekohärenzprozesse und zeigen für welche Prozesse die Zeitentwicklung mit einem effektiven, nichthermitschen Hamiltonian beschrieben werden kann. Anschließend verwenden wir diagrammatische Methoden zur Untersuchung eines einzelnen, in einem externen Potential propagierenden Polaritons. Durch die Summation aller Feynman-Diagramme lösen wir dieses System exakt.

Zwei kopropagierende Polaritonen— In Kapitel 3 verallgemeinern wir unsere theoretischen Methoden auf zwei und mehr kopropagierende Polaritonen [8]. Insbesondere leiten wir mit Feynman-Diagrammen die Streuung von zwei Polaritonen her. Wir bestimmen neue Parameterbereiche, in denen die Polariton-Polariton-Wechselwirkung repulsiv ist, was zu Antibunching von Photonen führt. Außerdem finden wir im Regime attraktiver Wechselwirkung mehrere gebundene Zustände aus zwei Polaritonen. Wir berechnen die Dispersion dieser Zustände und analysieren die resultierenden Streuresonanzen. Unsere Methoden ermöglichen es, eine effektive Vielteilchentheorie für Slow-Light-Polaritonen zu entwickeln und die früher ad hoc verwendete adiabatische Elimination rigoros zu rechtfertigen.

Phasengatter— In Kapitel 4 analysieren wir die Möglichkeit, mit zwei gegenläufigen Rydberg-Polaritonen ein Quantengatter mit hoher Fidelität zu bauen [3]. Wir leiten mit diagrammatischen Methoden alle Terme in führender Ordnung her, welche die Fidelität des Gatters verringern. Hierdurch lassen sich die für die experimentelle Umsetzung optimalen Parameter finden und die Grenzen des Rydberg-EIT-Schemas besser verstehen.

Kerr-Nichtlinearität— In Kapitel 5 untersuchen wir die Verbindung zwischen der klassischen Kerr-Nichtlinearität und einem wechselwirkenden, quantenmechanischen Vielteilchensystem aus Rydberg-Polaritonen im dispersiven Regime [1]. Wir zeigen, dass eine solche Verbindung besteht, wenn der Massenterm in der kinetischen Energie der Polaritonen vernachlässigbar ist. Dann ist die quantenmechanische Input-Output-Theorie für Polaritonen exakt lösbar, unabhängig von der Atomdichte und der Anzahl ankommender Photonen. Im klassischen Regime reduziert sich die Theorie zur gängigen Beschreibung der Kerr-Nichtlinearität. Unsere Methode macht es möglich, Lösungen nicht nur für Zwei- sondern auch für Mehrkörperwechselwirkungen zwischen den Polaritonen zu finden. Wir erklären, wie das mikroskopische Wechselwirkungspotential, insbesondere für Zwei- und Dreikörperwechselwirkungen, zwischen Rydberg-Polaritonen mit einer einfachen homodynen Detektion unter Verwendung eines kohärenten Input-Zustandes

untersucht werden kann. Zuletzt wurde herausgefunden, dass die selbstkonsistente Quantentheorie für eine lokale Kerr-Nichtlinearität nicht wohldefiniert ist. Zur Lösung dieses Problems wurde die Verwendung einer nichtlokalen Antwortzeit vorgeschlagen [44]. Wir zeigen mit unserem mikroskopischen Ansatz, dass in einem Rydberg-EIT-System solche Probleme nicht auftreten können, zum einen weil die Wechselwirkung langreichweitig ist und zum anderen wegen der quadratischen Korrekturen zur Dispersionsrelation der Polaritonen.

Förster-Resonanzen— In den beiden letzten Kapitel werden zwei Experimente, die von Sebastian Hofferberths Gruppe durchgeführt wurden, theoretisch beschrieben. In Kapitel 6 untersuchen wir, wie sich unter Ausnutzung von Förster-Resonanzen, die mithilfe des Stark-Effekts eingestellt wurden, die Effizienz von auf Rydberg-Physik basierenden Einzelphotonentransistoren und die nichtdestruktive Detektion einzelner Rydberg-Atome verbessern lässt [5]. Die meisten Messergebnisse können durch eine Analyse der Propagation eines einzelnen Rydberg-S-Zustand-Polaritons in Anwesenheit einer gespeicherten Rydberg-S-Zustand-Anregung erklärt werden. Auch wenn eine ähnliche Fragestellung für Van-der-Waals-Wechselwirkung zwischen einem Polariton und einer gespeicherten Anregung bereits untersucht wurde, ist die Physik im vorliegenden Fall grundlegend anders. So ist die weitverbreitete Annahme falsch, dass die Rydberg-Blockade für einen verschwindenden Förster-Defekt durch die resonante dipolare Wechselwirkung $\sim r^{-3}$ gegeben ist. Wir vergleichen unsere theoretischen Beschreibungen mit experimentellen Messungen und zeigen, dass diese sehr gut übereinstimmen.

Dipolare Dephasierung— In Kapitel 7 stellen wir die Ergebnisse aus dem zweiten Projekts vor, das Experiment und Theorie miteinander verbindet [7]. Wir untersuchen den Einfluss der anisotropen Rydberg-Wechselwirkung auf Slow-Light-Rydberg-Polaritonen im D-Zustand. Experimentatoren haben beobachtet, dass sich im Laufe der Zeit die Absorption der Signalphotonen erhöht. Wir erklären diese Erhöhung mit der Kopplung an entartete Zeeman-Subniveaus durch die Wechselwirkung, was dazu führt, dass Polaritonen in stationäre Rydberg-Anregungen umgewandelt werden. Dies hält wiederum andere Polaritonen davon ab, sich durch die Atomwolke zu bewegen. Um den beobachteten Effekt qualitativ beschreiben zu können, entwickeln wir ein Modell, das die Propagation der Zwei-Photonen-Wellenfunktion durch das System mit nichtperturbativen Berechnungen der anisotropen Rydberg-Wechselwirkung verbindet.

to my wife

Contents

The important thing is to not stop questioning. Curiosity has its own reason for existence. One cannot help but be in awe when he contemplates the mysteries of eternity, of life, of the marvelous structure of reality. It is enough if one tries merely to comprehend a little of this mystery each day.

Albert Einstein

Introduction

Photons interact with its environment much weaker than other quanta (e.g. electron spin, superconducting current) and are therefore excellent carriers of information. A long-standing goal is the realization of strong interaction between individual photons which may lead to ultralow-power all-optical signal processing [45, 46], quantum information processing and communication [47, 48] as well as other applications based on non-classical states of light [49, 50].

Means to engineer interactions between photons— A number of promising platforms to engineer suitable interactions between photons are being developed, see an excellent review by Chang et al. [51]. First ideas were based on the Kerr nonlinearity of conventional materials which unfortunately lead to extremely weak effects for single photons, even for highly nonlinear fibres [52]. In the microwave domain, a significant progress has been made using high-Q cavity quantum electrodynamics where a single confined electromagnetic mode is coupled to an atomic system [53–55] or to a superconducting circuit acting as an 'artificial atom' [19, 56]. In the optical domain, one approach is to map photons onto the collective states of an atomic ensemble [57, 58], which enabled the observation of electromagnetically-induced-transparency cross-coupling nonlinearities [59] and similar effects [60]. However, in order to achieve single photon effects [61, 62] cavities are necessary.

Rydberg-EIT— A promising approach that does not require optical resonators capitalizes on strong atom-atom interactions in the metastable Rydberg state $|s\rangle$ of an EIT scheme [32, 63]. These strong, tunable and long-range interactions [64] enabled a number of applications for quantum computing [65–68] and simulations [69–73] in which quantum information is encoded in the atomic degrees of freedom.

Short history of Rydberg-EIT— It is worth mentioning a few breakthroughs which laid the foundation for the field of Rydberg-EIT. In 2001, Lukin et al.

proposed to use the Rydberg blockade effect for the creation of non-classical states of light [63], however, their proposal lacked the EIT component. The idea to use EIT in order to couple photons to metastable Rydberg states was first proposed by Friedler et al. in 2005 [32]. The feasibility of these ideas was experimentally confirmed by Mohapatra in 2007 et al. [74]. This classical linear-optics experiment showed that dephasing and decoherence rates in ultracold Rydberg media can be low enough to observe a narrow EIT transparency window. The control of photons on the single quanta level was shown for the first time by three groups [24–26].

First applications of Rydberg-EIT— On the experimental side, the Rydberg-EIT approach [23, 75] enabled a variety of applications such as deterministic single photon source [24], observation of the quantum phenomena on a few photon level [76], atom-photon entanglement generation [77], a single photon switch [29] and a transistor [30, 31]. Moreover, in the regime of strong interactions between copropagating photons, the medium being transparent only to single photons [25] as well as the bound states of photons [28] were demonstrated.

Quantum gates— First steps towards an experimental realization of the Rydberg-EIT phase gate were done by demonstrating an optical π-phase shift created with a stored single-photon pulse by Tiarks et al. [37]. The extensions of the two-qubit photonic gate [38], employing spatial separation of photons [39] and performing quantum operations on the stored photons [78, 79], were proposed. In the one-dimensional free-space setups realized so far, the possible optical depth per blockade radius is limited by the interaction between ground state and Rydberg atoms [80]. This, in turn, sets constraints on the available amount of the dispersive interaction per photon for quantum information applications. To circumvent this limitation, an optical cavity can be employed to enhance the interaction per photon life-time [81, 82] and to construct high fidelity phase gates [83].

Rydberg states with orbital angular momentum— First Rydberg-EIT experiments mostly exploited interactions between s-states with the same principal quantum number where the angular dependence of the interaction is very weak. In recent experiments, Rydberg s- and p-states [26], or two different s-states [30, 31, 84] are simultaneously prepared. The interaction between different Rydberg states enables novel entanglement schemes [85] and additional flexibility in manipulation of few-photon light fields [86, 87]. Moreover, the angular dependence of the interaction between d-state polaritons can lead to the interaction-induced

dipolar dephasing of polariton pairs [7].

Förster resonances— The additional tunability of the interactions was investigated in setups close to a Förster resonance, where the interaction changes its character from van-der-Waals to dipolar. In the regime of zero E-field, an enhancement of the single-photon-transistor gain was shown [31], while in experiments on Rydberg atom imaging [88, 89] an increase in Rydberg excitation hopping was observed [84] in the regime of many photons. In addition, the Stark-tuned Förster resonances were used to further improve the efficiency and to study the coherent properties of the transistor [5].

Exotic states of light— Recently, it was shown that a Rydberg-EIT setup can give rise to new few- and many-body states of light. Two photons can form shallow [28] and deep bound states [8], which can be imagined as photons trapped by a Rydberg interaction in a deep nearly-square well. Interestingly, the effective three-body interaction between Rydberg polaritons can be as strong as the two-body interaction [4], which might lead to new exotic states of light. Pair of photons can also interact via an effective Coulomb potential, leading to a hydrogen-like diatomic molecule, in which photons are separated by a finite bond length [6]. Moreover, a single-photon absorber based on Rydberg-blockade effect [90] has been experimentally demonstrated [91]. Finally, the formation of a Wigner crystal of individual photons was predicted [36, 40].

It is also worth mentioning the progress towards many-body theory of strongly interacting Rydberg polaritons. In the dissipative regime, the dynamics of quantized light was analyzed in [35]. In the dispersive regime, the derivation of a low-energy Hamiltonian in the dilute regime was presented in [8]. The case of higher densities when the interaction is dominated by the purely repulsive part of the van der Waals interaction was studied in [36] . In the regime, where the effective interaction can be replaced by contact-interaction, the study of non-perturbative effects in N-body scattering of Rydberg polaritons using effective field theory (EFT) was presented in Ref. [92]. In the regime where the mass term is negligible, the analytical solution for arbitrary incoming photon number and shape of the atomic medium was shown in Ref. [1]. Moreover, a recently developed general input-output formalism to describe the dynamics of propagating strongly interacting photons in 1D [42, 43] can be applied to the Rydberg-polariton systems as well.

Rydberg-EIT in 2D and 3D— Most of the initial Rydberg-EIT research investigated effectively one-dimensional systems. A new promising direction are extensions to higher dimensions. For example, Rydberg-dressed photons in near-

degenerate optical cavities can behave as interacting, massive, harmonically trapped, two-dimensional particles in a synthetic magnetic field [93]. The experimental progress [94] makes Rydberg-cavity polaritons a promising platform for creating photonic quantum materials and topological states of light [41]. Moreover, the dynamics in the transversal direction of the copropagatingphotons can lead to tight beam focusing or spontaneous formation of ring structures [33].

1

Basic concepts

The main goal of this thesis is to study single photons strongly interacting by means of Rydberg-EIT. In the introduction, we have put this thesis into a broader perspective by describing other ways of making photons interact. We also presented the current state of the field by describing recent experimental demonstrations and theoretical proposals. In this chapter, we provide the reader with the tools and intuitions required to well understand interacting Rydberg slow light polaritons. We start with the discussion of classical nonlinearities. Then we present a description of EIT, introduce the concept of polaritons, and discuss properties of Rydberg atoms. Finally, we will show how Rydberg-EIT can lead to optical nonlinearities on both classical and quantum level.

1.1 Optical nonlinearities

Classical optical nonlinearities occur when the response of the medium to incident light depends on the intensity of the propagating electromagnetic field [95]. Depending on the number of involved fields, we can distinguish one-field effects (e.g., self phase modulation and frequency doubling), and two-field effects (e.g., cross-phase modulation and four-wave mixing).

The origin of classical nonlinearities: The classical origin of the nonlinear optical response of an atom is the following: The electric field strength $\mathcal{E}$ of the propagating light induces the average dipole moment $\langle d \rangle$ per atom. This leads

to an attenuation and a phase shift of the field described by the imaginary and real parts of the electric susceptibility $\chi_{\rm e}$, which is given by

$$\chi_{\rm e} \;=\; \frac{n_{\rm at}\langle d\rangle}{\epsilon_0 \mathcal{E}} \;, \tag{1.1}$$

with $n_{\rm at}$ the number density of atoms and ϵ_0 vacuum permittivity. Note that the electric susceptibility is connected to the complex refractive index of non-magnetic ($\mu = 1$) matter via the relation $n_{\rm refr}^2 = 1 + \chi_{\rm e}$.

The nonlinearity occurs when $\langle d\rangle$ is a nonlinear function of $\mathcal{E}$. Classically, the reason for that can be the anharmonic response of an oscillating charge. Such effects can be taken into account by expanding the susceptibility as a power series in $\mathcal{E}$

$$\chi_{\rm e} \;=\; \frac{N\langle d\rangle}{\epsilon_0 \mathcal{E}} = \chi_{\rm e}^{(1)} + \chi_{\rm e}^{(2)}\mathcal{E} + \chi_{\rm e}^{(3)}\mathcal{E}^2 + \cdots \;, \tag{1.2}$$

where $\chi_{\rm e}^{(1)}$ describes the linear response, whereas higher order terms depict the nonlinear response. Due to the inversion symmetry of atomic media, the second order vanishes (*i.e.*, $\chi_{\rm e}^{(2)} \approx 0$) and the dominant nonlinear term is $\chi_{\rm e}^{(3)}$, also know as *optical Kerr nonlinearity* [95].

The strength of the real part of the nonlinearity, denoted by $\chi_{\rm e,r}^{(3)}$, can be estimated by comparing the single-photon electric field with the binding field of electrons inside the Bohr's atom (for details see [96]) which leads to

$$\left|\chi_{\rm e,r}^{(3)}\right| \;\leq\; 10^{-23}\ {\rm V}^{-2}{\rm m}^2 \;. \tag{1.3}$$

Based on this result, one can deduce that optical nonlinearities in conventional media are approximately 20 orders of magnitude smaller than would be required for single-photon nonlinear optics.

Nonlinearity via resonant transition : Larger nonlinearities can be achieved by choosing the frequency of probe photons ω_p close to the transition frequency in the medium ω_{pg} between the ground state $|G\rangle$ and the excited state $|P\rangle$. The susceptibility of the two-level system reads

$$\chi_{\rm e}^{\rm 2-level} = \frac{1}{k l_{\rm a}} \frac{\gamma}{\delta - i\gamma} \;, \tag{1.4}$$

where $\delta = \omega_{pg} - \omega_p$, 2γ is a spontaneous decay rate of the excited state, $k = \omega_p/c = 2\pi/\lambda$ is a wavenumber, and $l_{\rm a} = (n_{\rm at}\sigma)^{-1}$ is the resonant attenuation

length, with σ the optical cross-section ($\sigma = 3\lambda^2/2\pi$ for a closed two-level transition).

Then the electric field of the photon causes an AC-stark shift of the excited level. Assuming that the absolute value of the detuning is much greater than the decay, *i.e.*, $|\delta| \gg \gamma$, the Kerr nonlinearity is

$$\chi^{(3)}_{\mathrm{e,r}} = \chi^{(1)}_{\mathrm{e,r}} \frac{d_{gp}^2}{(\hbar\omega_p)^2} \ , \tag{1.5}$$

where d_{gp} is the dipole moment for the transition between $|G\rangle$ and $|P\rangle$ states. The nonlinearity could be enhanced by choosing the detuning closer to the resonance, but this unfortunately coincides with an increase of the scattering rate due to the imaginary part of the susceptibility.

A very useful route to circumvent these issues is via coupling the excited state to an additional metastable state. This leads to the phenomenon of *electromagnetically induced transparency*, which will be discussed in the next section.

1.2 Electromagnetically induced transparency

Scientists try to understand and take advantage of remarkable and counterintuitive physical effects. One of such effects is the electromagnetically induced transparency (EIT): In this case, due to the interaction of light with coherently prepared atoms, an opaque medium becomes transparent. More precisely, quantum interference leads to the cancellation of a linear optical response to the probe photons when a coherent control field Ω is applied to the medium. EIT was first discussed by Harris et al. in 1990 [97], and experimentally realized by Boller et al. in 1991 [98].

In this section, we first explain the general idea and intuition behind EIT. We discuss the electric susceptibility of the medium, introduce the concept of *dark states*, and show experimental applications. More details regarding formalism and applications of EIT can be found in excellent reviews by Scully et al. (1997), Lukin et al. (2003), and Fleischhauer et al. (2005) [57, 99, 100].

Setup: We are interested in an ensemble of identical three-level atoms. Initially, all atoms are in the ground state $|G\rangle$. Since this dissertation treats *Rydberg-EIT*, we present EIT in the so-called ladder-scheme. In our case, the scheme

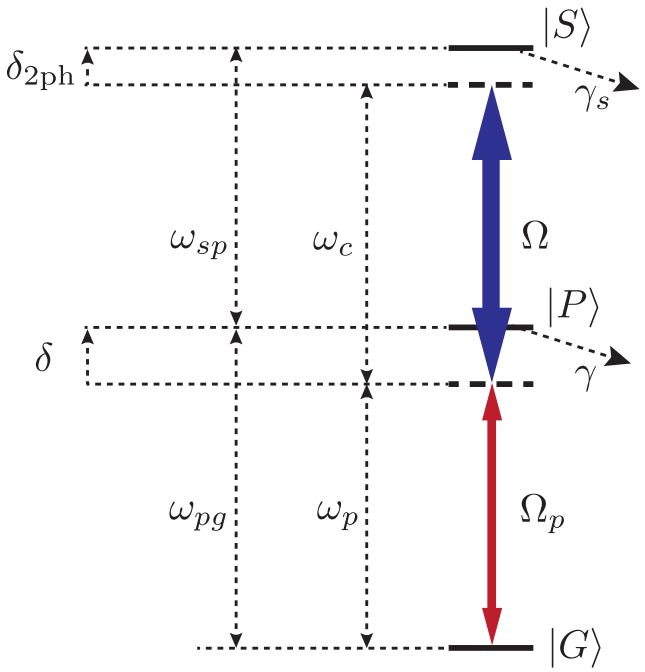

Fig. 1.1: EIT scheme: Three level atom driven by two coherent fields.

consists of a ground state $|G\rangle$, an excited short-lived state $|P\rangle$, and an excited long-lived state $|S\rangle$, where $|G\rangle$ and $|S\rangle$ have the same parity, see figure 1.1. The frequencies of the lower and upper transitions are ω_{pg} and ω_{sp}, respectively. Moreover, ω_p and $2\Omega_p$ are the frequency and Rabi frequency of the probe laser whereas ω_c and 2Ω describe the stronger coupling laser. The decay rate of the $|P\rangle$ state is equal to 2γ whereas the $|S\rangle$ state decays with $2\gamma_s$. The detuning of the $|P\rangle$-state is $\delta = \omega_{pg} - \omega_p$ and the two-photon detuning is equal to $\delta_{2\mathrm{ph}} = \omega_{pg} + \omega_{sp} - \omega_p - \omega_c = \delta + \delta_c$, with δ_c defined as $\delta_c = \omega_{sp} - \omega_c$.

Originally, theoretical and experimental work considered EIT in the so-called Λ-scheme which involves two ground states. The results are fully analogous, regardless of the type of the scheme, assuming that $|S\rangle$ is metastable.

Within the dipole approximation, the atom-laser interaction takes the form $H_{\mathrm{dipole}} = \mathbf{d} \cdot \mathbf{E}$. This interaction can be expressed in terms of the Rabi coupling $2\Omega = \mathbf{d} \cdot \mathbf{E}_0/\hbar$, where $\mathbf{E}_0$ is the amplitude of the electric field $\mathbf{E}$, and $\mathbf{d}$ is the transition's electric dipole moment. After applying the rotating-wave approximation, we arrive at a Hamiltonian of the three-level atom interacting with a coupling laser with real Rabi frequency Ω_{p} and a probe laser with Rabi

frequency Ω, which in the rotating frame has the form

$$H_{\text{int}} = \hbar \begin{pmatrix} 0 & \Omega_{\text{p}} & 0 \\ \Omega_{\text{p}} & \delta & \Omega \\ 0 & \Omega & \delta + \delta_c \end{pmatrix}. \tag{1.6}$$

Note that often other conventions are used: e.g., different signs of the of Rabi frequencies and with Rabi frequencies differing by factor of 2. We use the given convention because then most expressions have a much simpler form, *i.e.*, are without additional factors of 2 and -1.

1.2.1 Intuitive picture

The nearly perfect transmission at the EIT resonance can be understood intuitively. In this subsection, we present two ways of explaining this phenomena.

In the first picture, the absorption cancellation is caused by destructive interference between all possible excitation pathways $|G\rangle \to |P\rangle$, $|G\rangle \to |P\rangle \to |S\rangle \to |P\rangle$, $|G\rangle \to |P\rangle \to |S\rangle \to |P\rangle \to |S\rangle \to |P\rangle$, etc. at $\delta + \delta_c = 0$. A change of the detuning δ leads to imperfect destructive interference and, therefore, to the finite absorption of the medium shown in figure 1.3. The larger the coupling field Ω, the broader is the transparency window and the EIT-feature becomes more stable.

In order to explain the second intuitive picture, it proves useful to introduce the dressed state basis, $|+\rangle$ and $|-\rangle$, for the two upper states, see figure 1.2. Then, we see that the probe field does not directly couple to any of the dressed states $|+\rangle$ and $|-\rangle$. Moreover, the destructive interference occurs since the detunings of the dressed states have opposite signs. This destructive interference is nearly perfect, even for Ω comparable to γ, as long as we one is close to the two-photon resonance.

Finally, it is worth mentioning that the interference phenomenon of EIT is, in a sense, a classical effect as it can also occur in systems consisting of classical oscillators [101].

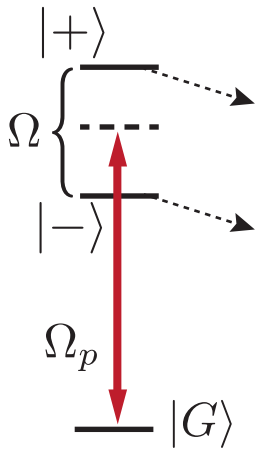

Fig. 1.2: Dressed states.

1.2.2 Linear susceptibility

Here we discuss the susceptibility of the coherently driven EIT medium in linear response with respect to a weak probe field. The presented results are based on the work of Gea-Banacloche et al. [102] , and more details can be found in the two reviews [57, 103].

The dynamics of the laser-coupled atomic system can be described by the Markovian master equation in Lindblad form for the atomic density operator ρ,

$$\frac{\mathrm{d}\rho}{\mathrm{d}t} = -\frac{i}{\hbar}\left[H_{\mathrm{int}}, \rho\right] + \sum_i \mathcal{L}_i(\rho)\,, \tag{1.7}$$

where $\mathcal{L}_i$ are Liouvillians describing different incoherent processes, like decays and dephasings indexed by i. For example, the Louvillian describing the decay of the intermediate p-state reads

$$\mathcal{L}_{pg}(\rho) = -\gamma\left[\hat{\sigma}_{pp}\rho + \rho\hat{\sigma}_{pp} - 2\hat{\sigma}_{gp}\rho\hat{\sigma}_{pg}\right], \tag{1.8}$$

and the Louvillian describing the dephasing of the $|S\rangle$ state takes the form

$$\mathcal{L}_{ss}(\rho) = -\gamma_s^{deph}\left[\hat{\sigma}_{ss}\rho + \rho\hat{\sigma}_{ss} - 2\hat{\sigma}_{ss}\rho\hat{\sigma}_{ss}\right], \tag{1.9}$$

where $\hat{\sigma}_{\mu\nu} = |\mu\rangle\langle\nu|$ are atomic internal-state operators with $\mu, \nu \in \{g, p, s\}$.

We are interested in the perturbative regime in the probe field (the so-called weak-excitation limit), hence we can set $\rho_{gg} = 1$, $\rho_{pp} = 0$, $\rho_{ss} = 0$ in the master equation. Then, we arrive at a set of equations for the coherences ρ_{gp}, ρ_{gs} and ρ_{ps}. From them, we get the expression for the coherence ρ_{gp} of the probe transition in the steady state. Next, we use the relation between the electric amplitude components of the electromagnetic field and the polarization,

$$P = \epsilon_0\chi_{\mathrm{e}}\mathcal{E}\,, \tag{1.10}$$

where $P = n_{\mathrm{at}}d$ is the polarization amplitude of the medium and $\mathcal{E} = |\mathbf{E}_0|$ is the amplitude of the electric field, with $n_{\mathrm{at}} = N/V$ the atomic density and the dipole moment d defined as $d = d_{gp}\rho_{gp}$. Based on this relation, we arrive at an the expression for the electric susceptibility of the three-level system,

$$\chi_{\mathrm{e}}^{3-\mathrm{level}} = \chi_{2-\mathrm{level}}\left[1 - \frac{\Omega^2}{\Omega^2 - (\delta + \delta_c - i\gamma_s)(\delta - i\gamma)}\right], \tag{1.11}$$

where the susceptibility of the two-level system ($\Omega = 0$) is given by Eq. (1.4). These susceptibilities are plotted in figure 1.3 and figure 1.4.

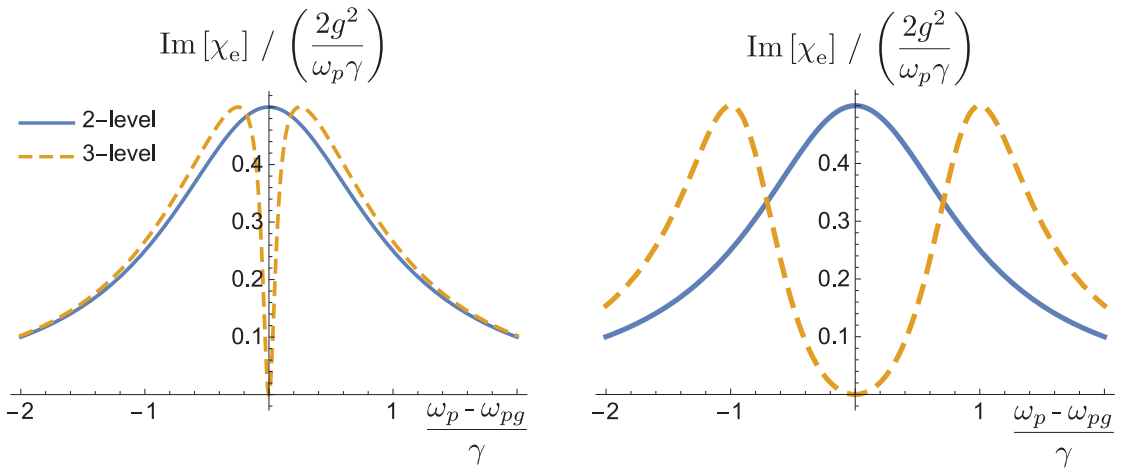

Fig. 1.3: The imaginary part of the electric susceptibility in the vicinity of the two photon resonance in the dissipative regime of fixed $\delta_c = 0$. (left) For $\Omega = \gamma/2$ we see a narrow transmission window at the center of the two-level feature. (right) For $\Omega = 2\gamma$ the EIT transmission window is broader.

From Eq. (1.11) we see that $\chi_e^{3-\text{level}}$ nearly vanishes at the two-photon resonance $\delta + \delta_c = 0$ as long as $|\gamma_s(\delta - i\gamma)| \ll \Omega^2$. Thus, a small decay rate of $|S\rangle$ can lead to nearly perfect transmission at the EIT-resonance. Equation (1.11) defines also the EIT-linewidth given by

$$\Gamma_{\text{EIT}} = \Omega^2/|\delta - i\gamma|. \tag{1.12}$$

In other words, the coupling by the laser field Ω causes the appearance of the narrow transmission window at the center of the two-level feature. In addition, the two peaks revealed in the imaginary part of the susceptibility correspond to the two dressed states.

We can distinguish two interesting regimes, depending on the detuning to the intermediate level δ: For small detuning $\delta \ll \gamma$ the system is in *dissipative* regime (see figure 1.3), whereas for large detuning $\delta \gg \gamma$ the system is in *dispersive* regime (see figure 1.4). Those two regimes will be discussed in section 1.5.2.

We see that in the dispersive regime, the imaginary part of both 2-level and 3-level susceptibilities can be very small. However, the real components can be large and different for the 3-level than for the 2-level susceptibility. In the next sections we will see how to switch between 2-level and 3-level susceptibilities on demand by using the dipolar interaction between Rydberg states.

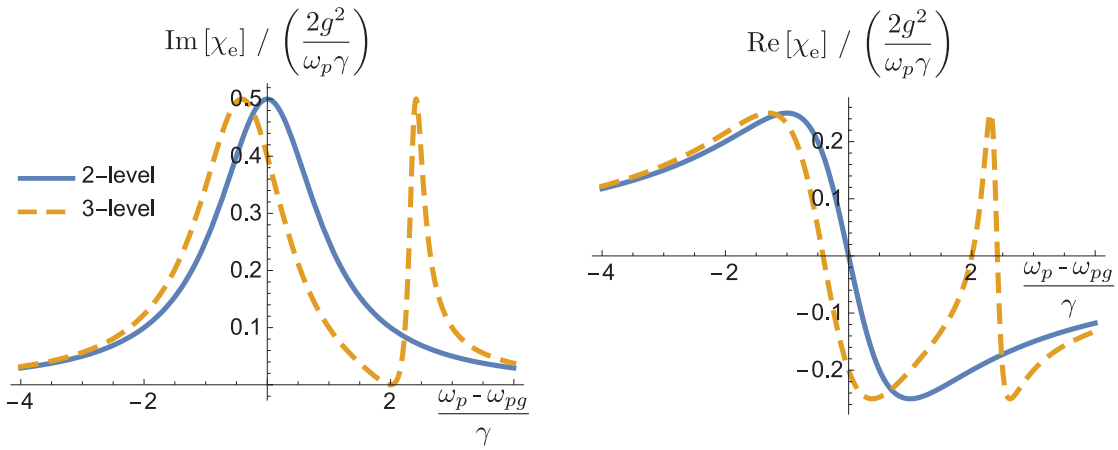

Fig. 1.4: Imaginary and real components of the susceptibilities for fixed $\delta_c = 2\gamma$ and $\Omega = 2\gamma$ in function of $\omega_p - \omega_{pg} = -\delta$. Note that in the vicinity of the two-photon resonance, a strong absorption feature is visible. This peak in $\mathrm{Im}[\chi_\mathrm{e}]$ resembles the Raman resonances corresponding to the AC-stark shifted Rydberg level.

In general, on EIT resonance one can achieve a Kerr nonlinearity given by

$$\chi_\mathrm{r}^{(3)} \approx \chi_\mathrm{r}^{(1)} \frac{d_{gp}^2}{(\hbar\Omega)^2} \,. \tag{1.13}$$

The enormous enhancement compared to the off – resonant 2-level case is immediately apparent as we have replaced the photon energy $\hbar\omega_p$ by $\hbar\Omega$, which differ by 8 orders of magnitude.

1.2.3 Dark state

The absorption cancellation at the EIT resonance can also be explained using the concept of a *dark state*. The dark state of the i-th atom is the eigenstate of Hamiltonian (1.6) having of form

$$|D_i\rangle = \frac{\Omega_p |S\rangle_i - \Omega |G\rangle_i}{\sqrt{\Omega_p^2 + \Omega^2}} \,. \tag{1.14}$$

Single atoms prepared in this steady state have no admixing of the $|P\rangle$-state, thus there is no possibility of a subsequent spontaneous emission from this short-lived state. Moreover, since the amplitudes of the atomic components are proportional to the light fields, the dark state is effectively decoupled from the electric field. This is a reason why both real and imaginary part of the susceptibility vanish at the two-photon resonance.

Note that the EIT effect is closely related to the *coherent populations trapping* (CPT) [104]. A difference is that for the CPT the evolution into the dark state is driven through the spontaneous decay from the $|P\rangle$-state, whereas for EIT the evolution into the dark state can be much more efficient by adiabatically time-varying the strength of the light fields [57].

1.2.4 Applications

After the first experimental realization of EIT [98], a lot of outstanding experimental and theoretical work has been done, which improved our fundamental understanding of light-matter interaction and demonstrated possible applications of EIT in quantum technologies.

For example, EIT allowed to slow down photons to group velocities many orders of magnitude smaller than the speed of light c, not only in quantum gases [105] but also in solids [106–108]. Moreover, using EIT, the excitation with localized, stationary electromagnetic energy – the so-called stationary light – was demonstrated [109–111]. EIT has been demonstated on the single photon level for in a gaseous medium [112, 113], and with single atoms in optical cavities [114, 115] as well as in a free space [116].

By time-varying a control field, it is even possible to bring light to full stop, as shown in proposed protocols [117–119] and in implementations for classical light in atomic ensemble [120–124] or for single atoms [125]. This *storage of light* on a single photon level [126–128] is especially appealing due to the possible applications in quantum information processing and quantum computation [51, 99]. This so-called *stored light* can be used as a photonic quantum memory [99, 126], and building block for quantum repeaters [129] exploiting protocols such as the Duan-Lukin-Cirac-Zoller (DLCZ) scheme [130].

In the next sections, we will show that EIT combined with Rydberg states can lead to even more amazing phenomena.

1.3 Dark state polariton

In previous sections we considered EIT from the semiclassical perspective where the continuous-wave (cw) classical fields interact with a single atom. In order to incorporate time-varying group-velocities and take into account the quantum nature of the probe field in the single photon limit one introduces the concept of a *polariton*. In the following, we present the general idea behind polaritons;

a full description (consistent with the formalism used throughout this thesis) will be presented in chapter 2.

Generally speaking, a polariton is a quasi-particle formed due to the coherent interaction of the probe field with the coherently dressed atoms. As we will see in section 2.4.1, we can distinguish a few types of polaritons depending on their life-time. The one which is metastable within the EIT-scheme is called *dark state polariton* – in analogy to the dark state introduced in section 1.2.3.

The quantum treatment of light propagation under EIT was first presented by Fleischhauer and Lukin [117, 118]. Using this treatment, the probe light propagation (within 1D approximation along the z direction) is described by slowly varying amplitude operator $\hat{\mathcal{E}}^\dagger(z)$ – which creates a photon at the position z – and a slowly varying polarizations $\hat{\mathcal{P}}^\dagger(z)$ and $\hat{\mathcal{S}}^\dagger(z)$ – which create atomic excitation at position z in $|P\rangle$ and $|S\rangle$ states, respectively. The necessary assumption behind this description is that during polariton dynamics, atoms are mostly in the ground state, and thus the condition $|g_0\mathcal{E}| \ll \Omega$ has to be satisfied. This last condition can be derived from Eq. (1.14), where the classical photon-field amplitude $\mathcal{E}$ is given by $\mathcal{E} = \langle\hat{\mathcal{E}}\rangle$.

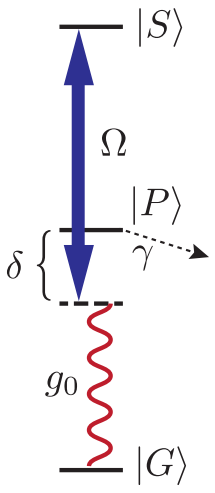

Fig. 1.5: Atomic scheme.

At the two photon resonance, the field operator creating the dark state polariton has the form

$$\hat{\Psi}_d^\dagger(z) = \frac{\Omega\hat{\mathcal{E}}^\dagger(z) - g\hat{\mathcal{S}}^\dagger(z)}{\sqrt{\Omega^2 + g^2}} \tag{1.15}$$

where g is a collectively enhanced coupling of probe photons to the $|P\rangle$ excitation, i.e. $g = g_0\sqrt{n_{\text{at}}}$. The dark state polariton consists of electromagnetic and collective atomic excitations, and inherits the features from both types of excitations. Its kinetics stems from the photonic component, leading to propagation, whereas the spin-wave component can gives rise to interactions with other polaritons or external fields.

In the strong coupling regime, $g \gg \Omega$, the photonic component is strongly quenched, leading to the suppression of the group velocity by a factor of Ω^2/g^2

compared to the speed of light. Therefore, in this regime, the dark state polariton is termed the *slow light polariton*. Additionally, polaritons in the medium are compressed compared to the size of the incoming photon outside the medium. Moreover, as we show in detail in section 2.4.1, the polaritonic dispersion relation consists of a linear part (described by the group velocity v_g), which is modified by higher order corrections. The second order correction leads to a mass term, which (similarly to the group velocity) can be controlled by tunable experimental parameters. As long as the spectral width of the incoming photon is much narrower than the EIT-width Γ_{EIT} (given by Eq. 1.12), we can neglect the mass term and the polariton propagates as a lossless and form-stable quasiparticle. All these properties make slow light polaritons excellent candidates for applications in quantum technologies.

Finally, there is a relation of dark state polaritons to the atomic dark-state (the latter was introduced in section 1.2.3). From the condition $\Omega_{\text{p}} = |g_0\mathcal{E}| \ll \Omega$, follows that for dark-state polaritons most atoms are in the ground state. But simultaneously, due to the collective enhancement of the coupling g, we can be in the regime of $g_0\sqrt{n_{\text{at}}} \gg \Omega$. Therefore the character of each single polariton can be mostly that of a matter excitation and much less contribution of a light excitation.

1.4 Rydberg atoms

One of the main goals in the field of AMO physics is to engineer and control strong and long-range interactions between single quanta [18, 19, 131]. There are many different approaches to this objective, for example, coulomb-interacting ions in paul-traps [132], dipolar quantum gases of atoms and molecules [133, 134], and atomic ensembles in cavities with photon-mediated interactions [135]. Another highly promising direction is to use Rydberg atoms for this purpose.

Rydberg states are defined as highly excited states of a valence electron in an atom or molecule, characterized by a large ($\gtrsim 20$) principal quantum number n. These states can be extremely large on their own, can interact strongly with each other, and can be highly sensitive to external electric and magnetic fields [136].

In this section we describe properties of Rydberg atoms and briefly summarize experimental and theoretical progress – especially in the context of hybrid Rydberg-EIT systems. For a detailed overview on Rydberg atoms, see Saffman

et al. [64], Löw et al. [137], Lim et al. [138], as well as Gallagher [136].

1.4.1 Properties of Rydberg atoms

Here, we review briefly properties of Rydberg atoms, especially those relevant for applications. Because the valence electron of the Rydberg atom is highly excited, many properties of Rydberg atoms follow hydrogenic scaling laws depending on the principal quantum number n. This often simplifies the description of Rydberg atoms tremendously and allows for simple estimates of the relevant quantities.

We start our presentation with the electron's Bohr radius which scales like $r \propto n^2$, and can reach sizes on the order of micrometers [139]. This huge size of the orbital radius leads to an enormous dipole moment with the same $\propto n^2$ scaling. The strength of the dipole moment together with the weak Coulomb interaction between nucleus and valence electron makes Rydberg atoms very sensitive to the environment. This is manifested by a strong response to electric fields with a DC polarizability $\alpha \propto n^7$. Their sensitivity to electric fields leads directly to applications of Rydberg atoms in precision electrometry [140–145] and nonlinear optics [23]. Due to this high sensitivity to the microwave frequencies, Rydberg atoms were used to probe few-photon fields in the Nobel-prize winning experiments by Haroche [146].

A small spatial overlap between the electronic wavefunctions of the ground state and the Rydberg state leads to a strong suppression of a spontaneous decay and therefore very long life-times $\propto n^3$ with values of the order of 100μs achievable in modern experiments. This metastability of the Rydberg states makes it also possible to use them as a third level in the EIT scheme.

The large dipole moment in combination with a millimeter energy spacing between Rydberg levels leads to a strong dipole-dipole interaction between Rydberg atoms. In most cases, the interaction $V(r)$ has a van der Waals character of the form $V(r) = C_6/r^6$ with the scaling $C_6 \propto n^{11}$ [147–149]. However, an external electric or microwave field can be used to engineer a longer range resonant dipole-dipole coupling of the form $V(r) = C_3/r^3$ [64, 150].

The strength of the van der Waals interaction between Rydberg atoms is comparable to the Coulomb interaction between ions and much stronger than the interaction between magnetic dipoles. This feature is illustrated in figure 1.6, which is taken from the excellent review of Saffman et al. [64]. Importantly, while the interactions between ions are always present in a setup, the Rydberg

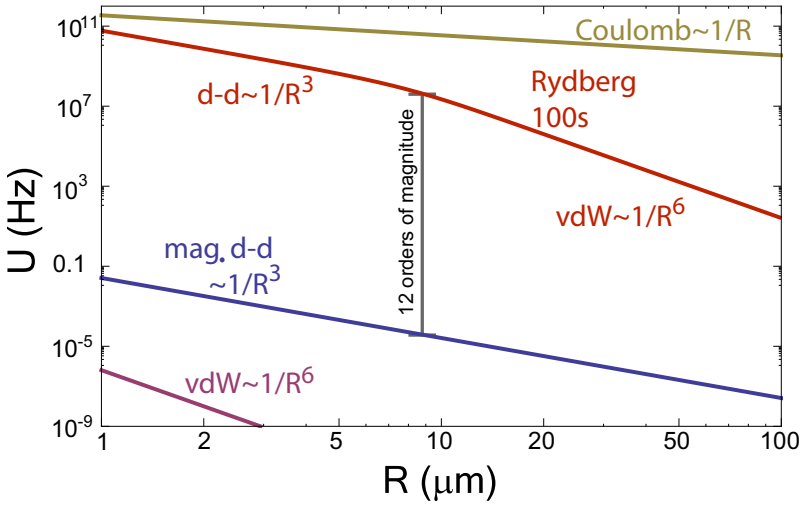

Fig. 1.6: Comparison of the interaction strengths for ground state Rb atoms: magnetic dipole-dipole (blue) and van der Waals (violet); for Rb atoms excited to the 100s level (red); and for ions (yellow). *Source: Saffman et al. [64].*

interaction can be easily switched on and off. This switching can be achieved by a coherent transfer between Rydberg states and ground states using light fields, together with the fact that interactions between ground states are more than ten order of magnitude smaller than between Rydberg states.

The highlighted properties of Rydberg atoms make them a great candidate for coherent manipulations of strongly interacting systems [64].

1.4.2 Dipolar interactions and Förster resonance

In this section, we will consider a simple two channel model in order to gain further intuition for the dipolar interactions between Rydberg atoms. This will lead us naturally to the notion of Förster resonances which will be explored thoroughly in the context of Rydberg-EIT in chapter 6.

Let us consider interatomic distances R greater than the LeRoy radius, i.e., $R \gg 2n^2 a_0$, where a_0 is the Bohr radius. Then we can neglect the effects due to the overlap between the atoms, and the leading electrostatic interaction between two Rydberg atoms 1 and 2 is the dipole-dipole interaction [151],

$$V_{\mathrm{dd}}(\mathbf{R}_{12}) = \frac{1}{4\pi\epsilon_0}\frac{1}{|\mathbf{R}_{12}|^3}\left[\mathbf{d}_1\cdot\mathbf{d}_2 - 3(\mathbf{d}_1\cdot\hat{\mathbf{R}}_{12})(\mathbf{d}_2\cdot\hat{\mathbf{R}}_{12})\right] = D_\varphi\frac{C_3}{|\mathbf{R}_{12}|^3}\,, \quad (1.16)$$

where $\mathbf{d}_1, \mathbf{d}_2$ denote dipole moments, $\mathbf{R} = \mathbf{R}_1 - \mathbf{R}_2$ is the difference between

the positions of the two atoms, and D_φ is a distance-independent but angle-dependent factor.

We are interested in two atoms excited by light to the same fine structure level, thus, the two-atom state at $R = \infty$ takes the form

$$\left|\psi^{(2)}\right\rangle = |nlj, nlj\rangle \,. \tag{1.17}$$

The dipolar interaction given by Eq. (1.16) couples $\left|\psi^{(2)}\right\rangle$ to other two-atom states $|n_1 l_1 j_1, n_2 l_2 j_2\rangle$. From the usual dipole selection rules, we get conditions on the angular momentum quantum numbers, i.e., $l_1, l_2 = l \pm 1$ and $j_1, j_2 = j \pm 0, 1$. Even though there is an infinite number of dipole-coupled states, in practice, the dipole-dipole interaction is dominated by only few two-atom states which are energetically nearby. The reason is twofold: First, the energy difference between two-atom states has to be small. Second, the dipole matrix element must not be too small. The latter quantity is proportional to the overlap of the electronic wave-functions and is strongly suppressed for large principal-quantum-number differences $|n - n_1|, |n - n_2| \gtrsim 3$ [149].

Next, let us additionally assume that the long-range interaction comes mainly from the coupling of just two states. We introduce the *Förster defect* equal to $\Delta_F = E_{n_1 l_1 j_1} + E_{n_2 l_2 j_2} - 2E_{nlj}$. Within this two-level approximation we arrive at the interaction Hamiltonian

$$H_{\text{int}} = \begin{pmatrix} 0 & V_{\text{dd}} \\ V_{\text{dd}} & \Delta_F \end{pmatrix} . \tag{1.18}$$

This leads to the two Förster eigen-energies [149]

$$V_\pm(R) = \frac{\Delta_F}{2} \pm \text{sign}(\Delta_F)\sqrt{\frac{\Delta_F^2}{4} + \frac{C_3^2}{R^6} D_\varphi^2} \,. \tag{1.19}$$

We can distinguish two limiting cases: First, for large inter-atom separations atoms in the $\left|\psi^{(2)}\right\rangle$ state interact via the perturbative van der Waals interaction-potential given by

$$V_{\text{vdW}}(R) \approx -\frac{C_3^2 D_\varphi^2}{\Delta_F R^6} = \frac{C_6}{R^6} \tag{1.20}$$

Note that the C_6 coefficient for Rydberg states can be positive or negative, depending on the sign of the Förster defect. On the other hand, for atoms in the ground state, the van der Waals interaction is always attractive.

In the second case, for small inter-atom separation, the interaction has a dipole-dipole character with

$$V_{\pm}(R) \approx \pm \operatorname{sgn}(\Delta_F) \frac{C_3 D_\varphi}{R^3}. \tag{1.21}$$

The crossover between the two regimes takes place at the distance $R_c \sim |V_{\mathrm{dd}}/\Delta_F|^{1/3}$. This crossover distance is usually much smaller then the distance between excitations due to the blockade effect, which will be discussed in the next section.

Importantly, one can change the character of the interaction for large distances from van der Waals to dipolar by either applying external electric fields [152–157], which corresponds to tuning $\Delta_F \to 0$, and via microwave fields [26, 158, 159].

An interesting aspect of Förster resonances with Rydberg states is the study of resonant energy transfer processes in ensembles of atoms [160, 161]. It is envisioned that this research will help to shed light on the physics behind e.g. light harvesting complexes [162], which play an important role in biological systems.

We point out that the accuracy of the presented simple description of dipolar interactions by using C_3 and C_6 coefficients was directly validated by a number of beautiful experiments conducted by the Palaiseau group [163–166].

1.4.3 Rydberg blockade

An important and distinctive phenomenon in Rydberg physics is the so-called *Rydberg blockade* [63, 167], also know under the name of *dipole blockade* or just *blockade effect*. The Rydberg blockade describes the strong suppression of multiple Rydberg excitations due to position dependent level shifts. As illustrated in figure 1.7, once a single Rydberg atom is excited to the $|S\rangle$ state, the excitation of a second one is strongly suppressed for distances smaller than the *blockade radius* ξ. For the excitation of ground states to Rydberg states using coherent laser fields, the blockade radius is defined as the distance at which the interaction $V(R)$ equals the laser linewidth $\hbar\Omega_S$ of the Rydberg-state excitation process,

$$V(\xi) \stackrel{!}{=} \hbar\Omega_S\,, \tag{1.22}$$

where $V(r)$ can be a resonant dipole-dipole interaction or a van der Waals interaction. For large principal quantum numbers, the blockade radius can

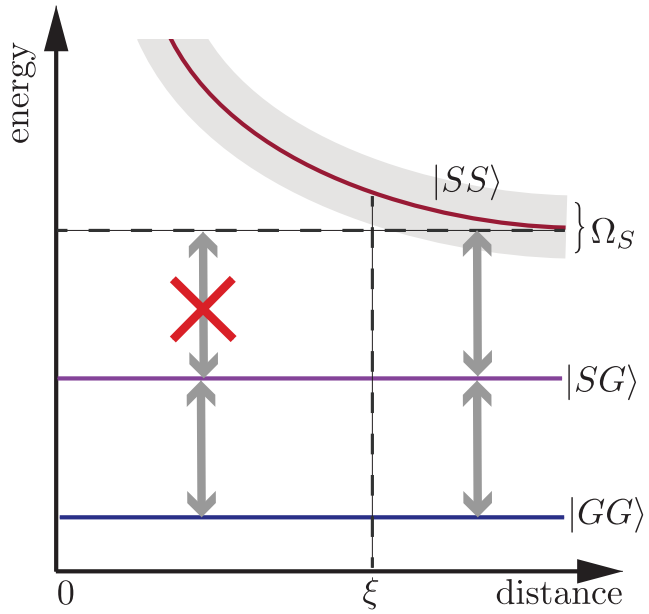

Fig. 1.7: Illustration of the Rydberg blockade.

reach sizes of the order of tens of microns. In this thesis, we will demonstrate that the blockade effect is also an important feature of Rydberg-EIT systems.

It should be mentioned that an effective interaction, as well as entanglement created using Rydberg blockade, is insensitive to the exact values of the interactions. Thus, it is *not* necessary to control the strength of the interaction to high precision, which in turn leads to less demanding requirements on atom positions and temperature control.

Closely related to the blockade effect is the notion of a *superatom* [64, 168]. To understand this concept, imagine an ensemble of N atoms with size smaller than the blockade radius ξ. Then it is only possible to create a single collective excitation in the system, described by the collective state $|W\rangle$, which reads

$$|W\rangle = \frac{1}{\sqrt{N}} \sum_i |g_1, g_2, g_3, ..., e_i, ...g_N\rangle \,. \tag{1.23}$$

In other words, the ensemble of atoms effectively behaves as a two-level atom with collectively enhanced coupling $\Omega_N = \sqrt{N}\Omega$, which motivates the term "superatom".

1.4.4 Applications

Due to their amazing properties, Rydberg atoms give rise to a plethora of interesting phenomena, some of which can find applications in quantum technologies. For example, Rydberg atoms can be used for quantum information processing [64, 169] and as quantum simulators [72, 73, 170]. Based on the blockade effect, it is possible to realize a source of single photons [24, 63, 171] and atoms [171, 172]. Moreover, great progress in imaging and loading of atoms in microtrap arrays [173–175] and optical lattices [69] facilitated the direct observation of super-atom dynamics [176, 177] and Rydberg blockade [69, 70]. Finally, the scattering between the Rydberg electron and ground state atoms can lead to strong interactions and subsequently to the formation of ultra-long-range molecules [80, 139, 178–181].

1.5 Rydberg-EIT

The study of strongly interacting Rydberg polaritons is the main subject of this dissertation. This setup is an extremely promising approach to engineer nonlinearities on the single photon level. Its premise is based on the combination of Rydberg state properties (like blockade effect) with properties of EIT (like strong and coherent atom-light coupling).

In this section, building on already described results, we will give a brief introduction to Rydberg nonlinear optics. We start with the general concept and explain Rydberg-EIT nonlinearities in two regimes: classical and quantum. Finally, we shortly discuss Rydberg-EIT applications and experimental results, we will concentrate on those which are not discussed in the next chapters. An additional overview of the Rydberg-EIT field can be found in the introduction. For more detailed description of Rydberg-EIT we refer the reader to the great works by Pritchard et al. [96], Firstenberg et al. [103], and Murray et al. [182].

Note that there are also other ways of using dipolar interactions to engineer interactions between photons. One approach is to use single emitters. However, for this setup the mode matching between input and output modes is challenging and limits efficiencies to about $\sim 10\%$ [183–186]. Another approach (which solves mode matching problem) is to combine Rydberg atoms with cavity QED or waveguides [62, 187–189]. In this case, the challenge is to control the complexity of a hybrid system. In contrast, the Rydberg-EIT setup in free-space achieves strong interactions by compressing photons in the atomic ensemble

via the slow light effect. Additionally, photonic input and output efficiencies in Rydberg-EIT systems are nearly perfect – in contrast to the cavity setups.

1.5.1 General concept

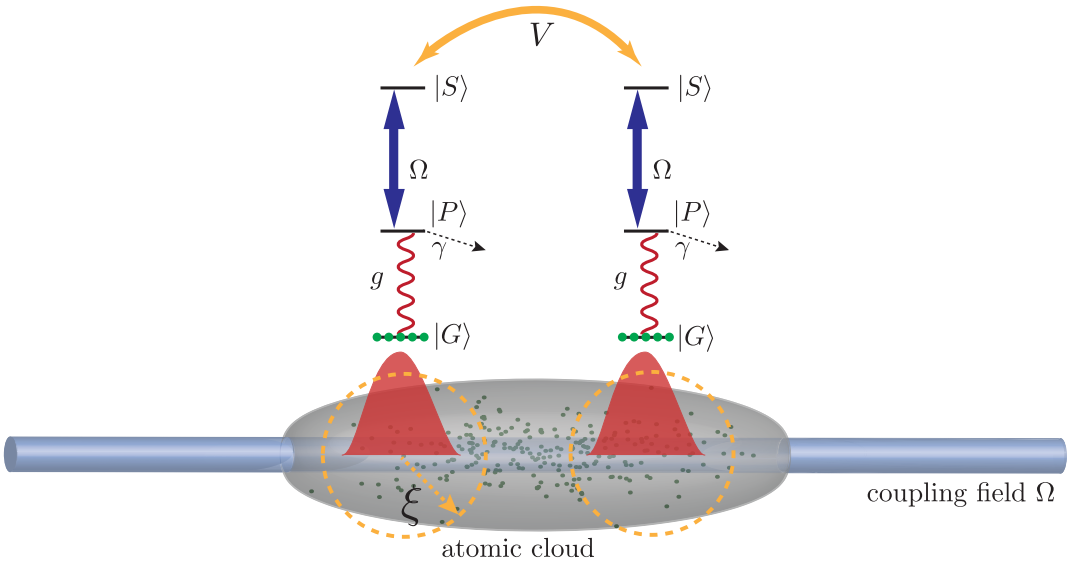

Fig. 1.8: Setup of Rydberg slow light polaritons: Each atom consists of three relevant levels, ground state $|G\rangle$, intermediate state $|P\rangle$ and Rydberg state $|S\rangle$; the latter are coupled by a strong laser Ω. Photons are propagating in the medium as slow light Rydberg polaritons. The interaction between the Rydberg states provides an interaction V between the polaritons. Dashed circles depict the characteristic length-scale ξ of the interaction.

The general idea behind Rydberg-EIT is to map Rydberg interactions onto effective photon interactions by means of electromagnetically induced transparency. This is achieved by using Rydberg states as $|S\rangle$ state in the three-level EIT scheme, as shown in figure 1.8. EIT is a sensitive quantum interference effect and can be easily perturbed. The Rydberg-EIT takes advantage of this feature: Once two propagating photons are close by, the Rydberg component is shifted out of the two-photon resonance and the EIT condition is broken.

Rydberg blockade: The blockade effect gives rise to the characteristic range of the interaction in terms of the blockade radius, which was discussed in the context of Rydberg excitations in section 1.4.3. For polaritons the Rydberg

blockade ξ is defined as distance at which the dipolar interaction equals to the EIT linewidth,

$$V(\xi) \stackrel{!}{=} \Gamma_{\text{EIT}}. \tag{1.24}$$

The blockade radius reach values on the order of tens of microns – much larger than the optical wavelength of the probe photons.

1.5.2 Intuition based on electric susceptibility

The Rydberg optical nonlinearity can be understood intuitively as a controlled switching between three-level and two-level optical responses, given by Eqs (1.4) and (1.11). As discussed in section 1.2.2, the susceptibility of the medium vanishes at the two-photon resonance. Thus, the figure of merit comes from the two-level susceptibility, see Eq. (1.4). As already mentioned in section 1.2.2, we differentiate two regimes depending on the detuning δ to the intermediate level: The *dissipative* regime for small detuning $\delta \ll \gamma$, and the *dispersive* regime for large detuning $\delta \gg \gamma$.

In the dissipative regime the two-level susceptibility takes the form

$$\chi_{\text{e}}^{2-\text{level}} = i\frac{1}{kl_{\text{a}}}\ , \tag{1.25}$$

which corresponds to the strong absorption of two photons separated by less than the blockade radius. In order to quantify this dissipative feature, we introduce the optical depth $OD = g_0^2 n_{\text{at}} L/(c\gamma)$. It describes the exponential attenuation e^{-OD} of the probe-field after propagation through the medium of length L in the absence of the control field. In other words, OD characterizes the strength of the collective optical coupling to the atomic ensemble. A closely related quantity is the optical depth per blockade radius $OD_b = g^2\xi/(c\gamma)$ which characterizes the effective interaction strength between photons.

Note that the first Rydberg-EIT nonlinear effects where observed in the dissipative regime. Pritchard et al. observed the decrease of transmission peak of the EIT signal with increasing probe field strength [75]. Moreover, they measured that the output intensity (at the exit of the medium) saturated at low values.

In the dispersive regime, the two-level susceptibility is dominated by its real part with a small imaginary contribution,

$$\chi_{\text{e}}^{2-\text{level}} = \frac{1}{kl_{\text{a}}}\frac{\gamma}{\delta}\left(1 + i\frac{\gamma}{\delta}\right)\ . \tag{1.26}$$

In this regime, the blockade effect leads to an additional phase shift for the closely propagating photons. In this thesis we will mostly study the dispersive effects involving Rydberg polaritons.

We stress that, in analogy to the electric susceptibilities in other system discussed above, see Eqs (1.5) and (1.13), we can also describe Rydberg-EIT by the third order susceptibility. And since there are N_b atoms within the blockade sphere, the maximum nonlinearity on resonance is enhanced approximately by a factor of N_b, i.e.,

$$\chi_\mathrm{e}^{(3)} \sim N_\mathrm{b}\chi_\mathrm{e}^{(1)}\frac{d_{gp}^2}{(\hbar\Omega)^2} . \tag{1.27}$$

Finally, Rydberg-EIT can be thought of as a Rydberg dressing of photons – in analogy to the Rydberg dressing of ground state atoms [190–192] in which an admixture of Rydberg states leads to an effective interaction between ground state atoms.

1.5.3 Classical and quantum nonlinearities

In the previous section we differentiated Rydberg optical nonlinearities depending whether the dipolar interactions give rise to the dispersive or dissipative effects. Another way of characterizing optical nonlinearities is based on the interaction strength per photon as shown in figure 1.9. For Rydberg-EIT systems the strength of interaction can be quantified by OD_b in the dissipative regime and by $OD_b\,\gamma/\delta$ in the dispersive regime. In order to distinguish between classical and quantum effects, we introduce the two-photon correlation function $g^{(2)}(t_2 - t_1)$, where t_1 and t_2 denote the measurement time of the first and second photon, respectively. In the weakly interacting regime, *i.e.*, for $OD_b\,\gamma/|\delta - i\gamma| \ll 1$, the interaction does not affect the statistics of a coherent input field, thus, $g^{(2)}(0) = 1$. Note that the interaction can still lead to strong classical nonlinear effects. In the strongly interacting regime, $OD_b\,\gamma/|\delta - i\gamma| > 1$, the interaction leads to nonclassical correlations, best visible in the two-photon equal-time correlation function, *i.e.*, $g^{(2)}(0) \neq 1$.

1.6 Classical Rydberg-EIT nonlinearities

In this section we review the main achievements related to the *classical* Rydberg-EIT nonlinearities. This will help us better understand *quantum* nonlinearities.

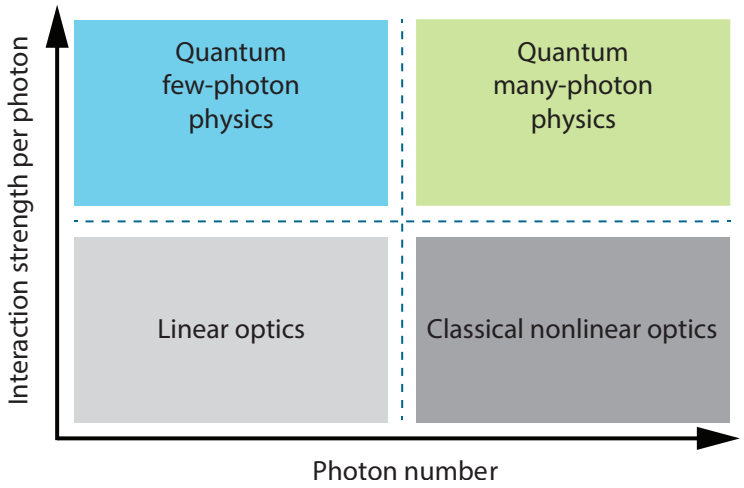

Fig. 1.9: Phenomena involving photons can be characterized according to the interaction strength per photon and the number of photons involved. Four different regimes can be distinguished: First, *linear optics*, in which interaction can be neglected at all. Second, *classical nonlinear optics*, in which the interactions only appear for large numbers of photons and they can be well described using averaged fields. In the regimes of *quantum few- and many-photon physics*, the interactions strongly modify statistics and correlations between photons on single-quanta level. In this dissertation, we mainly concentrate on quantum few-photon physics, but often we will also describe the two regimes with a large number of photons. *Source: Figure adapted from Chang et al.* [51].

In the weakly interacting regime, $OD_b\,\gamma/|\delta - i\gamma| \ll 1$, the theoretical descriptions can be simplified a lot. Since photon correlations are weak, the light propagation can be described by the classical photon-field amplitude $\mathcal{E} = \langle\hat{\mathcal{E}}\rangle$. Then, any appearing correlations stem from strong correlations between interacting Rydberg excitations, but we neglect any back-action of photons on the atomic correlations.

1.6.1 Optical nonlinearities

In the simplest case, we can neglect propagation effects and describe the probe field on the lower transition by the Rabi frequency Ω_p. Then interactions between Rydberg atoms can lead to various interesting effects: nonclassical light emission [193, 194], dissipative preparation of entangled N-atom states [85, 195–197], and quantum gate operations [198–201].

In general, even in this simplest case, the theoretical description of atomic ensembles is computationally hard. Thus, in recent years, a number of approx-

imate theoretical methods were used, e.g., variational approaches [202–204] and the cluster expansion method [205]. Another theoretical approach takes advantage of strong dissipation on the lower optical transition. This way one can treat the problem classically, considering only atomic level populations, via classical rate equations [206–208].

1.6.2 Nonlinear light propagation

In this section we discuss the nonlinear propagation through a Rydberg-EIT medium. In the classical regime, this propagation can be described by an effective equation for the coherent photon field $\mathcal{E}(\mathbf{r}) = \left\langle \hat{\mathcal{E}}(\mathbf{r}) \right\rangle$, for details see Ref. [33]. In this regime we can still assume that the interactions do not change the classical nature of the coherent input field. The photon propagation is determined by correlations between Rydberg spin wave excitations. The latter can be described using a hierarchy of equations for many-body correlations [33, 209]. Interestingly, one can tune between defocusing nonlinearities for repulsive effective interactions $\Delta > 0$ and focusing for $\Delta < 0$. It was also argued that in this classical regime it is possible to observe tight beam focusing and the spontaneous formation of ring structures [33].

1.7 Quantum Rydberg-EIT nonlinearities

In preceding sections we presented all building blocks for the Rydberg-EIT scheme. Since this thesis is treating quantum nonlinearities, we will present motivation for and explanation of the involved quantum phenomena in the corresponding chapters. An overview of the field was already given in the introduction to this dissertation.

The theoretical foundations of the description of quantum Rydberg-EIT nonlinearities will be presented in chapter 2. More details related to...

- photonic molecules will be discussed in chapter 3.
- applications in quantum technologies like quantum gates and all-optical transistors are surveyed in Chapters 4 and 6.
- the connection of Rydberg-EIT to the optical Kerr nonlinearities is described in chapter 5.
- Förster resonances and the related tunability of the interaction can be found in chapter 6.

- the angular dependence of Rydberg interactions and Rydberg polaritons with higher angular quantum numbers than $l = 0$ are discussed in chapter 7.

2

Theoretical foundations

In this chapter, we present the theoretical foundations our work [1–5, 7, 8, 41] presented in next chapters is based on. We start from the derivation of a microscopic Hamiltonian describing the polariton propagation in one-dimensional free-space. We analyze decoherence processes using a Master equation approach and show for which processes the evolution can be described using the Schrödinger equation with an effective non-Hermitian Hamiltonian. Using this approach, we present a straightforward derivation of the equations of motion in the Schrödinger picture for the example of two polaritons. Next, we introduce well-established in condensed-matter diagrammatic methods to describe Rydberg-EIT. Here, we apply diagrammatic methods to the setup consisting of a single polariton propagating in an external potential. For this setup, we show the exact solution by a summation of all Feynman diagrams. The intuition gained from this problem will be very profitable for the understanding the enhancement of nonlinearities by Förster resonances presented in chapter 6. Note also that the diagrammatic method will be very useful to describe the two-body problem [8], as we show in chapter 3.

2.1 Microscopic Hamiltonian derivation

In this section, we derive a microscopic Hamiltonian describing the propagation of a weak probe light pulse through an atomic medium under the EIT condition.

We start with the description of single photons propagating along the z-axis

in a free space. In the following, the relevant modes have only small deviations from the carrier probe frequency ω_c and momentum $\hbar k_c = \hbar\omega_c/c$. Moreover, we will study the experimentally relevant one-dimensional setup. The light field distribution u_k, characterized by a single transverse mode $u_\perp$, has the form

$$u_k(\mathbf{x}) = \frac{e^{iz(k_c+k)}}{\sqrt{L_q}} u_\perp(\mathbf{R}), \tag{2.1}$$

with L_q being the quantization length. For each longitudinal mode k, we introduce the creation operator $a_k^\dagger$. Then, the electric field operator reduces to

$$\mathbf{E}(\mathbf{x}) = \sqrt{\frac{\hbar\omega_c}{2\epsilon_0}} \sum_k \left[\varepsilon_k u_k(\mathbf{x}) a_k^\dagger + \varepsilon_k^* u_k^*(\mathbf{x}) a_k\right], \tag{2.2}$$

with the polarization ε_k. Here, each mode is characterized by a shift in energy from the leading frequency ω_c. This gives rise to the Hamiltonian in the rotating frame

$$H_{\text{ph}} = \sum_k \hbar kc\, a_k^\dagger a_k \tag{2.3}$$

with $\hbar kc \ll \hbar\omega_c$.

Next, we study the interaction of a single photon with the atoms in the medium. For each atom, there are three relevant states within the EIT setup:

The ground state $|g\rangle$, an intermediate state $|p\rangle$, and finally the Rydberg state $|s\rangle$, see Fig. 2.1(a). Within the rotating frame and using the rotating wave approximation, the strong coupling between the intermediate state $|p\rangle$ with detuning δ and the Rydberg state $|s\rangle$ with Rabi frequency 2Ω gives rise to dressed states

$$\begin{aligned} |+\rangle &= \alpha|p\rangle + \beta|s\rangle, \qquad \Delta_+ = \left(\delta + \sqrt{\delta^2 + 4\Omega^2}\right)/2, \\ |-\rangle &= \beta^*|p\rangle - \alpha^*|s\rangle, \qquad \Delta_- = \left(\delta - \sqrt{\delta^2 + 4\Omega^2}\right)/2, \end{aligned} \tag{2.4}$$

with energies $\hbar\Delta_\pm$. Note, that the spontaneous emission from the intermediate state with decay rate 2γ can be incorporated by replacing δ with a complex detuning $\Delta = \delta - i\gamma$, for details see Section 2.2. The probe light modes couple the states $|g\rangle$ with $|p\rangle$. For simplicity, we restrict the analysis to a situation where only a single polarization couples matter with light, with the dipole moment $d = \langle g|\mathbf{d}\cdot\varepsilon|p\rangle$. Then, the Hamiltonian, describing the interaction between the atoms and the light modes reduces to

$$H_{\text{lm}} = \hbar g \sum_i \left[\psi_e(\mathbf{x}_i)\, |p\rangle\langle g|_i + \psi_e^\dagger(\mathbf{x}_i)\, |g\rangle\langle p|_i\right] \tag{2.5}$$

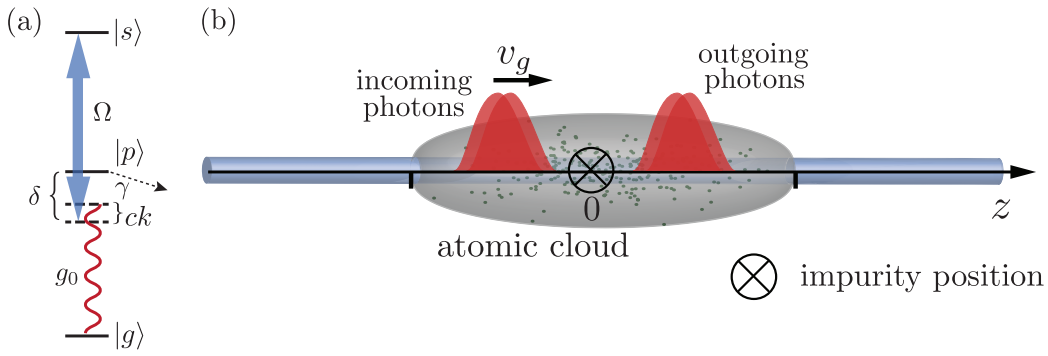

Fig. 2.1: (a) Setup for the electromagnetically induced transparency: the probe field couples the atomic ground state $|g\rangle$ to the p-level $|p\rangle$ with the single-particle coupling strength g_0, while a strong coupling laser drives the transition between the p-level and the Rydberg state $|s\rangle$ with Rabi frequency Ω and detuning δ. Furthermore, 2γ denotes the decay rate from the p-level. The single-particle coupling g_0 is related to the collective coupling $g = \sqrt{n}g_0$ with n the particle density. (b) Single photons propagate through the atomic medium with the reduced group velocity $v_g \ll c$. In this chapter we will be interested in case, in which a single polariton propagates in an external potential generated by, for example, a stored Rydberg excitation (impurity).

with $g = \sqrt{\frac{\omega_c}{2\hbar\epsilon_0}}\, d$. In addition, we have introduced the field operator for the electric field

$$\psi_e^\dagger(\mathbf{x}) = \sum_k u_k(\mathbf{x}) a_k^\dagger. \tag{2.6}$$

In the following, in the continuum limit, we describe the atoms by a field operator $\bar{\Psi}$, with the internal structure of the atoms properly accounted for by a spinor degree of freedom of $\bar{\Psi}$, i.e.,

$$\bar{\Psi}(\mathbf{x}) = \begin{pmatrix} \Psi_g(\mathbf{x}) \\ \Psi_+(\mathbf{x}) \\ \Psi_-(\mathbf{x}) \end{pmatrix}. \tag{2.7}$$

This operator can either be a fermionic or a bosonic field operator, depending on the statistics of the atoms. Next, we define two new operators, describing a transition from the ground state $|g\rangle$ into an excited state $|\pm\rangle$,

$$b^\dagger(\mathbf{x}) = \frac{1}{\sqrt{n(\mathbf{x})}} \bar{\Psi}^\dagger(\mathbf{x}) S^+ \bar{\Psi}(\mathbf{x}), \tag{2.8}$$

$$c^\dagger(\mathbf{x}) = \frac{1}{\sqrt{n(\mathbf{x})}} \bar{\Psi}^\dagger(\mathbf{x}) T^+ \bar{\Psi}(\mathbf{x}), \tag{2.9}$$

with the spinor operator $S^+ = |+\rangle\langle g|$ and $T^+ = |-\rangle\langle g|$. In addition, $n(\mathbf{x})$ denotes the atomic density. Then, these operators always satisfy the bosonic commutation relation, for example:

$$\left[b(\mathbf{x}), b^\dagger(\mathbf{y})\right] = \frac{\Psi_g^\dagger \Psi_g - \Psi_+^\dagger \Psi_+}{n(\mathbf{x})}\, \delta(\mathbf{x}-\mathbf{y}) \simeq \delta(\mathbf{x}-\mathbf{y}). \tag{2.10}$$

Here, we have used that fact, that the atomic density is much higher than the photon (polariton) density and, therefore, almost all atoms are in the ground state, i.e., $\Psi_g^\dagger \Psi_g \simeq n(\mathbf{x}) \gg \Psi_+^\dagger \Psi_+$. It immediately follows, that $b^\dagger$ and $c^\dagger$ are bosonic field operators, and the Hamiltonian describing the light field and the interaction with the atoms reduces to a quadratic Hamiltonian for three coupled bosonic fields,

$$H = \hbar \int \mathrm{d}\mathbf{x} \begin{pmatrix} \psi_e^\dagger \\ b^\dagger \\ c^\dagger \end{pmatrix} \begin{pmatrix} -ic\partial_z & g\sqrt{n}\alpha & g\sqrt{n}\beta \\ g\sqrt{n}\alpha & \Delta_+ & 0 \\ g\sqrt{n}\beta & 0 & \Delta_- \end{pmatrix} \begin{pmatrix} \psi_e \\ b \\ c \end{pmatrix}, \tag{2.11}$$

where we have Fourier-transformed the photonic part.

The Hamiltonian in Eq. (2.11) may be written in a more convenient way by introducing the fields $\psi_p^\dagger(\mathbf{x}) = -\beta b^\dagger(\mathbf{x}) + \alpha c^\dagger(\mathbf{x})$ and $\psi_s^\dagger(\mathbf{x}) = \alpha b^\dagger(\mathbf{x}) + \beta c^\dagger(\mathbf{x})$. These operators describe bosonic fields for the creation of excitation in $|p\rangle$-state and $|s\rangle$-state, respectively. Then, the Hamiltonian reduces to

$$H = \hbar \int \mathrm{d}\mathbf{x} \begin{pmatrix} \psi_e \\ \psi_p \\ \psi_s \end{pmatrix}^\dagger \begin{pmatrix} -ic\partial_z & g & 0 \\ g & \delta & \Omega \\ 0 & \Omega & 0 \end{pmatrix} \begin{pmatrix} \psi_e \\ \psi_p \\ \psi_s \end{pmatrix}. \tag{2.12}$$

Note, that our derivation can be straightforwardly generalized to the light fields confined in a cavity.

Next, we integrate out the transverse mode $u_\perp$ in order to arrive at a one-dimensional theory. Assuming a homogeneous particle distribution along the longitudinal mode, the light field couples to the following matter mode

$$\psi_p^\dagger(\mathbf{x}) = \sqrt{\frac{n(\mathbf{R})}{\bar{n}}} u_\perp(\mathbf{R}) \psi_p^\dagger(z) \tag{2.13}$$

with the effective particle density

$$\bar{n} = \int \mathrm{d}\mathbf{R}\, n(\mathbf{R}) |u_\perp(\mathbf{R})|^2. \tag{2.14}$$

Analogously, we can define the one-dimensional field operator $\psi_s(z)$ accounting for the Rydberg state. Then, the operators $\psi_e(z)$, $\psi_p(z)$, $\psi_s(z)$ describe a one-dimensional field theory with the Hamiltonian

$$\mathcal{H} = \hbar \int \mathrm{d}z \begin{pmatrix} \psi_e^\dagger \\ \psi_p^\dagger \\ \psi_s^\dagger \end{pmatrix} \begin{pmatrix} -ic\partial_z & g & 0 \\ g & \delta & \Omega \\ 0 & \Omega & 0 \end{pmatrix} \begin{pmatrix} \psi_e \\ \psi_p \\ \psi_s \end{pmatrix}. \tag{2.15}$$

2.2 Decoherence description within Master equation approach

In this section, we analyze the decoherence of Rydberg polaritons within the formalism developed in the previous section. The source of the decoherence can be, e.g., spontaneous emission from excited states, motional dephasing or dephasing caused by the interactions between ground and Rydberg states. In order to understand the impact of these processes on polaritons, we study the system evolution using the Master equation. In the case of a Markovian evolution, it can be written in the Lindblad form

$$\dot{\rho} = -\frac{i}{\hbar}[\mathcal{H}, \rho] + \sum_i \mathcal{L}_i(\rho), \tag{2.16}$$

where $\mathcal{L}_i$ are Liouvillians describing different incoherent processes, $\mathcal{H}$ describes the coherent evolution and ρ is a density matrix

$$\rho = \sum_{n=0}^{N} \rho^{(n)}, \tag{2.17}$$

where $\rho^{(n)}$ contains n excitations (atomic or photonic). Moreover, we neglect correlations between the $N+1$ terms in (2.17). Note that we truncated the Hilbert space by introducing the maximal number of excitations N present in the system. Such a cut-off is justified for most of the experiments investigating quantum phenomena on a few-photon level with Rydberg-polaritons [5, 25, 28, 30, 31, 36]. In these experiments, a low intensity laser field is used as a photon source and, thus, the probability of having N excitations in the system is much higher than the probability of having $N+1$ excitations.

As an example, let us consider the case of a single incoming photon, for which the full density matrix takes the form

$$\rho(t) \;=\; \rho^{(0)}(t) + \rho^{(1)}(t) = \epsilon(t)|0\rangle\langle 0| + \rho^{(1)}(t). \tag{2.18}$$

The single-particle component of the density matrix $\rho^{(1)}$ can be characterized using density matrix components $\rho_{AB}(x,y,t)$ defined as $\rho_{AB}(x,y,t) = \mathrm{Tr}[\rho^{(1)}(t)\psi_A^\dagger(x)\psi_B(y)]$, i.e.,

$$\rho^{(1)}(t) = \sum_{\mathrm{AB}} \int \mathrm{d}x \int \mathrm{d}y\, \rho_{\mathrm{AB}}(x,y,t)\psi_{\mathrm{B}}^\dagger(y)|0\rangle\langle 0|\psi_{\mathrm{A}}(x), \tag{2.19}$$

where $\mathrm{AB} \in \{ee, ep, pe, es, se, sp, ps, ss\}$.

In the following, we will only be interested in the evolution of $\rho^{(N)}$. First, we will show that in such a situation, the description of the system can be substantially simplified in the case of decoherence due to the decay of the excited states. Afterwards, we comment on the impact of dephasing on the system evolution.

2.2.1 Decay

Here, we consider decoherence in the system due to the finite lifetime of the excited states. For the sake of simplicity, we analyze the decay on the example of the intermediate p-state with the decay rate 2γ. The Louvillian for such a process reads

$$\mathcal{L}_{pg} = -\gamma \int \mathrm{d}y \left[\psi_p^\dagger(y)\psi_p(y)\rho + \rho\psi_p^\dagger(y)\psi_p(y) - 2\psi_p(y)\rho\psi_p^\dagger(y)\right]. \tag{2.20}$$

The first two terms describe the decay of the probability that the system contains N excitations. The last term depicts the "quantum jump" from the $(N+1)$-excitation manifold to the N-excitation manifold. Since we consider the case $\rho^{(N+1)} = 0$, this process can be neglected. Using this observation we can rewrite Master equation as

$$\dot{\rho}^{(N)} = -\frac{i}{\hbar}(H_0\rho^{(N)} - \rho^{(N)}H_0^\dagger), \tag{2.21}$$

where we defined the non-Hermitian Hamiltonian

$$H_0 = \mathcal{H} - i\hbar\gamma \int \mathrm{d}y\, \psi_p^\dagger(y)\psi_p(y). \tag{2.22}$$

Next, we write density operator in the general form $\rho^{(N)} = \sum_j p_j |\Phi_j\rangle\langle\Phi_j|$. Together with (2.21) we see that, rather than solving the Master equation (2.21), we can solve the Schrödinger equation

$$i\hbar\frac{d}{dt}|\Phi_j\rangle = H_0|\Phi_j\rangle \tag{2.23}$$

for the pure state $|\Phi_j\rangle$, which is much more convenient. Note that there are no approximations in this simplification. The only assumption is that we can neglect the occupation of any Hilbert subspace with more than N excitations and that we are only interested in the time evolution of $\rho^{(N)}$. Let us illustrate this simplification on the previously described example of a single incoming photon (2.18). Assuming that at initial time $t = 0$ the excitation can be described by a pure state $|\psi_1(0)\rangle$, the full density matrix simplifies to

$$\rho(t) \;=\; \epsilon(t)|0\rangle\langle 0| + |\psi_1(t)\rangle\langle\psi_1(t)|. \tag{2.24}$$

Note, that due to the non-Hermitian nature of the effective Hamiltonian, the probability leaks from the single excitation subspace. It corresponds to an increase in time of the probability $\epsilon(t)$ to have zero excitations.

Analogously to the decay of the p-level, we can include the decay $2\gamma_s$ of the Rydberg s-state. Together with (4.2) leads to the non-Hermitian Hamiltonian of the form

$$H_0 = \hbar \int \mathrm{d}z \begin{pmatrix} \psi_e \\ \psi_p \\ \psi_s \end{pmatrix}^\dagger \begin{pmatrix} -ic\partial_z & g & 0 \\ g & \delta - i\gamma & \Omega \\ 0 & \Omega & -i\gamma_s \end{pmatrix} \begin{pmatrix} \psi_e \\ \psi_p \\ \psi_s \end{pmatrix}. \tag{2.25}$$

Note, that even though for typical experimental conditions $\gamma_s \ll \gamma$, it can be the decoherence of the Rydberg level that has a leading impact on the losses of a single photon inside the medium at the two-photon resonance.

2.2.2 Dephasing

In general there exist processes which decrease coherences of the density matrix without affecting the populations. In this chapter, we call such processes *dephasing*. In Rydberg-EIT setups the dephasing can result from a variety of sources, for example, finite linewidth of the laser field, atom-atom interactions or motion of the atoms. In general, dephasing can not be rigorously treated by an imaginary part in an effective Hamiltonian. In this section we show the impact of dephasing on the description of polaritons propagation.

We start with the Liouvillian describing the dephasing [**Fleischhauer2005a**, 210] of the s-state

$$\mathcal{L}_{ss} = -\gamma_s^{\mathrm{deph}} \sum_j \left(P_j P_j \rho + \rho P_j P_j - 2 P_j \rho P_j\right) \tag{2.26}$$

with $P^j = |s\rangle\langle s|_j$ being the projection onto the Rydberg state. In second quantization, and written using field operators ψ_s, it takes the form

$$\mathcal{L}_{ss} = -\gamma_s^{\text{deph}} \int \mathrm{d}y \left(\psi_s^\dagger(y)\psi_s(y)\rho - \frac{\psi_s^\dagger(y)\psi_s(y)\,\rho\,\psi_s^\dagger(y)\psi_s(y)}{n(y)} + h.c. \right).$$

In general, the second term in the parentheses is nonzero even for $\rho^{(N)}$. To better understand the impact of this term, we analyze an exemplary time evolution of a single excitation $\rho^{(1)}$. For this purpose, we use the representation of the density matrix given by (2.19). Next, we project the Master equation onto different components $\rho_{\mu\beta}$ of the single excitation subspace:

$$\begin{aligned} \dot{\rho}_{\mu\beta}(x,y,t) &= \langle\psi_\mu(x)|\dot{\rho}|\psi_\beta(y)\rangle \\ &= \left\langle \psi_\mu(x) \middle| -\frac{i}{\hbar}[\mathcal{H},\rho] + \mathcal{L}_{ss}(\rho) + \mathcal{L}_{sg}(\rho) \middle| \psi_\beta(y) \right\rangle, \end{aligned} \tag{2.27}$$

where $|\psi_\beta(y)\rangle = \psi_\beta^\dagger(y)\,|0\rangle$. We also included the decay of the s-state by the Liouvillian $\mathcal{L}_{sg}$ analogous to $\mathcal{L}_{pg}$ for the decay of the p-state, see Eq. (2.20).

Specifically, the equation of main interest, i.e., for ρ_{ss} takes the form

$$\begin{aligned} \partial_t \rho_{ss}(z,z',t) &= i\Omega\left(\rho_{es}(z,z',t) + \rho_{se}(z,z',t)\right) - \gamma_s \rho_{ss}(z,z',t) \\ &\quad -\gamma_s^{\text{deph}} \rho_{ss}(z,z',t) + \gamma_s^{\text{deph}} \rho_{ss}(z,z',t) \frac{\delta(z-z')}{n(z)}. \end{aligned} \tag{2.28}$$

Where the last term in the first line depicts the decay due to the finite lifetime, while the two terms in the second line describe dephasing. We see that the dephasing differs from the decay by the last term which is nonzero for $z = z'$. Because of this difference one can not use an effective non-Hermitian Hamiltonian for the rigorous description of dephasing.

2.3 Interaction between polaritons

In this section, we include the strong interaction between the Rydberg atoms. It takes the form

$$\begin{aligned} H_{\text{rr}} &= \frac{1}{2}\sum_{i\neq j} V^{\text{3D}}(\mathbf{x}_i - \mathbf{x}_j) P_i P_j \\ &= \frac{1}{2}\int \mathrm{d}\mathbf{x} \int \mathrm{d}\mathbf{y}\, V^{\text{3D}}(\mathbf{x}-\mathbf{y}) : \Psi_r^\dagger(\mathbf{x})\Psi_r(\mathbf{x})\Psi_r^\dagger(\mathbf{y})\Psi_r(\mathbf{y}) : \end{aligned} \tag{2.29}$$

with $P_i = |s\rangle\langle s|_i$ the projection onto the Rydberg state. The notation $: \; :$ means normal ordering, which is included in order to avoid self-interactions.

On the same level of approximation as for the non-interacting Hamiltonian H_0, this interaction can then be expressed in terms of the bosonic fields as

$$H_{\text{rr}} = \frac{1}{2}\int \mathrm{d}\mathbf{x} \int \mathrm{d}\mathbf{y}\, V^{\text{3D}}(\mathbf{x}-\mathbf{y}) : \psi_s^\dagger(\mathbf{x})\psi_s(\mathbf{x})\psi_s^\dagger(\mathbf{y})\psi_s(\mathbf{y}) : \tag{2.30}$$

with the bosonic field operator $\psi_s^\dagger(\mathbf{x})$ creating an s-excitation at position $\mathbf{x}$.

In the one-dimensional limit, the interaction between the Rydberg levels is described by

$$H_{\text{rr}} = \frac{1}{2}\int \mathrm{d}z \int \mathrm{d}z' V(z-z')\psi_s^\dagger(z)\psi_s^\dagger(z')\psi_s(z')\psi_s(z), \tag{2.31}$$

where the interaction potential V results from the microscopic interaction potential by an average over the transverse modes

$$V(z) = \int \mathrm{d}\mathbf{R} \int \mathrm{d}\mathbf{R}' \frac{n(\mathbf{R})n(\mathbf{R}')}{\bar{n}^2} |u_\perp(\mathbf{R})|^2 |u_\perp(\mathbf{R}')|^2 V^{\text{3D}}(\mathbf{R}-\mathbf{R}', z). \tag{2.32}$$

Note, that the transverse mode spacing naturally introduces a cut-off to the van der Waals interaction. In this chapter, we neglect this effect by taking $V(z) = C_6/z^6$, which is an excellent approximation for high Rydberg states, such that the blockade radius is greater than the size of the transverse mode. For additional insights see Ref. [40].

In the following, the quadratic Hamiltonian in Eq. (4.2) for the bosonic fields ψ_e, ψ_p, and ψ_s together with the interaction H_{rr} in Eq. (2.31) allows us to apply standard diagrammatic Green's function techniques to study the properties of the system. The only relevant approximations are, that the light modes are restricted to low energies $\hbar\omega \ll \hbar\omega_c$ and that the photonic density is always much smaller than the atomic density $n(\mathbf{x})$.

2.3.1 Equations of motion in Schrödinger picture

Here, we derive the equations of motion within the Schrödinger picture using an effective non-Hermitian Hamiltonian. The Schrödinger equation has the form

$$i\hbar\partial_t \left|\psi(t)\right\rangle = \left(H_0 + H_{\text{rr}}\right)\left|\psi(t)\right\rangle. \tag{2.33}$$

As an exemplary case, we present the analysis for the wavefunction describing two excitations,

$$\begin{aligned}|\psi(t)\rangle &= \int \mathrm{d}x \int \mathrm{d}y \Big[\varphi_{ep}(x,y,t)\psi_e^\dagger(x)\psi_p^\dagger(y) + \varphi_{es}(x,y,t)\psi_e^\dagger(x)\psi_s^\dagger(y) \\ &+ \varphi_{ps}(x,y,t)\psi_p^\dagger(x)\psi_s^\dagger(y) + \frac{1}{2}\varphi_{ee}(x,y,t)\psi_e^\dagger(x)\psi_e^\dagger(y) + \\ &+ \frac{1}{2}\varphi_{pp}(x,y,t)\psi_p^\dagger(x)\psi_p^\dagger(y) + \frac{1}{2}\varphi_{ss}(x,y,t)\psi_s^\dagger(x)\psi_s^\dagger(y) \Big] |0\rangle \,. \quad (2.34)\end{aligned}$$

We will arrive at equations of motion for the two particle amplitudes by projecting Eq. (2.33) onto all possible components $|\psi_{\mathrm{A}}(z)\psi_{\mathrm{B}}(z')\rangle = \psi_{\mathrm{A}}^\dagger(z)\psi_{\mathrm{B}}^\dagger(z')\,|0\rangle$. For example, the time evolution of $\varphi_{ep}(z,z')$ is given by $\langle\psi_e(z)\psi_p(z')|\,(-i\hbar\partial_t + H_0 + H_{\mathrm{rr}})\,|\psi(t)\rangle = 0$. Without loss of generality, we take $\varphi_{ee}(x,y) = \varphi_{ee}(y,x)$, $\varphi_{pp}(x,y) = \varphi_{pp}(y,x)$ and $\varphi_{ss}(x,y) = \varphi_{ss}(y,x)$. The full set of equations has the form

$$\begin{aligned}
i\partial_t\varphi_{ee}(z,z') &= -ic(\partial_z + \partial_{z'})\varphi_{ee}(z,z') + g(\varphi_{ep}(z,z') + \varphi_{ep}(z',z)), \\
i\partial_t\varphi_{ep}(z,z') &= (-ic\partial_z + \Delta)\varphi_{ep}(z,z') + g(\varphi_{ee}(z,z') + \varphi_{pp}(z,z')) + \Omega\varphi_{es}(z,z'), \\
i\partial_t\varphi_{es}(z,z') &= (-ic\partial_z - i\gamma_s)\varphi_{es}(z,z') + g\varphi_{ps}(z,z') + \Omega\varphi_{ep}(z,z'), \\
i\partial_t\varphi_{pp}(z,z') &= 2\Delta\varphi_{pp}(z,z') + g(\varphi_{ep}(z,z') + \varphi_{ep}(z',z)) \\
&+ \Omega(\varphi_{ps}(z,z') + \varphi_{ps}(z',z)), \\
i\partial_t\varphi_{ps}(z,z') &= (\Delta - i\gamma_s)\varphi_{ps}(z,z') + g\varphi_{es}(z,z') + \Omega(\varphi_{pp}(z,z') + \varphi_{ss}(z,z')), \\
i\partial_t\varphi_{ss}(z,z') &= -i2\gamma_s\varphi_{ss}(z,z') + \Omega(\varphi_{ps}(z,z') + \varphi_{ps}(z',z)) \\
&+ V(z-z')\varphi_{ss}(z,z').
\end{aligned}$$

Alternatively, one can describe the system in the Heisenberg picture. Then, the equation of motion for the time dependent field operators $\psi_A(z,t)$ can be derived from Heisenberg-Langevin equations

$$\partial_t\psi_e = \frac{i}{\hbar}[\mathcal{H} + H_{\mathrm{rr}}, \psi_e], \quad (2.35)$$

$$\partial_t\psi_p = \frac{i}{\hbar}[\mathcal{H} + H_{\mathrm{rr}}, \psi_p] - \gamma\psi_p + F_p, \quad (2.36)$$

$$\partial_t\psi_s = \frac{i}{\hbar}[\mathcal{H} + H_{\mathrm{rr}}, \psi_s] - \gamma_s\psi_s + F_s, \quad (2.37)$$

where $\mathcal{H} + H_{\mathrm{rr}}$ describes the coherent evolution, see Eqs (2.15) and (2.31), while F_p and F_s are the Langevin noise operators corresponding to the decay rates γ and γ_s, respectively. These equations are the starting point of the analysis presented, for example, in [25, 36, 38, 40].

2.4 Diagrammatic methods

The microscopic Hamiltonian describes three bosonic fields with a non-interacting quadratic part [Eq. (4.2)] and a quartic interaction [Eq. (2.31)]. In the past, such systems have been studied extensively using diagrammatic methods; see for example [211]. However, it is important to stress that the quadratic Hamiltonian exhibits a rather unconventional form, as the only dynamics is given by the light velocity of the photon. It is this property, which is crucial for the following analysis using diagrammatic methods and gives rise to novel phenomena.

In our previous work [8], we successfully applied diagrammatic methods to the case of two copropagating polaritons. Here, we first use the diagrammatic formalism to describe a single polariton propagating in an external potential. We show that this problem can be solved by an exact summation of all Feynman diagrams. Note, that in section 3.2.5 we will show another exact solution, *i.e.*, of a two-body problem in the weakly interacting regime.

2.4.1 Dispersion relation

First, we analyze the unconventional form of the quadratic Hamiltonian, by looking at its spectrum, see Fig 2.2. It is obtained by diagonalizing the quadratic Hamiltonian (4.2), which reduces to $H_0 = \sum_{\mu\in 0,\pm 1} \epsilon_\mu(k)\tilde{\psi}^\dagger_\mu(k)\tilde{\psi}_\mu(k)$. Here, $\mu \in \pm 1$ accounts for the two bright polariton states, while $\mu = 0$ denotes the dark state polariton mode. The new field operators take the form $\tilde{\psi}_{\mu k} = \sum_{\beta\in\{e,p,s\}} U^\beta_\mu(k)\psi_{\beta k}$ with $\mu \in \{0, \pm 1\}$, and its inverse $\bar{U} \equiv U^{-1}$ providing $\tilde{\psi}^\dagger_{\mu k} = \sum_{\beta\in\{e,p,s\}} \bar{U}^\mu_\beta(k)\psi^\dagger_{\beta k}$. Note, that the diagonalizing matrix U is not unitary, due to the imaginary part in the Hamiltonian (4.2). For the clarity of the expressions, we set the decay of the s-state to zero in the rest of this chapter, i.e., $\gamma_s = 0$. This approximation is well justified for highly excited Rydberg states used in nowadays experiments, because the propagation time of the photon in the medium is much shorter than the life-time of the Rydberg state.

In the regime of low-momentum and low-energy, i.e., $\omega, v_g k \ll \min[\Omega, |\Delta|, g]$, the dispersion relation for the dark state polariton is well accounted for by the two terms in

$$\epsilon_0(k) = \hbar v_g k - \frac{\hbar^2}{2m}k^2, \tag{2.38}$$

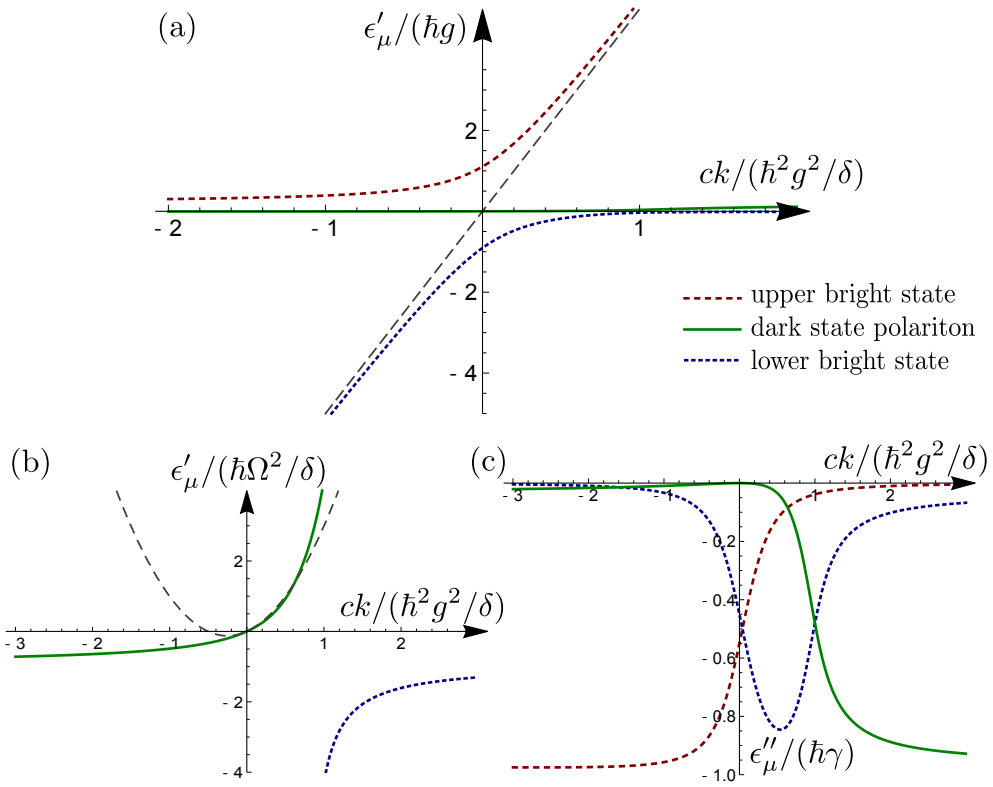

Fig. 2.2: Dispersion relation for the three non-interacting polariton branches for $g = 4\delta$, $\Omega = 0.25\delta$ and $\Delta = (4 - i)\gamma$. (a) The real part of the energy $\epsilon'_\mu(k)$. The gray dashed line depicts light mode dispersion relation. (b) The low energy range of the dispersion relation illustrating dark state polariton behavior: For low momenta the dispersion relation $\epsilon_0(k)$ can be approximated by linear and quadratic contributions. The gray dashed line shows the contribution from these two terms, see Eq. (2.38). (c) The imaginary part of the energy $\epsilon''_\mu(k)$: For low momenta the imaginary part of the dark state energy vanishes. Note different characteristic energy scales for each figure.

with group velocity and polariton mass

$$v_g = \frac{\Omega^2}{g^2 + \Omega^2} c, \qquad m = \frac{\left(g^2 + \Omega^2\right)^3}{2c^2 g^2 \Delta \Omega^2}. \tag{2.39}$$

Finally, it is worth pointing out that while the general expressions for the dispersion relation are complicated, the expression for momentum as a function of energy has a simple analytical form

$$\hbar c k(\omega) \;=\; \hbar\omega \left(\frac{g^2}{\Omega^2} \frac{1}{1 + \frac{\Delta\omega - \omega^2}{\Omega^2}} + 1 \right). \tag{2.40}$$

2.4.2 Polariton propagation in external potential

In this section, building on the understanding of single-body physics, we describe the polariton propagation in an external potential $V(z)$, acting only on the Rydberg s-state

$$H_{\text{ext}} = \int \mathrm{d}z\, \psi_s(z)^\dagger V(z) \psi_s(z). \tag{2.41}$$

This potential can be a result of an interaction between the polariton and a stationary Rydberg excitation in state $|s'\rangle$. Such a configuration is relevant for recent experimental realizations of single photon switch and transistor [5, 29–31]. Note, that in order to neglect readout of the stored excitation, the state $|s'\rangle$ has to be different than the state $|s\rangle$ in the EIT scheme. Moreover, alternative ways of treating this problem can be found, for example, in Ref. [38, 212].

We start by pointing out, that the Hamiltonian conserves the total energy $\hbar\omega$. Then, the single polariton scattering properties can be well accounted for using the T-matrix formalism. As the interaction acts only between the Rydberg states, it is sufficient to study the T-matrix for the Rydberg states alone, which will be denoted as $T_{kk'}(\omega)$. Here, $\hbar k$ denotes the momentum of the incoming particle, and $\hbar k'$ the momentum of the outgoing state. The relation between the T-matrix and the s-state amplitude φ_s by definition is provided by the relation

$$\varphi_s(z) = \frac{1}{V(z)} \int \frac{\mathrm{d}k'}{2\pi}\, e^{ik'z}\, T_{kk'}. \tag{2.42}$$

For single polaritons, the T-matrix is expressed as a resummation of all ladder diagrams, figure 2.3, which gives rise to the integral equation [211]

$$T_{kk'}(\omega) = V(k-k') + \int \frac{\mathrm{d}q}{2\pi}\, T_{kq}(\omega)\chi_q(\omega)V(q-k'). \tag{2.43}$$

Here, χ_q denotes the full propagation of a single polariton and its overlap with the Rydberg state

$$\chi_q(\omega) = \sum_{\mu\in\{0,\pm1\}} \frac{\bar{U}_s^\mu(q) U_\mu^s(q)}{\hbar\omega - \epsilon_\mu(q) + i\eta} \tag{2.44}$$

It is a special property of the polariton Hamiltonian, that χ_q reduces to two terms

$$\chi_q = \bar{\chi}(\omega) + \frac{\alpha(\omega)}{\hbar c\, k(\omega) - \hbar c\, q + i\eta}. \tag{2.45}$$

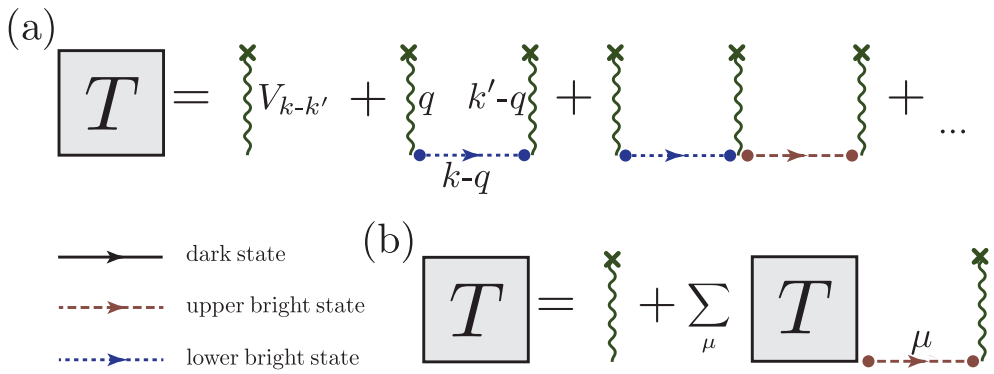

Fig. 2.3: (a) Illustration of ladder diagrams up to the third order: the interaction V is denoted by a wavy line, while the straight lines with an arrow are Green's functions for the three polariton modes $1/(\hbar\omega - \epsilon_\mu + i\eta)$, and the dots mark the overlap factors U_μ^s and $\bar{U}_s^\mu$ of the polariton with the Rydberg state. The T-matrix includes all diagrams up to arbitrary order with all possible intermediate polaritons. (b) Illustration of the integral equation (2.43).

Here, $\bar{\chi}(\omega)$ accounts for the saturation of the polariton propagation at large momenta $q \to \pm\infty$ and takes the form

$$\hbar\bar{\chi}(\omega) \;=\; \frac{\Delta}{\Omega^2}\frac{1-\frac{\omega}{\Delta}}{1+\frac{\Delta\omega}{\Omega^2}-\frac{\omega^2}{\Omega^2}}, \tag{2.46}$$

which for $\omega \ll \Omega^2/\Delta$ simplifies to $\hbar\bar{\chi}(\omega) = \Delta/\Omega^2$. The second term in Eq. (2.45) characterizes the pole structure of the propagating polariton. This term reduces to the propagator of a single polariton with momentum $\hbar k(\omega)$, given by (2.40), and α depends on the energy ω of the incoming polariton:

$$\alpha(\omega) \;=\; \frac{g^2}{\Omega^2}\frac{1}{\left((\Delta-\omega)\omega/\Omega^2+1\right)^2}. \tag{2.47}$$

In order to eliminate the saturation-term $\bar{\chi}$, we Fourier transform the T-matrix equation (2.43) to real space

$$T_k(z) \;=\; V(x)e^{ikz} + \bar{\chi}(\omega)V(z)T_k(z) + V(z)\int \mathrm{d}y\, G(\omega, z-y)T_k(y)$$

with $G(\omega, z) = -i\alpha(\omega)\,\theta(z)e^{ik(\omega)z}$ being the Fourier transform of the second term in Eq. (2.45), where $\theta(z)$ is the Heaviside step function. Introducing the effective interaction potential

$$V^{\text{eff}}(z) = \frac{V(z)}{1-\bar{\chi}(\omega)V(z)}, \tag{2.48}$$

the equation for the T-matrix reduces to

$$T_k(z) = V^{\text{eff}}(z)e^{ikz}\left(1 - i\frac{\alpha}{\hbar c}\int_{-\infty}^{z} \mathrm{d}y\, e^{-iky}T_k(y)\right). \tag{2.49}$$

This equation can be solved analytically leading to the expression for T-matrix

$$T_k(z) = e^{ikz}V^{\text{eff}}(z)\exp\left[-i\frac{\alpha}{\hbar c}\int_{-\infty}^{z} \mathrm{d}y\, V^{\text{eff}}(y)\right]. \tag{2.50}$$

Based on the solution for $T_k(\omega)$ we can derive all components of the wavefunction describing a single polariton. For this purpose, we start from the relation between the T-matrix and the outgoing state

$$\varphi_k^{\beta}(z) = e^{ikz}u_k^{\beta} + u_k^{s}\int\frac{\mathrm{d}q}{2\pi}\, e^{iqz}T_{kq}\chi^{s\beta}(\omega, q), \tag{2.51}$$

where the index $\beta \in \{e, p, s\}$ depicts components of the incoming u_k^{β} and the outgoing φ_k^{β} states. In order to arrive at formula (2.51) we used the fact that the only non-vanishing element of the T-matrix is between s-states. Moreover, we introduced $\chi^{s\beta}(\omega, q)$ which is the generalization of $\chi_q(\omega)$, see Eq. (2.44), and describes the propagation of a single polariton and its overlap with s-state and β-state

$$\chi^{s\beta}(\omega, q) = \sum_{\mu\in\{0,\pm1\}}\frac{\bar{U}_s^{\mu}(q)U_{\mu}^{\beta}(q)}{\hbar\omega - \epsilon_{\mu}(q) + i\eta}. \tag{2.52}$$

Moreover, analogously to Eq. (2.45), $\chi^{s\beta}(\omega, q)$ can be re-written in the following form

$$\chi^{s\beta}(\omega, q) = \bar{\chi}^{\beta}(\omega) + \frac{\alpha^{\beta}(\omega)}{\hbar c k(\omega) - \hbar c q + i\eta}. \tag{2.53}$$

Note that in the newly introduced notation, by definition, the following relations are satisfied: $\bar{\chi}^s \equiv \bar{\chi}$ and $\alpha^s \equiv \alpha$. Next, we Fourier transform Eq. (2.51), and then insert to it the solution for T-matrix, given by Eq. (2.50). Furthermore, we use the relation $u_k^s/u_k^{\beta} = \alpha^s/\alpha^{\beta}$ and finally arrive at the expressions for the wavefunction components

$$\varphi_k^{\gamma}(z) = e^{ikz}u_k^{\gamma}\exp\left[-i\frac{\alpha}{\hbar c}\int_{-\infty}^{z} \mathrm{d}y\, V^{\text{eff}}(y)\right]\left(1 + V^{\text{eff}}(z)\bar{\chi}^{\gamma}\frac{\alpha}{\alpha^{\gamma}}\right). \tag{2.54}$$

From this solution, we see that for distances much larger than the range of the interaction the outgoing state is proportional to the incoming one. Thus, due to the interaction, all components pick up a common exponent. Next, we comment on the form of each component separately. For van der Waals interaction $V(r) = C_6/r^6$, all of them are shown in figure 2.4.

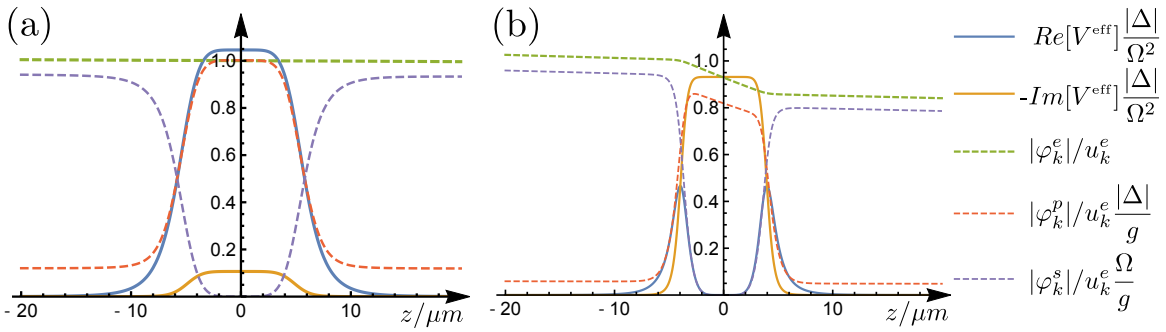

Fig. 2.4: Wavefunction components and effective interaction in function of distance. (a) The dispersive regime with $\Delta = (10 - i)\gamma$, (b) The dissipative regime with $\Delta = -i\gamma$. All other parameters are the same for both regimes: $\omega = 0.05‰^2/|\Delta|$, $g = 1500\gamma$, $‰ = 1.4\gamma$, $C_6 = 3.3 \times 10^4\gamma\ \mu m^6$.

First, for the photonic component the saturation vanishes, i.e. $\bar{\chi}^e = 0$, which leads to

$$\varphi_k^e(z) = e^{ikz}u_k^e \exp\left[-i\frac{\alpha}{\hbar c}\int_{-\infty}^{z} \mathrm{d}y\, V_e(y)\right]. \tag{2.55}$$

We see that even close to the impurity the photonic component only picks up a phase factor as a result of the interaction with the impurity. Note, that due to the finite γ this phase factor is complex what leads to the decay of φ_k^e.

Secondly, for the Rydberg component expressed using u_k^e we arrive at

$$\varphi_k^s(z) = -e^{ikz}\frac{g}{\Omega}\frac{1}{1 + \frac{\omega\Delta}{\Omega^2} - \frac{\omega^2}{\Omega^2}} \exp\left[-i\frac{\alpha}{\hbar c}\int_{-\infty}^{z} \mathrm{d}y\, V_e(y)\right]\frac{1}{1 - \bar{\chi}^s V(z)}u_k^e, \tag{2.56}$$

from which we see that the Rydberg component is suppressed at distances shorter than the so-called Rydberg blockade ξ defined via $|V(\xi)\bar{\chi}| = 1$. The reason is the following: At short distances, due to the interaction, the Rydberg-level is shifted out of resonance and can not be excited [63].

Finally, the p-state component has the form

$$\varphi_k^p(z) \;=\; -e^{ikz}\frac{g}{\Omega}\frac{1}{1+\frac{\Delta\omega}{\Omega^2}-\frac{\omega^2}{\Omega^2}}\frac{1}{\Omega}\frac{V-\omega}{1-\bar{\chi}V}\exp\left[-i\alpha\int\limits_{-\infty}^{z}\mathrm{d}y\,V_e(y)\right]u_k^e. \quad (2.57)$$

This component vanishes for distances much greater than the blockade length, i.e., $x \gg \xi$, as long as $\omega \ll \Omega^2/|\Delta|$. The last condition corresponds to the EIT transparency condition. Once this condition is broken, the polariton has a significant admixture of the p-state, which causes the decay of the polariton inside the medium. Moreover, for short distances $z < \xi$ with $\omega \ll \Omega^2/|\Delta|$, the p-state component saturates at $|\varphi_k^p| \sim \frac{g}{|\Delta|}u_k^e$. Hence, in the dissipative regime with small detuning $\delta < \gamma$ the p-component is larger than in dispersive regime with $\delta \gg \gamma$. It corresponds to smaller losses in the dispersive regime, as shown in figure 2.4.

3

Scattering resonances and bound states for strongly interacting Rydberg polaritons

In this chapter, we provide a rigorous framework for describing a low-density gas of slow-light polaritons propagating in one dimension under the conditions of electromagnetically induced transparency and interacting via strong Rydberg-Rydberg interactions. For this purpose, we formulate the problem in the condensed matter language using a well-established Feynman-diagrams approach. Specifically, we use a diagrammatic method to analytically derive the scattering properties of two polaritons. We discover previously unexplored parameter regimes where polariton-polariton interactions are *repulsive*. Furthermore, in the regime of *attractive* interactions, we identify multiple two-polariton bound states and calculate their dispersion relation. We analytically derive the low energy scattering length and find the appearance of resonances; we expect the corresponding tunability of the scattering length to play the role that Feshbach resonances play in ultra-cold atomic gases [213]. Moreover, we present the exact solution of the two-body problem in a weakly interacting regime. This result facilitates better understanding of losses from the dark state polaritons to the bright polaritons [8]. Finally, the two-particle scattering properties allow us to derive the exact low-energy many-body Hamiltonian.

This theoretical platform is also a foundation for a better understanding of other Rydberg-polariton phenomena presented in this thesis, especially, the dipolar dephasing of $D-$state polaritons and the quantum theory of Kerr-

nonlinearity for Rydberg-polaritons presented in chapters 7 and 5, respectively.

3.1 Introduction

First, we would like to shortly put our research into a broader perspective. The goal of this project was to study the Rydberg-EIT system, in which photons entering the atomic gas are converted into a slow-light polariton with a substantial admixture of the Rydberg state. It is this latter admixture which maps the Rydberg-Rydberg interaction onto an effective interaction between slow light polaritons. The propagation and interaction effects can be experimentally probed by looking at the correlations between outgoing photons. Within such a setup, two impressive two-body effects have been demonstrated by the collaboration of MIT and Harvard physicists, i.e., the antibunching of single-photons [25] and the formation of bound states of Rydberg polaritons [28]. These experiments were an additional motivation to study the two-body problem more carefully.

3.1.1 Setup

The atomic scheme and theoretical description of non-interacting polaritons were extensively described in chapters 1 and 2. Here, in order to make the description more consistent, we shortly repeat the notation used to describe Rydberg polaritons.

We start with the microscopic Hamiltonian for a one-dimensional setup with the light field described by a single transverse mode, for details see section 2.1. Then the electric field is described by the operator $\psi_e^\dagger(z)$ which creates a photon at position z in the transverse mode. The matter is well described by the bosonic field operators $\psi_p^\dagger(z)$ which depicts an atomic excitation into the p-state at position z, while $\psi_s^\dagger(z)$ accounts for the creation of a Rydberg excitation. We then obtain the non-interacting part of the microscopic Hamiltonian within the rotating

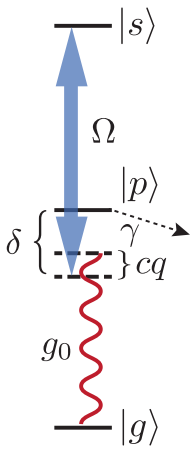

Fig. 3.1: Scheme

frame, for details see Eq. (4.2),

$$H_0 = \hbar \int dz \begin{pmatrix} \psi_e \\ \psi_p \\ \psi_s \end{pmatrix}^\dagger \begin{pmatrix} -ic\partial_z & g & 0 \\ g & \Delta & \Omega \\ 0 & \Omega & 0 \end{pmatrix} \begin{pmatrix} \psi_e \\ \psi_p \\ \psi_s \end{pmatrix}. \tag{3.1}$$

with 2Ω the Rabi frequency of the coupling laser and $g = \sqrt{\bar{n}} g_0$ the collective coupling, where $\bar{n}$ accounts for the effective atomic density for the coupling and depends on the transverse shape of the photonic mode. The atomic scheme is shown in figure 3.1 (as well as in figure 2.1). Note that the kinetic energy of the photons $-i\hbar c\partial_z$ only accounts for the difference to the EIT condition, and in the momentum space takes the form $\hbar cq$. Furthermore, the detuning $\Delta = \delta - i\gamma$ includes the decay rate γ from the p-level. The interaction between the Rydberg levels is described by

$$H_{\text{rr}} = \frac{1}{2} \int \mathrm{d}z \int \mathrm{d}z' \, V(z - z') \psi_s^\dagger(z) \psi_s^\dagger(z') \psi_s(z') \psi_s(z). \tag{3.2}$$

In the following, we focus on a van der Waals interaction $V(r) = C_6/r^6$. The microscopic Hamiltonian $H_0 + H_{\text{rr}}$ describes three bosonic fields with a non-interacting quadratic part and a quartic interaction. Such systems have been extensively studied in the past using diagrammatic methods, *cf.* Ref. [211]. However, it is relevant to emphasize that the quadratic Hamiltonian has an unconventional form, as the dynamics is only due to the light velocity of the photon. This is crucial to the following analysis using diagrammatic methods and gives rise to novel phenomena. This property can already be seen from the spectrum of the non-interacting Hamiltonian, already discussed in section 2.4.1 and Fig 2.2.

3.2 Two-body problem

Pseudo-potential: We start with analyzing the scattering properties and bound-state structure for two dark-state polaritons. Subsequently, this will help us to understand the many-body properties of the system. The main idea is to derive the scattering length a_{1D}, which in turn allows for the description of the many-body theory in terms of a pseudo-potential. In one dimension, the pseudo-potential takes the form

$$V_{\text{1D}}(r) = -\frac{2\hbar^2}{m\, a_{\text{1D}}} \delta(r), \tag{3.3}$$

where m plays the role of the polariton mass. This approach is in analogy to cold atomic gases, where it is extremely successful [213].

The description of two polaritons requires, in the most general case, a nine-component, two-particle wavefunctions $\psi_{\mu\nu}(z, z')$ with $\mu, \nu \in \{e, p, s\}$, which denotes the amplitude of finding particles in states μ and ν at z and z', respectively [38]. To utilize the conservation of energy and momentum, we rewrite $\psi_{\mu\nu}$ in the center-of-mass $R = (z + z')/2$ and relative $r = z - z'$ coordinates and parametrize it in terms of temporal and spatial Fourier components (ω, K), leaving r the only degree of freedom.

3.2.1 Diagrammatic approach

We start by pointing out, first, that the Hamiltonian conserves the total energy $\hbar\omega$ and momentum $\hbar K$. Second, the two-polariton scattering properties are well accounted for by the T-matrix. As the interaction acts only between the

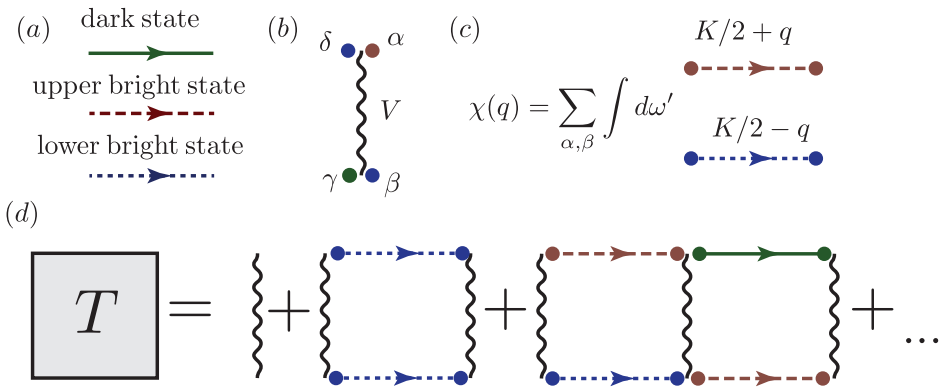

Fig. 3.2: Diagrammatic representation: (a) The diagonalization of H_0 gives rise to three propagator accounting for the different polaritons. (b) The interaction between the polaritons is given by the microscopic interaction between the Rydberg levels (wavy line) and the overlap U_s^α with each polariton (dots). (c) The full two-particle propagator for the Rydberg state χ is the summation of all individual pair propagation of two polaritons. (d) Illustration of ladder diagrams up to third order: the interaction $V(r)$ is denoted by a wavy line, while the straight lines with an arrow are Green's functions for the three polariton modes $1/(\hbar\omega - \epsilon_\mu + i\eta)$, and the dots mark the overlap factors U_μ^s and $\bar{U}_s^\mu$ of the polariton with the Rydberg state. The T-matrix includes all diagrams to arbitrary order with all possible intermediate polaritons.

two Rydberg states, it is sufficient to study the T-matrix for the Rydberg states alone, denoted as $T_{kk'}(K, \omega)$. Here, k is the relative momentum of the incoming

two polaritons and k' the relative momentum of the outgoing polaritons. The relation between the T-matrix and the scattering wave function is provided by the relation

$$\psi_{ss}(r) = \frac{1}{V(r)} \int \frac{\mathrm{d}k'}{2\pi} e^{ik'r} T_{kk'} \tag{3.4}$$

where $\psi_{ss}(r)$ denotes the amplitude to find both Rydberg polaritons in the Rydberg state at relative separation r. For two-polaritons, the T-matrix can be determined as a resummation of all ladder diagrams, which gives rise to the integral equation [211]

$$T_{kk'}(K,\omega) = V_{k-k'} + \int \frac{\mathrm{d}q}{2\pi} V_{k-q}\, \chi_q(K,\omega) T_{qk'}(K,\omega), \tag{3.5}$$

Here, the full pair propagation of two polaritons and its overlap with the Rydberg state is denoted by

$$\chi_q(K,\omega) = \sum_{\alpha,\beta\in\{0,\pm1\}} \frac{\bar{U}_s^\alpha(p) U_\alpha^s(p) \bar{U}_s^\beta(p') U_\beta^s(p')}{\hbar\omega - \epsilon_\alpha(p) - \epsilon_\beta(p') + i\eta}, \tag{3.6}$$

with $q = p - p'$ and $K = (p+p')/2$, where diagonalizing matrix U was introduced and discussed in section 2.4.1. Note that in the following, we will drop the explicit dependence on K and ω as the latter are conserved. It is a special property of our polariton Hamiltonian, that the pair propagation reduces to three terms,

$$\chi_q = \bar{\chi} + \frac{\alpha}{\hbar\bar{\omega} - \hbar^2 q^2/m + i\eta} + \frac{\alpha_{\mathrm{B}}}{\hbar\bar{\omega}_{\mathrm{B}} - \hbar^2 q^2/m + i\eta}. \tag{3.7}$$

Here, $\bar{\chi}(\omega)$ accounts for the saturation of the pair propagation at large momenta $q \to \pm\infty$ and takes the form

$$\bar{\chi}(\omega) = \frac{1}{\hbar} \frac{\Delta - \frac{\omega}{2} - \frac{\Omega^2}{\Delta-\omega}}{\omega\left(\Delta - \frac{\omega}{2}\right) + 2\Omega^2}. \tag{3.8}$$

The second term in Eq. (4.5) is the pole structure for the propagation of the two incoming polaritons. This term reduces to the propagator of a single massive particle, where α and $\bar{\omega}$ depend on the center-of-mass momentum K and total energy ω. The latter defines the relative momentum $k = \pm\sqrt{\bar{\omega}}$ of the incoming scattering states.

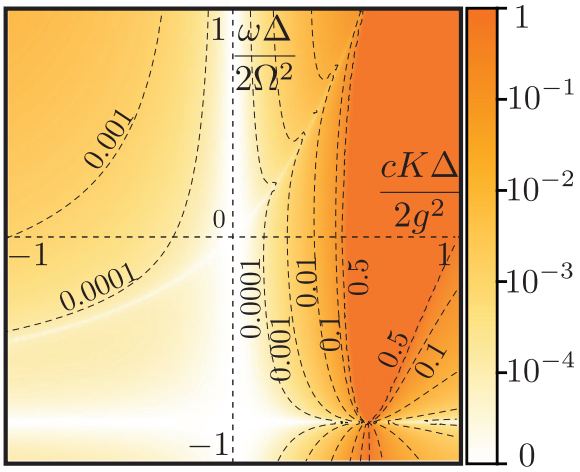

Fig. 3.3: Parameter $\zeta(K,\omega)$ measuring the influence of the second pole for $\Omega \ll g$ and $\Omega/\Delta = 0.5$. In the low energy and in the low momentum limit, the second pole can be safely neglected, however its influence strongly increases for $cK\Delta/2g^2 \to 1$.

Losses to the bright channel: The last term in Eq. (4.5) accounts for a second pole, describing the phenomenon of resonant scattering of two incoming polaritons into a different outgoing channel, *e.g.*, the conversion of two dark polaritons into an upper and a lower bright polariton, and therefore denoted by '$_{\mathrm{B}}$', for illustration see figure 3.5. The influence of the second pole is measured by the dimensionless parameter $\zeta(K,\omega) = \sqrt{|(\bar{\omega}\alpha_{\mathrm{B}}^2)/(\bar{\omega}_{\mathrm{B}}\alpha^2)|}$. Especially, $\zeta(K,\omega)$ is strongly suppressed in the two regimes discussed below, *i.e.*, *the low momentum and low energy regime*, and *the far-detuned regime*. In these cases the second pole can be dropped in leading order in the small parameter $\zeta \ll 1$. An illustration demonstrating the strong suppression is shown Fig. 3.3, while the analytical expressions are provided in the subsection 3.2.4.

Effective potential: The saturation $\bar{\chi}$ can be eliminated by introducing the effective interaction potential

$$V_{\mathrm{eff}}(r) = \frac{V(r)}{1 - \bar{\chi}(\omega)V(r)}. \tag{3.9}$$

Then, the equation for the T-matrix reduces to

$$T_{kk'} = V^{\mathrm{eff}}_{k-k'} + \int \frac{\mathrm{d}q}{2\pi}\, V^{\mathrm{eff}}_{k-q}\, \frac{\alpha}{\hbar\bar{\omega} - \hbar^2 q^2/m}\, T_{qk'}. \tag{3.10}$$

Consequently the T-matrix describes a system of a single massive particle in the effective interaction potential V_{eff} with the relative coordinate as the degree

of freedom and is fully described by the Schrödinger equation

$$\hbar\bar{\omega}\psi(r) = \left[-\frac{\hbar^2}{m}\partial_r^2 + \alpha V^{\text{eff}}(r)\right]\psi(r). \tag{3.11}$$

with the effective potential given by Eq. (4.8) and polariton mass (discussed in detail in section 2.4.1)

$$m = \hbar\frac{(g^2+\Omega^2)^3}{2c^2g^2\Delta\Omega^2}. \tag{3.12}$$

Here, $\hbar\bar{\omega}(K,\omega)$ plays the role of energy, and the dimensionless parameter $\alpha(K,\omega)$ can be interpreted as the overlap of the polaritons with the Rydberg state.

The relation $\psi(r) = \psi_{ss}(r)[1-\bar{\chi}V(r)]$ follows from the relation between the T-matrix and the scattering wave function $\psi_{ss}(r)V(r) = \int \mathrm{d}k'\, e^{irk'}T_{kk'}/(2\pi) = \psi(r)V^{\text{eff}}(r)$. Note that this relation captures the blockade phenomenon: the amplitude $\psi_{ss}(r)$ to find two Rydberg states essentially vanishes at distances shorter than the blockade radius $\xi = (|C_6\bar{\chi}|)^{1/6}$. In addition, the wavefunction $\psi(r)$ is proportional to the electric field amplitude $\psi_{ee}(r)$. We would like to stress once again that equation (3.11) is valid in several experimentally relevant regimes, including the low-momentum and low-energy regime, and the far-detuned regime. The analytical expressions for $\alpha, \bar{\omega}$, and $\bar{\chi}$ are discussed below. In the following, we will analyze the behavior of the two-particle properties in these two important regimes. Note that, throughout our analysis, we assume $|\delta| \gg \gamma$, thus providing the results in the limit $\gamma = 0$. Then, the inclusion of a finite decay rate γ is obtained by an analytical continuation in $\Delta = \delta - i\gamma$.

3.2.2 Low momentum and low energy regime

We start with the *low momentum and low energy regime*, which allows us to analytically derive the low-energy scattering length $a_{1\text{D}}$, see figure 3.4. The characteristic energy scale is given by $\omega_c = \min\{|\Delta|, \Omega^2/|\Delta|\}$, and the corresponding characteristic momentum is $q_c = \omega_c/v_g$ with $v_g = \Omega^2/(\Omega^2+g^2)c$ the slow-light velocity. Expanding the two-particle propagator for $|\omega| < \omega_c$ and $|K| < q_c$, the parameters for the first pole take the form

$$\bar{\omega} = \omega - v_g K, \qquad \alpha = \frac{g^4}{(g^2+\Omega^2)^2}. \tag{3.13}$$

The strength of the second pole α_{B} is strongly suppressed and vanishes as $\alpha_{\text{B}} \sim (\omega - cK)^2$, see figure 3.3, and is thus negligible in the low energy/momentum

limit. Furthermore, $\bar{\chi}$ reduces to

$$\hbar\,\bar{\chi} = \frac{\Delta}{2\Omega^2} - \frac{1}{2\Delta}. \tag{3.14}$$

Scattering length and interaction tunability: Most importantly, we identify that $\bar{\chi}$ exhibits a zero crossing for $\Omega = |\Delta|$ and consequently changes sign.

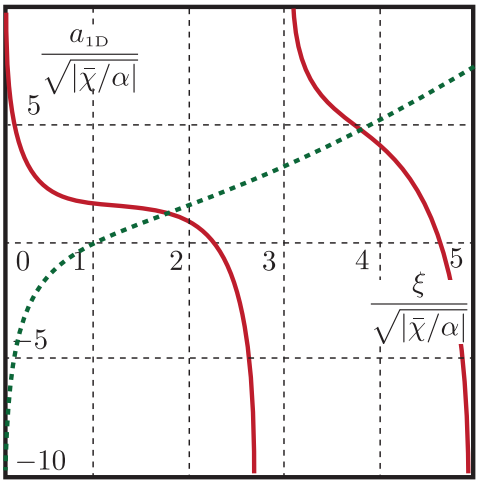

Fig. 3.4: Low-energy scattering length a_{1D}: for attractive interactions (solid line), we obtain scattering resonances associated with the appearance of additional bound states. For repulsive interactions (dashed line), we find a single zero crossing.

Therefore, it is possible to realize *repulsive* polariton-polariton interactions for $\Omega > |\Delta|$ with $C_6\delta > 0$ (the latter condition is required in order to avoid a singular behavior of V_{eff}). In this regime, we obtain a transition from a negative to a positive 1D scattering-length a_{1D} for increasing interactions, see figure 3.4. Using the blockade radius $\xi = (-C_6\bar{\chi})^{1/6}$, we obtain the asymptotic behavior $a_{1D} = (3/\pi)\bar{\chi}/\alpha\xi$, valid for weak interactions with $|\xi| < \sqrt{|\bar{\chi}/\alpha|}$, where the interaction potential can be replaced by a δ-function. Note that for $\gamma = 0$, the scattering length is negative, while for a finite decay rate, we obtain an imaginary contribution to the scattering length accounting for the losses from the p-level during the collision. For increasing interactions $|\xi| > \sqrt{|\bar{\chi}/\alpha|}$, we eventually obtain a zero crossing of a_{1D}, and recover the positive scattering length $a_{1D} \approx 0.7\,(\alpha C_6)^{1/4}$, where the full tail of the van der Waals interaction dominates.

In the *attractive* regime $\Omega < |\Delta|$ with $C_6\delta < 0$, the system generally gives rise to bound states. For weak interaction $|\xi| < \sqrt{|\bar{\chi}/\alpha|}$, a single bound state

is present, and we recover the positive scattering length $a_{1D} = (3/\pi)\bar{\chi}/\alpha\xi$. For increasing interactions $|\xi| > \sqrt{|\bar{\chi}/\alpha|}$, additional bound states will appear. Each additional bound state is associated with a resonance in the scattering length in analogy to Feshbach resonances in cold atomic gases [213]. The exact determination of the scattering length a_{1D} requires the full treatment of the effective interaction potential $V_{\text{eff}}(r)$; the latter is easily achieved numerically, see Fig. 3.4. It clearly demonstrates, that we can tune the strength of the scattering length to arbitrary values by controlling the single parameter $\xi/\sqrt{|\bar{\chi}/\alpha|}$, which defines the strength of the interaction potential.

3.2.3 Far detuned regime

In general, the bound states will violate the condition of low energy and are thus more appropriately studied in the *far-detuned regime* with $\Omega \ll |\Delta|$, which is valid for all momenta K with the weak constraint on the energy $|\omega| \ll |\Delta|$. In this regime, the weight of the second pole is suppressed by a factor $|\Omega/\Delta|^6$ and can again be safely ignored. Then, we obtain $\hbar\,\bar{\chi}(\omega) = [\omega + 2\Omega^2/\Delta]^{-1}$, the blockade radius reduces to $\xi = (|C_6\Delta/2\Omega^2\hbar|)^{1/6}$, while the analytic but lengthy expressions for $\bar{\omega}$ and α are presented in the section 3.2.4. In the experimentally most interesting regime of slow light with $g \gg \Omega$ with $g \gtrsim |\Delta|$, we find

$$\alpha = \frac{1 - \frac{cK\Delta}{2g^2}}{\left(1 + \frac{\omega\Delta}{2\Omega^2}\right)^2}, \tag{3.15}$$

while the expression for the energy $\hbar\bar{\omega}$ is defined through

$$\frac{\bar{\omega}\Delta}{2\Omega^2} = \frac{\frac{\omega\Delta}{2\Omega^2}}{1 + \frac{\omega\Delta}{2\Omega^2}} - \frac{1 + 2\frac{\omega\Delta}{2\Omega^2}}{1 + \frac{\omega\Delta}{2\Omega^2}} \frac{cK\Delta}{2g^2} + \left(\frac{cK\Delta}{2g^2}\right)^2. \tag{3.16}$$

Finally, the relation to the electric field amplitude ψ_{ee} is again closely related to the wavefunction ψ via $(g^2 - cK\Delta/2)\psi_{ee} = (\Omega^2 + \omega\Delta/2)\psi$.

In contrast to a conventional massive particle, here the on-shell condition at $\omega = 0$ takes the form $K^2/4 - k^2 = Kg^2/2\Delta c$ with opposite sign between relative and center-of-mass momenta. This parameter regime has previously been analyzed using adiabatic elimination [28, 38]. It is important to stress that, in this limit, the diagrammatic result completely agrees with the approach utilizing adiabatic elimination, see section 3.3 for details. However, the diagrammatic approach provides the strength of the second pole and therefore

serves as a microscopic justification for the adiabatic elimination. Moreover, the diagrammatic approach also provides a natural extension to finite energies ω and thus to time-dependent phenomena.

3.2.4 Influence and strength of the second pole

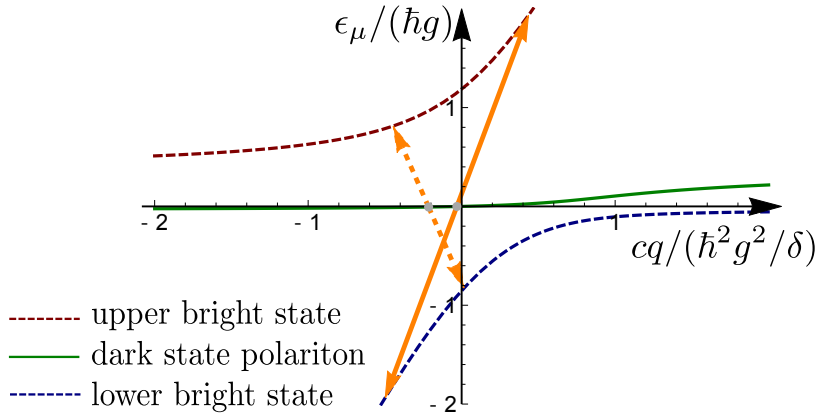

Fig. 3.5: Illustration of a resonant excitation of two bright polaritons from two dark polaritons for $g = 3\delta$, $\Omega = \delta/3$ and $\gamma = 0$. Two different cases of the total energy $\hbar\omega$ of the incoming dark-state polaritons are shown. In both situations the relative momentum is zero, $\hbar k = 0$. Orange solid arrow shows the case of $\omega = -0.06\Omega^2/\delta$, while orange dashed line the case of $\omega = -0.35\Omega^2/\delta$. Resonant excitation conserves center of mass momentum $\hbar K$, as well as the total energy, $\hbar\omega = 2\epsilon_0(K/2) = \epsilon_-(K/2 - k_\mathrm{B}/2) + \epsilon_+(K/2 + k_\mathrm{B}/2)$, where $\hbar k_\mathrm{B} = \pm\sqrt{\hbar\bar{\omega}_\mathrm{B} m}$.

In the following, we estimate the relevance of the second pole in Eq. (A.7), characterized by α_B and $\bar{\omega}_\mathrm{B}$, which gives rise to the resonant scattering into a different outgoing channel, see figure 3.5. First, we concentrate on the low momentum and energy regime. The analytical expressions for α and $\bar{\omega}$ describing the first pole are given in Eq. (3.13). In turn, the parameters for the second pole derived by the diagrammatic method take the form

$$\alpha_\mathrm{B} = -\frac{(\omega - cK)^2\Omega^6}{4\Delta^2(g^2+\Omega^2)^3}, \tag{3.17}$$

$$\bar{\omega}_\mathrm{B} = \frac{4\Omega^2 g^4}{(g^2+\Omega^2)^3}\frac{\Delta^2}{\omega - cK}. \tag{3.18}$$

Note that the weight α_B of the pole vanishes quadratically, when $\hbar|\omega|, \hbar|K|v_g \ll \hbar\min\{|\Delta|, 2\Omega^2/|\Delta|\}$, where $v_g = \Omega^2/(\Omega^2+g^2)c$ the slow light velocity, and can therefore be safely dropped.

Next, we analyze the influence of the second pole in the regime of far-detuned Rydberg polaritons with $|\omega|, \Omega \ll |\Delta|, g$. The diagrammatic approach provides the analytic expressions

$$\begin{aligned} \alpha_{\mathrm{B}} &= -\frac{\Omega^6(1+\frac{cK}{2\Delta})(\omega-cK)^2}{4\Delta^2(g^2+\Omega^2)^3\left(1-\frac{cK\Delta}{2g^2}\right)^2}, \\ \bar{\omega}_{\mathrm{B}} &= -\left(1+\frac{cK}{2\Delta}\right)^2\left(1-\frac{cK\Delta}{2g^2}\right)\frac{4\Omega^2 g^4}{(g^2+\Omega^2)^3}\frac{\Delta^2}{cK-\omega}. \end{aligned} \tag{3.19}$$

We find that, in the regime $cK\delta/2g^2 < 1$, the dimensionless parameters $\zeta(K,\omega)$ is strongly suppressed by the factor $(\Omega/\Delta)^6$. However, it is important to stress that the strength of the second pole diverges in a narrow parameter regime around $cK\delta/2g^2 \approx 1$.

3.2.5 Exact solution for weak interactions

In the section 3.2.1, we claimed that the influence of the second pole can be measured by the dimensionless parameter $\zeta(K,\omega) = \sqrt{|(\bar{\omega}\alpha_{\mathrm{B}}^2)/(\bar{\omega}_{\mathrm{B}}\alpha^2)|}$. We also have shown that $\zeta(K,\omega)$ is strongly suppressed in several relevant regimes. In this subsection, we will show how the parameter $\zeta(K,\omega)$ relates to the solution of two-body problem in the weakly interacting regime.

The interaction strength can be conveniently quantified by the dimensionless parameter $\xi/\bar{\lambda}$, where $\bar{\lambda} = \sqrt{|\hbar^2\bar{\chi}/(\alpha m)|}$ is the de Broglie wavelength associated with the depth (or height) $|\alpha/\bar{\chi}|$ of the effective potential. Here, we present exact solution of the two-body problem for weak interactions, i.e., for $\xi/\bar{\lambda} \ll 1$, in which case the interaction potential can be replaced by a δ-function. We start by rewriting the equation for the T-matrix, see Eq. (3.5), using the effective potential $V^{\mathrm{eff}}(r) = V(r)/(1-\bar{\chi}(\omega)V(r))$ and explicitly including the pole structure,

$$T_{kk'}(K,\omega) = V^{\mathrm{eff}}_{k-k'} + \int\frac{\mathrm{d}q}{2\pi}\,T_{kq}(K,\omega)\left(\frac{\alpha}{\hbar\bar{\omega}-\frac{\hbar^2q^2}{m}+i\eta}+\frac{\alpha_{\mathrm{B}}}{\hbar\bar{\omega}_{\mathrm{B}}-\frac{\hbar^2q^2}{m}+i\eta}\right)V^{\mathrm{eff}}_{q-k'},$$

This equation is equivalent to the Lippmann-Schwinger equation for φ, defined by $\varphi(r)V^{\mathrm{eff}}(r) = \int\mathrm{d}k'\,e^{irk'}T_{kk'}/(2\pi)$,

$$\varphi(r) = \varphi_0(r) + \int\mathrm{d}y\,\mathcal{G}(r-y)\;\alpha\,V^{\mathrm{eff}}(y)\,\varphi(y). \tag{3.20}$$

As already mentioned, the wavefunction component φ_{ss} describing two Rydberg excitations can be expressed using T-matrix, *i.e.*, $\varphi_{ss}(r)V(r) = \int\mathrm{d}k'\,e^{irk'}T_{kk'}/(2\pi)$.

Moreover, the incoming wave $\varphi_0(r) = e^{ikr}$, and the propagator $\mathcal{G}$ in real space has the form

$$\mathcal{G}(r) = -\frac{i}{2}\frac{m}{\hbar^2}\left(\frac{e^{ik|r|}}{k} + \frac{\alpha_{\mathrm{B}}}{\alpha}\frac{e^{ik_{\mathrm{B}}|r|}}{k_{\mathrm{B}}}\right), \tag{3.21}$$

with $k = \sqrt{\bar{\omega}m/\hbar}$ and $k_{\mathrm{B}} = \sqrt{\bar{\omega}_{\mathrm{B}}m/\hbar}$. Then, the solution of (3.20) can be found via the re-summation of all orders in Born expansion

$$\begin{aligned}\varphi(r) &= \varphi_0(r) + \int \mathrm{d}y\, \mathcal{G}(r-y)\, \alpha\, V^{\mathrm{eff}}(y)\, \varphi_0(y) \\ &+ \int \mathrm{d}y \int \mathrm{d}y'\, \mathcal{G}(r-y)\, \alpha\, V^{\mathrm{eff}}(y)\, \mathcal{G}(y-y')\, \alpha\, V^{\mathrm{eff}}(y')\, \varphi_0(y') + ...\end{aligned} \tag{3.22}$$

In the case of weak interactions $\xi \ll \bar{\lambda}$, we can replace the effective interaction by the potential $v\delta(r)$, where $v = \int \mathrm{d}r\, \alpha V^{\mathrm{eff}}(r)$. It enables us to simplify the expression for φ to

$$\begin{aligned}\varphi(r) &= \varphi_0(r) + \mathcal{G}(r)v\left(1 + \mathcal{G}(0)v + (\mathcal{G}(0)v)^2 + ...\right) \\ &= \varphi_0(r) + v\, \mathcal{G}(r)\frac{1}{1 - v\, \mathcal{G}(0)} \\ &= e^{ikr} - \frac{1}{1 + \frac{k}{k_B}\frac{\alpha_B}{\alpha} - 2i\frac{\hbar^2 k}{mv}}\left(e^{ik|r|} + \frac{\alpha_B}{\alpha}\frac{k}{k_{\mathrm{B}}}e^{ik_{\mathrm{B}}|r|}\right).\end{aligned} \tag{3.23}$$

We see that the dimensionless parameter $\zeta(K,\omega) = |(k\alpha_{\mathrm{B}})/(k_{\mathrm{B}}\alpha)|$ controls the influence of the second pole. Since the term proportional to $e^{ik_{\mathrm{B}}|r|}$ accounts for the resonant excitation of an upper and lower bright polariton, this process is strongly suppressed for small parameter $\zeta(K,\omega) \ll 1$.

3.3 Comparison with adiabatic elimination

In the following, we compare our diagrammatic approach with the previously successfully-applied study of the two-particle equation for the wave function in the regime $\omega = 0$, where the p-level has sometimes been adiabatically eliminated [25, 28, 38]. Furthermore, we will present the natural extension of adiabatic elimination for finite frequencies. The two-particle wave function contains four components: ψ_{ee} describes the amplitude for two photons, ψ_{ss} the amplitude for two Rydberg atoms, and $\psi_{es\pm}$ the amplitude for one photon and one Rydberg atom with even (odd) symmetry. The Schrödinger equation reduces to (see

Refs. [25, 28, 38] for more details)

$$\omega\psi_{ee} = -ic\partial_R\psi_{ee} - \frac{2g^2}{\Delta}\psi_{ee} - \frac{2g\Omega}{\Delta}\psi_{es+}, \tag{3.24}$$

$$\omega\psi_{es+} = -\frac{ic}{2}\partial_R\psi_{es+} - ic\partial_r\psi_{es-} - \frac{g^2+\Omega^2}{\Delta}\psi_{es+} - \frac{g\Omega}{\Delta}\left(\psi_{ee}+\psi_{ss}\right), \tag{3.25}$$

$$\omega\psi_{es-} = -\frac{ic}{2}\partial_R\psi_{es-} - ic\partial_r\psi_{es+} - \frac{g^2+\Omega^2}{\Delta}\psi_{es-}, \tag{3.26}$$

$$\omega\psi_{ss} = -\frac{2\Omega^2}{\Delta}\psi_{ss} - \frac{2g\Omega}{\Delta}\psi_{es+} + \frac{V(r)}{\hbar}\psi_{ss}, \tag{3.27}$$

where r denotes the relative coordinate and R the center-of-mass coordinate. For the translational invariant system, the latter coordinate is expressed in Fourier space with the total momentum K. We can solve the first, third and fourth equations for ψ_{ee}, ψ_{es-}, and ψ_{ss}, respectively. Inserting these expressions into Eq. (3.25), we obtain a single differential equation involving only the wave function ψ_{es+},

$$\hbar\bar{\omega}\psi_{es+} = -\frac{\hbar^2}{m}\partial_r^2\psi_{es+} + \alpha V_{\text{eff}}(r)\psi_{es+}. \tag{3.28}$$

This equation takes exactly the form of Eq. (3.11) with the identification $\psi_{es+} \sim \psi$. The expressions for α and $\bar{\omega}$ within the adiabatic elimination reduce to

$$\begin{aligned}
\frac{\alpha m}{\hbar^2} &= \frac{g^2\Omega^2}{c^2\hbar\Delta^2}\frac{2(\omega+\frac{g^2+\Omega^2}{\Delta}) - cK}{\left(\omega+2\frac{\Omega^2}{\Delta}\right)^2}, \\
\bar{\chi} &= \frac{1}{\hbar}\frac{1}{\omega+2\Omega^2/\Delta}, \\
\frac{\bar{\omega}m}{\hbar} &= \left[cK - 2(\omega+\frac{\Omega^2+g^2}{\Delta})\right]^2 \frac{2\omega\frac{\Omega^2+g^2}{\Delta} + \omega(\omega-cK) - \frac{2\Omega^2}{\Delta}cK}{4c^2\left(\omega+\frac{2\Omega^2}{\Delta}\right)\left(\omega-cK+\frac{2g^2}{\Delta}\right)}.
\end{aligned} \tag{3.29}$$

These expressions fully agree with the result derived within the diagrammatic approach in the limit of large detuning $\Omega \ll |\Delta|$ and energies $|\omega| \ll |\Delta|$. In the physically interesting situation of Rydberg polaritons with $g \gtrsim |\Delta|$, we finally obtain the expressions (3.15) and (3.16).

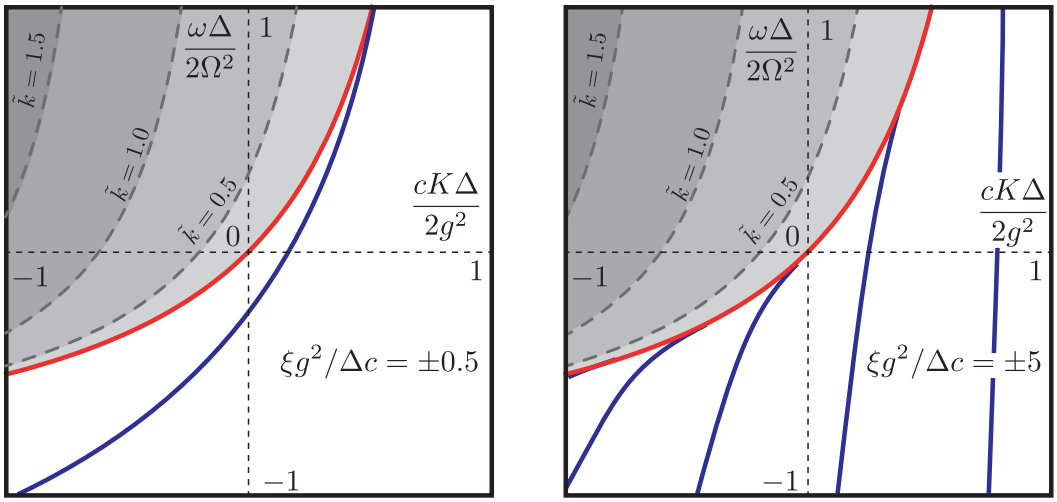

Fig. 3.6: Bound-state structure ($\gamma = 0$): For weak interactions $\xi g^2/\Delta c = \pm 0.5$, we obtain a single bound state below the continuum of scattering states, while for strong interactions $\xi g^2/\Delta c = \pm 5$, we observe the existence of several bound states giving rise to scattering resonances. The dashed lines mark the lines with fixed incoming relative momentum $\tilde{k} = k\Delta c/g^2 = 0.5, 1.0, 1.5$ for the scattering states.

3.4 Bound states

The effective equation Eq. (3.11) allows us to derive the bound states and their group velocity in addition to the scattering states. The spectrum of two Rydberg polaritons is shown in figure 3.6: it exhibits a continuum of scattering states as well as bound states. Note that the interaction potential as well as $\bar{\omega}$ depend on the energy ω, and therefore the bound-state energies have to be determined self-consistently. The condition of weak interaction reduces to $|\xi g^2/\Delta c| < 1$, and we recover a single bound state, which is well described by replacing the effective interaction potential by a δ-function. For increasing interaction strength $|\xi g^2/\Delta c| > 1$, we observe the appearance of additional bound states. Then, the exact bound state energy requires the numerical treatment of the full effective interaction potential Eq. (4.8). These bound states can be probed in two different ways: first, at fixed energy, one can determine the center of mass momentum of the bound state, as it has been demonstrated experimentally [28]. Alternatively at a fixed center of mass $K = 0$, we can probe the bound state by a two-color input field via probing the excitation frequency; the latter method is the standard method in condensed matter physics to probe the spectrum.

3.5 Low energy many-body Hamiltonian

The full understanding of the scattering properties allows us now to derive the *low energy many-body Hamiltonian for Rydberg polaritons*. Here, the fundamental assumption is that each scattering process of the polaritons is independent of each other. This condition is well satisfied in the dilute regime $n_d\, r_0 \ll 1$, where the density n_d of Rydberg polaritons is low compared to the range r_0 of the interaction potential. The latter is determined either by the blockade radius or the van der Waals length, *i.e.*, $r_0 = \max\{|\xi|, (|\alpha C_6|)^{1/4}\}$. Then, the interaction is fully determined by the scattering length a_{1D} via the pseudo-potential in Eq. (3.3), and the many-body theory reduces to the Hamiltonian

$$H = \int \mathrm{d}z \left[\psi_d^\dagger \left(-i\hbar v_g \partial_z - \frac{\hbar^2}{2m}\partial_z^2\right)\psi_d - \frac{2\hbar^2}{m a_{1D}}\psi_d^\dagger \psi_d^\dagger \psi_d \psi_d\right].$$

Here, $\psi_d^\dagger$ (ψ_d) denotes the bosonic field operator creating (annihilating) a Rydberg polariton. The kinetic energy in the low momentum limit is well described by the slow-light velocity v_g and the effective mass $m = \hbar(g^2 + \Omega^2)^3/(2c^2 g^2 \Delta\Omega^2)$. Note that the change in sign for the center-of-mass momentum term K^2 in Eq. (3.16) is a higher-order process and is irrelevant in the low-momentum limit. Here we can control the scattering length a_{1D} by the strength of the interactions, see Fig. 3.4. We can therefore study continuously the crossover from a Lieb-Liniger gas with $a_{1D} < 1$ to the Super-Tonks-Girardeaux gas $a_{1D} > 1$ by tuning the parameters through a zero crossing of the scattering length [214–216]. In contrast to cold atomic gases [217, 218], the zero crossing of the scattering length is not associated with losses in the system. Using the experimental parameters characteristic for Ref. [28] with $\Omega \approx 5$ MHz, $\delta \approx 18$ MHz and $g \approx 5$ GHz, we find that the range of the potential is determined by the Blockade radius with $\xi \approx 18$ μm, while the interaction strength reduces to $\xi g^2/c|\Delta| = 0.54$. Consequently, these experiments are in the regime close to the appearance of an additional bound state.

Complementary approaches: Finally, we point out that a complementary derivation of an effective low-energy theory can also be achieved at high densities, if the interaction is dominated by the purely repulsive part of the van der Waals interaction, as proposed in Ref. [36]. This behavior is obtained in the parameter regime with $1/(|\alpha C_6|)^{1/4} < n_{1D} < q_c, 1/|\xi|$; note that here we provide a microscopic derivation for the correct blockade radius χ.

We have demonstrated that this regime is most interesting to study at the point $\Delta = \pm\Omega$ and $C_6\Delta > 0$, where $\bar{\chi} = 0$ vanishes, and the effective interaction reduces to the pure van der Waals repulsion $V_{\text{eff}}(r) = C_6/r^6$ and allows one to observe the crossover into a regime where crystalline correlation dominate the ground state.

3.6 Outlook

The microscopic analysis presented here has several implications for experiments. First, the existence of a parameter regime with a purely repulsive interaction will give rise to photon anti-bunching for the two-photon correlations in an experimental setup similar to that of Ref. [28]. The experimental requirements are strong Rabi frequency $\Omega \gtrsim |\Delta|$, and $\gamma \ll |\delta|$ to distinguish the repulsion from losses. In turn, the analysis of the bound-state structure allows for the determination of the group velocity. As can be seen in figure 3.6, the group velocity of the bound states is larger than the slow light velocity, and the bound states will travel ahead of the continuum. This will allow one to spatially separate the bound photon pairs in a pulsed experiment. Finally, the scattering length defines the phase shift two polaritons pick up during a collision; it has been proposed to use such collisions to realize photonic two-qubit gates [32, 38]. Here, the predicted zero-crossing of the scattering length corresponds to the optimal π-phase shift. A direct measurement of these resonances is possible in a setup with frequency difference $\Delta\omega$ and spatially-resolved detection of the polaritons inside the medium. Therein, the correlation function in the relative coordinate will oscillate with a wavevector $\Delta k = \Delta\omega/v_g$. The maxima of these oscillations will shift for increasing scattering length by a phase ϕ via $\cot(\phi) = -a_{1\text{D}}\Delta k$. The details of these observations depend on the experimental setup and on the precise boundary conditions but can be efficiently addressed within the presented framework.

4

Two-photon conditional phase-gate based on Rydberg slow light polaritons

4.1 Introduction

Since photons only interact weakly with their environment, propagate with the speed of light and provide a high bandwidth, they are an excellent carrier of information. However, for applications in quantum information processing [219], interactions on the level of single quanta is necessary. Such interactions can be achieved by coupling photons to matter [53, 76, 220–222], with Rydberg-EIT (rEIT) being a specially promising approach [57, 74, 75, 223–226].

Once a strong effective interaction is available in the system, an important question can be posed: Can one use this interaction to engineer a two-photon conditional phase-gate? The principle behind the phase gate is that the source photon picks up a phase shift depending on the state of the control photon. Moreover, this phase shift should be spatially homogeneous, shouldn't change the shape of both source and gate photons, and for most applications in the quantum information processing should be on the order of π.

A photonic phase gate using Rydberg-EIT in a counter-propagating setup was first discussed by Friedler et al. [32] and an extended description was shown by Gorshkov et al. [38]. However, a study including all effects that decrease the fidelity of the phase gate is still missing; in this chapter, we attempt to fill this gap.

It is worth mentioning that for the co-propagating setup with the linear dispersion, the condition of a homogeneous phase shift requires a compression of photons to the size of the blockade radius. However, the latter violates the conditions for the mass negligence. In turn, adding the mass term leads to strong mode distortion precluding the realization of a photonic quantum gate in co-propagating setup. Thus, the homogeneous phase shift between two photons might be possible only if they pass each other either by for example being counter-propagating [32, 227–229] or having different group velocities [230].

Note that a number of new proposals [78, 79] were (at least partially) motivated by the believe that, from fundamental grounds, the link between propagation and interaction [44, 231] precludes high-fidelity gates whenever a cross-phase modulation (XPM) on a single photon level is used. We would like to point out that this argument does not apply to the Rydberg-EIT setup because the interaction between Rydberg polaritons is nonlocal, whereas no-go theorems [44, 231, 232] assume local interactions.

Moreover, we would like to comment on a new proposal [39], in which the authors use a semiclassical approach to describe the evolution of two polaritons in a Rydberg medium. There is no need to use the semiclassical approach since the equations of motion for two polaritons [8, 25, 38] do not assume a steady state. In other words, the quantum mechanical approach used by us fully describes both the propagation as well as the state evolution. Using this approach, we derive analytical and compact expressions for the fidelity and phase shifts. Finally, once this Hamiltonian is restricted to two photons, the decay rates can be exactly included by an imaginary contribution in the detuning. Such an inclusion is fully equivalent to solving the master equation. We consider this another fundamental advantage of the presented approach, which allows for a nearly analytical solution.

It deserves mentioning that first steps towards an experimental realization of the Rydberg-EIT phase gate were done by the group of G. Rempe, which demonstrated an optical π-phase shift created with a stored single-photon pulse [37]. An alternative promising route to engineer a phase gate is by using a Rydberg-state dependent reflection of the cavity, as shown by Das et al. [83].

4.1.1 General concept

Photons after entering the Rydberg medium are propagating as polaritons, see figure 4.1. After passing each other, they pick-up the phase shift due to the

strong interaction between Rydberg atoms. The information can be encoded in the polarization of probe photons. The excitation into the Rydberg levels can depend on this polarization [28], leading to the interaction induced phase shift only between photons having a specific polarization. We define the fidelity F and phase shift ϕ of the gate as the overlap between the two-photon wave-functions with ($\mathcal{EE}$) and without ($\mathcal{EE}^{V=0}$) the interaction $V(r)$ between the polaritons:

$$\sqrt{F}e^{i\phi} = \left\langle \mathcal{EE}^{V=0} \middle| \mathcal{EE} \right\rangle \Big/ \left\langle \mathcal{EE}^{V=0} \middle| \mathcal{EE}^{V=0} \right\rangle. \tag{4.1}$$

Such a definition, in which two output states are normalized, is often used [39, 232, 233] and is related to the concept of conditional fidelity and efficiency commonly applied in the context of quantum storage [78, 234]. This way, the effects of single photon losses are included in the efficiency Θ defined by $\Theta = \left\langle \mathcal{EE}^{V=0} \middle| \mathcal{EE}^{V=0} \right\rangle$.

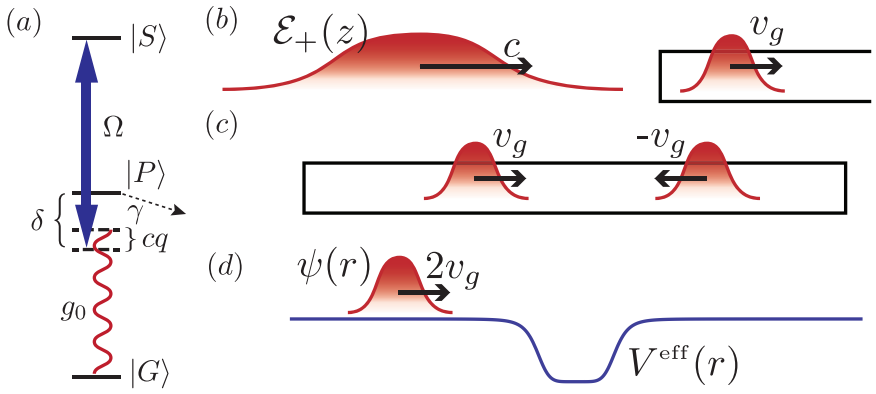

Fig. 4.1: (a) The probe field couples the atomic ground state $|G\rangle$ to the p-level $|P\rangle$ with the single-particle coupling strength g_0, while a strong coupling laser drives the transition between the p-level and the Rydberg state $|S\rangle$ with Rabi frequency 2Ω and detuning δ. Furthermore, 2γ denotes the decay rate from the p-level. The single-particle coupling g_0 is related to the collective coupling $g = \sqrt{n_{\mathrm{at}}}g_0$ with n_{at} the particle density. Note that the kinetic energy of the photons $\pm\hbar cq$ accounts for the difference to the EIT condition, and in the position space takes the form $\mp i\hbar c\partial_z$. (b) Photon entering the EIT medium is compressed by factor v_g/c. (c) Two counterpropagating polaritons inside the medium. (d) In the center of mass frame, a problem simplifies to the scattering on the effective potential $V^{\mathrm{eff}}(r)$, which leads to the imprint of the phase shift on the two-body wave-function $\psi(r)$.

4.2 Propagation inside the medium

We consider photons inside an atomic ensemble propagating in one dimension (the light field distribution is characterized by a single transverse mode) under the EIT conditions, where the atomic ground state is coupled to a Rydberg s-state via an intermediate short-lived p-state, see Fig. 4.1(a). We introduce the electric field operators $\hat{\mathcal{E}}_+^\dagger(z)$ and $\hat{\mathcal{E}}_-^\dagger(z)$ creating at position z photons propagating to the right and left, respectively. For the atomic density much higher than the photonic density, the excitations of atoms generated by left- and right- moving photons into s-level and p-level are well-described by the bosonic field operators $\hat{\mathcal{S}}_\pm^\dagger(z)$ and $\hat{\mathcal{P}}_\pm^\dagger(z)$, respectively. Then, we obtain the non-interacting part of the microscopic Hamiltonian [8, 38], i.e., $H_+ + H_-$, under the rotating-wave approximation in the rotating frame, where

$$H_\pm = \hbar \int dz \begin{pmatrix} \hat{\mathcal{E}}_\pm \\ \hat{\mathcal{P}}_\pm \\ \hat{\mathcal{S}}_\pm \end{pmatrix}^\dagger \begin{pmatrix} \mp ic\partial_z & g & 0 \\ g & \Delta & \Omega \\ 0 & \Omega & 0 \end{pmatrix} \begin{pmatrix} \hat{\mathcal{E}}_\pm \\ \hat{\mathcal{P}}_\pm \\ \hat{\mathcal{S}}_\pm \end{pmatrix}. \tag{4.2}$$

Here, g denotes the collective coupling of the photons to the matter via the excitation of ground state atoms into the p-level, while 2Ω denotes the Rabi frequency of the control field between the p-level and the Rydberg state. Note that the kinetic energy of the photons $\mp i\hbar\partial_z$ accounts for the deviation from the EIT condition. We introduced the complex detuning $\Delta = \delta - i\gamma$, which accounts for the detuning δ of the control field and the decay rate 2γ from the p-level. While we are interested in two counter-propagating polaritons the interaction between the Rydberg levels is described by

$$H_{\rm rr} = \frac{1}{2}\int \mathrm{d}z \int \mathrm{d}z'\, V(z-z')\hat{\mathcal{S}}_+^\dagger(z)\hat{\mathcal{S}}_-^\dagger(z')\hat{\mathcal{S}}_-(z')\hat{\mathcal{S}}_+(z).$$

We obtain the real time evolution by decomposing the incoming photons into the frequency components. It is then natural to analyze interaction of two counter-propagating photons as the scattering process. The two-polariton scattering properties are well accounted for by the T-matrix. As the interaction acts only between Rydberg states, it is sufficient to study T-matrix for the Rydberg states alone. The resummation of all ladder diagrams [8] leads to the integral equation

$$T_{kk'}(K,\omega) = V_{k-k'} + \int \frac{dq}{2\pi} V_{k-q}\, \chi_q(K,\omega) T_{qk'}(K,\omega), \tag{4.3}$$

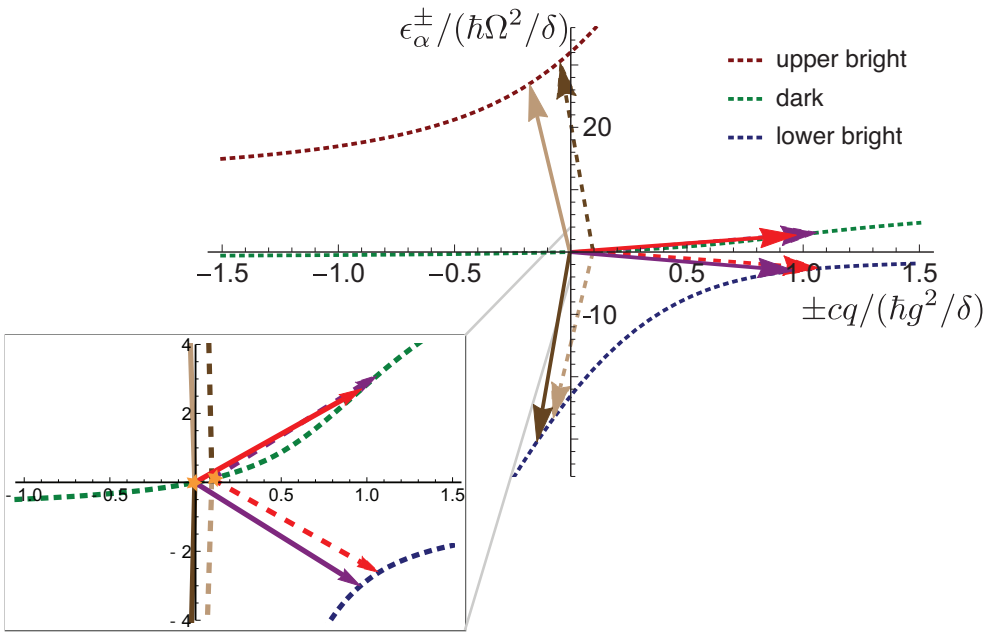

Fig. 4.2: Dispersion relations for the right- and left- propagating fields are shown using the property that $\epsilon_\alpha^-(-q) = \epsilon_\alpha^+(q)$, and therefore the curves overlap. For each direction of propagation, three noninteracting polariton branches exist. Two dark state polaritons (denoted by stars in the inset for low energy and momentum) can scatter into four channels, each represented by different colour of arrows. Solid lines correspond to right-propagating and dashed lines to left- propagating polaritons. Note, that the total momentum $\hbar K$ and energy $\hbar\omega$ are conserved during the scattering process. Strongly suppressed losses into two bright polaritons are described by light and dark brown arrows. Crucial losses into bright-dark polariton pair are depicted by red and purple arrows. Results are presented for $g = 3\,\delta, \delta = 3\,\Omega, \gamma = 0, \omega = 0.1 \times 2\Omega^2/|\Delta|, K = -0.1\,g^2/|\Delta|c$.

where $\hbar k$ is the relative momentum of the two incoming polaritons and $\hbar k'$ the relative momentum of the outgoing polaritons. The full pair propagator of two polaritons and its overlap with the Rydberg state takes the form

$$\chi_q\,(K,\omega) = \sum_{\alpha,\beta\in\{0,\pm1\}} \frac{\bar{U}_s^\alpha(p)U_\alpha^s(p)\bar{U}_s^\beta(p')U_\beta^s(p')}{\hbar\omega - \epsilon_\alpha^+(p) - \epsilon_\beta^-(p') + i\eta}, \tag{4.4}$$

with $p = K/2 + q$ and $p' = K/2 - q$. It is a special property of our polaritonic Hamiltonian that the pair propagation reduces to six terms [8],

$$\chi_q(K,\omega) = \bar{\chi}(\omega) + \frac{\alpha_D}{\hbar\bar{k}_D - \hbar q + i\eta} + \sum_{i=2}^{5} \frac{\alpha_i}{\hbar\bar{k}_i - \hbar q + i\eta}. \tag{4.5}$$

Here, $\bar{\chi}(\omega)$ accounts for the saturation of the pair propagation at large momenta

$\hbar q \to \pm\infty$. The second term in Eq. (4.5) is the pole structure for the propagation of the two incoming dark-state polaritons. The last sum accounts for the resonant scattering of the two incoming polaritons into four outgoing channels containing at least one bright polariton, see figure 4.2. Note that in contrast to the copropagating equation, where the massive-like behavior of the dark-dark polariton pair can be neglected only in certain regimes (see chapter 5), here, the kinetic part is always linear in relative momentum. Thus, the large phase shift is possible without a drop of the fidelity caused by the distortion of the wave-packet shape.

4.2.1 Scattering matrix description

The scattering into four bright channels can be neglected in the experimentally relevant regime of slow light $g \gg \Omega$, with large single photon detuning $\Delta \gg \Omega$, with small center of mass momentum $K \ll g^2/|\Delta|c$, and with a weak constraint on the total energy $|\omega| \leq 2\Omega^2|/\Delta|$; we will discuss the derivation of these constraints below. In this regime, the initial problem simplifies tremendously: the only nonvanishing T-matrix element is the one between two dark-state polaritons and has the form $T_{kk} = i\hbar c(e^{i\varphi} - 1)$. This corresponds to the elements of scattering $S-$matrix for two incoming dark-polaritons (depicted by "$_{DD}$"):

$$S_{DD;IJ}(k - k') = 2\pi\ \delta_{D,I}\delta_{D,J}\delta(k - k')\exp[i\varphi], \tag{4.6}$$

with $I, J \in \{D, U, L\}$, where indices U and L denote "U"pper and "L"ower bright polariton. Therefore, due to the interaction, dark polaritons only pick-up the exponent φ, which imaginary part describes losses in the system.

4.3 The phase shift

The exponent φ can be conveniently calculated by Fourier transforming equation (4.3) and introducing ψ defined by $\psi(r)V^{\text{eff}}(r) = \int \mathrm{d}k'\, e^{irk'}T_{kk'}/(2\pi)$, which leads to the effective Schrödinger equation [8],

$$\frac{\hbar\omega}{1 + \frac{\omega\Delta}{2\Omega^2}}\psi(r) = \left(-i2\hbar c\frac{\Omega^2}{g^2}\,\partial_r + \frac{1}{(1 + \frac{\omega\Delta}{2\Omega^2})^2}V^{\text{eff}}(r)\right)\psi(r), \tag{4.7}$$

where we defined an effective potential

$$V^{\text{eff}}(r) = \frac{V(r)}{1 - \bar{\chi}(\omega)V(r)} \tag{4.8}$$

with $\hbar\bar{\chi}(\omega) = (\omega + 2\Omega^2/\Delta)^{-1}$. The blockade radius has the form $\xi = (|C_6\bar{\chi}|)^{1/6}$; note that $\bar{\chi}$ has the same form as in the copropagating setup, see Eq. (3.8). Equation (4.7) can be interpreted as an evolution of a massless particle in the effective potential, see figure 4.1(d). This interpretation will be useful later for the estimation of transverse size effects. The analytical solution of Eq. (4.7) for $r \gg \xi$ has the form $\psi(r) = \exp[ik_{\text{D}}r + i\varphi]$ where

$$\varphi = \frac{2\pi g^2 \xi(-\text{sgn}[C_6]\Delta)^{1/6}}{3c|\Delta|^{1/6}\Delta\left(\frac{\Delta\omega}{2\Omega^2}+1\right)^{7/6}}, \quad k_{\text{D}} = \frac{g^2}{2\Omega^2 c}\frac{\omega}{1+\frac{\omega\Delta}{2\Omega^2}}. \tag{4.9}$$

In the limit of two photon resonance, *i.e.*, $\omega = 0$, the solution agrees with Ref. [38]. For $\gamma \ll |\delta|$ the exponent φ simplifies to $\phi + i\eta = 2\pi g^2\xi(1 + i\frac{5}{6}\frac{\gamma}{\delta})/(3\delta c)$, where η describes dissipation, whereas ϕ denotes the phase shift and can be expressed using optical depth κ_ξ per blockade radius: $\phi = (\pi/3)\kappa_\xi\gamma/\delta$.

4.4 Estimate of the scattering to other channels

Next, we discuss the (presented in section 4.2.1) conditions on the negligence of the scattering dark polaritons into bright polaritons. In general, the corrections $\delta\psi_i$ due to the scattering to other channels can be estimated using the exponent φ and pole strengths α_i, see Appendix B,

$$\left|\frac{\delta\psi_i}{\psi}\right| \lesssim \left|\frac{\alpha_B\left(e^{i\varphi}\varphi - \sin(\varphi)\right)}{2\alpha_D}\right| \tag{4.10}$$

which for $\phi \ll \pi$ scales like $\sim \left|\alpha_B\varphi^2/2\alpha_D\right|$, whereas for $\phi \gtrsim \pi$ like $\sim |\alpha_B\varphi/2\alpha_D|$. Interestingly, the sign of the detuning matters, and in order to minimize scattering to bright polaritons $\delta < 0$ is preferable. In order to simplify the presentation of the rest of results, we define $f(\varphi) = \left|e^{i\varphi}\varphi - \sin(\varphi)\right|/2$. Based on this estimate, scattering corrections can be neglected when the ratio of poles strength $\zeta_i = \alpha_i/\alpha_D$ is small, $\zeta_i \ll 1$. First, let us consider two poles α_{LU}, α_{UL} corresponding to outgoing "U"pper and "L"ower bright polariton pair. The parameters ζ_{LU}, ζ_{UL} scale like $\Omega^6/(g^2 + \Delta^2)^3/2$ and therefore this loss channel is strongly

suppressed for $\Omega \ll g$. We observed similar suppression in case of copropagating polaritons in chapter 3, but there the bright-bright resonance was the only scattering channel. Here, a pair of dark and lower bright polariton can also be resonantly excited, for which $|\zeta_{LD}|+|\zeta_{DL}| \lesssim 2(g^2+\Delta^2)\Omega^2/(g^2\Delta^2)+(K|\Delta|c/g^2)^2/4$. This estimate leads to the conditions $K \ll g^2/|\Delta|c$ and $\Omega \ll |\Delta|$, which are more demanding than the one from UL and LU channels.

4.5 Finite size corrections

Up to now we considered single frequency component of the photons. In the following we will show the impact of the finite size of photons on the phase gate fidelity. Outside the medium photons are described by slowly varying envelopes,

$$\mathcal{E}_{\pm}(z,t) = \frac{1}{2\pi}\int \mathrm{d}\nu\, \mathcal{E}_{\pm}(\nu)\exp[ik_{\pm}z - i\nu t], \tag{4.11}$$

where the momentum k is related to frequency ν via $k_{\pm}(\nu) = \pm\nu/c$. Inside the medium, photons are converted into compressed polaritons figure 4.1(b). Once the size of polariton is much less than the length of the medium $\sigma_z < L$, the interaction between polaritons does not impact their entrance into the medium. Thus, the energy $\omega_{\pm}$ of each component is conserved, whereas momentum $k_{\pm}(\omega_{\pm})$ is changed. Inside the medium, the interaction between polaritons leads to losses from the $p-$level as well as the imprint of the phase shift– both taken into account by the $S-$matrix, see Eqs (4.6) and (4.9). Including these effects, the propagation through the medium of the pair of dark polaritons with energy components $\{\omega_+, \omega_-\}$ can be described by the factor

$$\exp\left[i\varphi(\omega_+,\omega_-) + i\left(k_+(\omega_+) - k_-(\omega_-)\right)L + \hbar(\omega_+ + \omega_-)t\right]. \tag{4.12}$$

For large times– such that both photons already left the medium, the fidelity F [defined in Eq. (4.1)] does not depend on the time and is given by, for details see Appendix B,

$$\begin{aligned}\sqrt{F}e^{i\phi} &= \frac{1}{\Theta}\left(\frac{1}{2\pi}\right)^2 \int \mathrm{d}\omega_1 \int \mathrm{d}\omega_2 |\mathcal{E}_+(\omega_1)|^2 |\mathcal{E}_-(\omega_2)|^2 \\ &\times \exp\left\{2\mathrm{Im}\left[k_-(\omega_2) - k_+(\omega_1)\right]L + i\varphi(\omega_1,\omega_2)\right\}.\end{aligned} \tag{4.13}$$

Because of the losses from the $p-$state, the best efficiency Θ can be achieved for both polaritons close to the EIT resonance, *i.e.*, $\omega_{\pm} \approx 0$. Assuming that

both photons have the same shape, we conveniently define polaritons by their frequency components (introduced in (4.11)) outside the medium

$$\mathcal{E}_{\pm}(\nu) = \exp\left[-(\nu/\sigma^{\omega})^2/2\right]/\sqrt{\sqrt{\pi}\sigma^{\omega}}, \tag{4.14}$$

with $\sigma^{\omega}\delta/\Omega^2 \ll 1$, where the width in energy space is connected to the width in position space via $\sigma^{\omega} = c\Omega^2/(g^2\sigma_z)$. Next, we estimate the drop of the gate efficiency due to the single photon losses and the deviations from the linear dispersion relation. To this end, we use expression for momentum in the regime of $g, |\Delta| \gg \Omega$ but for bigger energies $|\nu| \lesssim \Omega^2/|\Delta|$ which takes the form

$$k_{\pm}(\nu) = \pm\frac{g^2}{\Delta c}\frac{\nu\Delta}{2\Omega^2}\Big/\left(\frac{\nu\Delta}{2\Omega^2}+\frac{1}{2}\right), \tag{4.15}$$

therefore, the losses in the leading order of γ/δ are equal to

$$2\mathrm{Im}\left[k_{-}(\omega_{-}) - k_{+}(\omega_{+})\right]L = -2\frac{Lg^2}{\delta c}\frac{\delta^2(\omega_{+}^2+\omega_{-}^2)}{\Omega^4}\frac{\gamma}{\delta}, \tag{4.16}$$

which leads to the drop of the efficiency by factor

$$\Theta = \frac{1}{1+2\frac{Lg^2}{\delta c}\frac{\delta^2\sigma_{\omega}^2}{\Omega^4}\frac{\gamma}{\delta}}. \tag{4.17}$$

Which for the length of the medium L on the order of polaritons size σ_z leads to negligible corrections, suppressed additionally by γ/δ. Moreover, by making the medium longer and simultaneously keeping the ratio σ_z/L fixed, we can make this correction arbitrary small.

Finite size of the wavepacket leads to the increase of the losses into bright-dark channel. We already estimated the strength of this scattering process by

$$\frac{\delta\psi(\omega_{+},\omega_{-})}{\psi(\omega_{+},\omega_{-})} \leq \left(\frac{\Omega^2}{|\Delta|^2}+\left(\frac{K|\Delta|c}{2g^2}\right)^2\right)\frac{f(\varphi)}{2} \tag{4.18}$$

for $g \gg |\Delta|$, which after averaging over wavepacket shape gives

$$\delta F = \langle\psi|\delta\psi\rangle \leq \left(\frac{\Omega^2}{|\Delta|^2}+\left(\frac{\sigma_{\omega}|\Delta|}{2\Omega^2}\right)^2\right)\frac{f(\varphi)}{2}. \tag{4.19}$$

Finally, we will estimate the effect caused by energy dependence of the exponent $\varphi(\omega, K)$, which leads to the inhomogeneity of the phase shift. For this estimate, we neglect scattering to bright channels but include dependence

on K of dark pole α_D, which leads to the analytical solution $\psi(r)$ of Eq. 4.7 with modified exponent φ having the form

$$\left(\frac{1}{\sqrt{\left(\frac{c\Delta K}{g^2}\right)^2\left(\frac{\Delta\omega}{2\Omega^2}+1\right)^2+1}}+1\right)\frac{2\pi g^2\xi(-\mathrm{sgn}[C_6]\Delta)^{1/6}}{6c|\Delta|^{1/6}\Delta\left(\frac{\Delta\omega}{2\Omega^2}+1\right)^{7/6}}, \tag{4.20}$$

which can be expanded in ω_+, ω_- up to the second order. After integration over Gaussian wavepackets the expression for the fidelity and phase shift, which contains corrections up to the second order in small parameters γ/δ and σ^ω/ω_c, takes the form

$$\sqrt{F}e^{i\phi} = \exp\left[i\phi - \frac{5}{6}\frac{\gamma}{\delta}\phi - \frac{1}{2}\left(7^2\,\phi^2 + i\,19\,\phi\right)\left(\frac{\sigma^\omega|\Delta|}{12\Omega^2}\right)^2\right] \tag{4.21}$$

It shows that the setup with far detuned $\delta \gg \gamma$ and long polaritons $\sigma_z \gg g^2/|\Delta|c$ enables a construction of the phase gate with fidelity F close to the unity, unconstrained fundamentally.

4.6 Effects due to the transversal extend of the photons

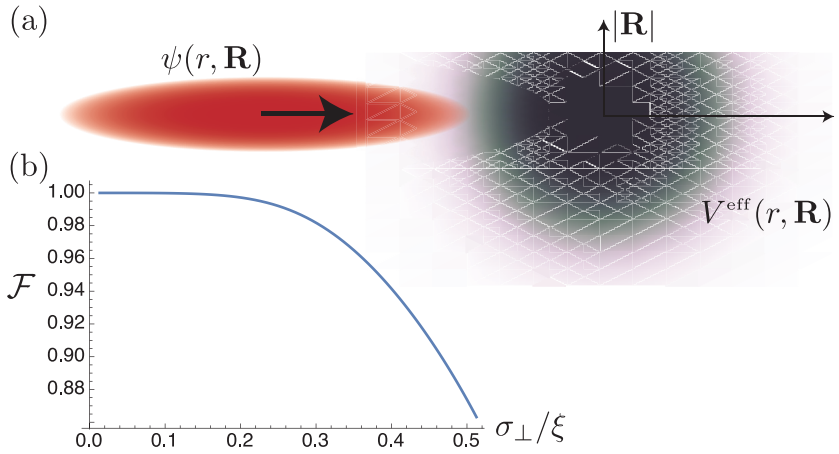

Fig. 4.3: (a) Two-photon wave-function, having finite transverse size, scatters in center-of-mass (*i.e.*, $z_- + z_+ = const.$ and $\mathbf{R}_+ + \mathbf{R}_- = const.$) frame on the effective potential $V^{\mathrm{eff}}(r,\mathbf{R})$, where $\mathbf{R} = \mathbf{R}_+ - \mathbf{R}_-$. (b) Fidelity in function of a transverse width $\sigma_{R_\perp}$ for the phase shift $\phi = \pi/2$: The drop of the fidelity for $\sigma_\perp/\xi < 0.25$ is negligible. Thus, due to the plateauing of V^{eff}, photons experience a homogeneous phase shift.

Next, we analyze the impact of a transversal size of photons, which in general is limited by the diffraction limit or the finite width of a waveguide, on the phase

gate fidelity. The interaction potential V^{eff} depends on the relative distance, what leads to the inhomogeneity of the phase shift, [32, 235]. We estimate this phase-inhomogeneity effect by calculating the fidelity $\mathcal{F}$ in the limit of $\gamma/\delta \to 0$ and for long photons. For two colliding wave-packets having the transverse size $\sigma_\perp$, described by $\mathcal{E}_\pm(z_\pm, \mathbf{R}_\pm) = \mathcal{E}(z_\pm)u(\mathbf{R}_\pm)$ with $u(\mathbf{R}) = \exp[-(x^2+y^2)/\sigma_\perp^2]/\pi\sigma_\perp^2$, the fidelity is given by

$$\mathcal{F} = \int \mathrm{d}\mathbf{R}_+ \int \mathrm{d}\mathbf{R}_- \, |u(\mathbf{R}_+)u(\mathbf{R}_-)|^2 \exp[i\phi(|\mathbf{R}_+ - \mathbf{R}_-|, \xi)].$$

From the figure 4.3(b) we see that the fidelity drop due to the transversal size can be neglected for $\sigma_\perp/\xi < 0.25$, which is within current experimental capabilities, e.g., for $\sigma_\perp = 3\,\mu\text{m}, n\text{S}= 100\text{S}, \Omega = \Gamma$, and $\Delta = 5\Gamma$ we get $\sigma_\perp/\xi = 0.12$. The reason for this behavior is that polaritons interact via V^{eff} which is nearly constant for the distances shorter than the blockade radius, Eq. (4.7). It is an important feature of Rydberg polaritons, resulting in the phase shift being nearly homogeneous also in the transverse direction.

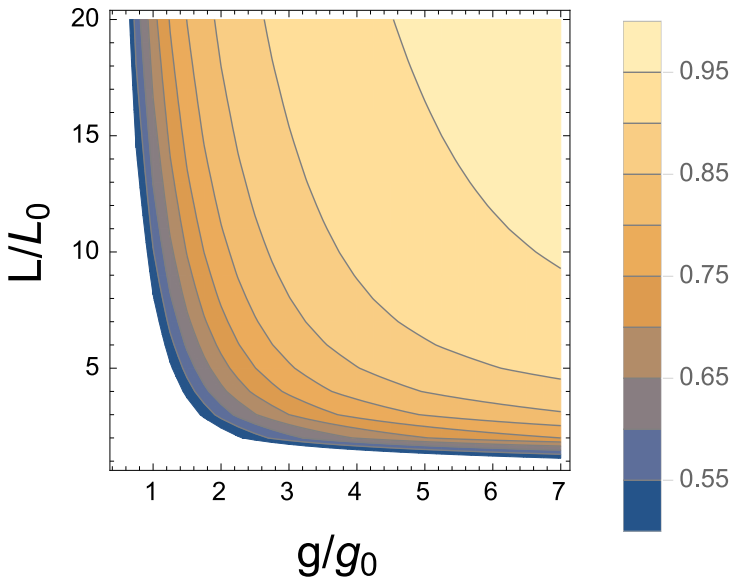

Fig. 4.4: The $\sqrt{F}$ including all presented corrections for $\phi = \pi/2$ in function of collective coupling g and length of the medium L with parameters characteristic for [28, 30]: $L_0 = 160\mu m$ and $g_0/2\pi = 4.4\text{GHz}$. All our estimates assume that the corrections are small and a pulse is long $\sigma_z g^2/|\Delta|c \gg 1$. Therefore, the estimates are not valid in the regimes where F drops much below 1, therefore, we do not plot F there.

4.7 Estimate of the optimal parameters for the phase gate

Based on the estimates of all the detrimental effects, we numerically find optimal parameters δ and Ω for fixed C_6, g, L and ϕ in case of ^{87}Rb atoms (for which $\gamma/\pi = 6.1$MHz). A resulting fidelity for 100S state and $\phi = \pi/2$ as a function of the g and L is presented in the figure 4.4. In order to neglect interaction effects for the entering and leaving the medium, as well as to ensure that photons will completely interact with each other, we take $\sigma_z = L/8$. Some of the corrections are overestimated, like scattering to other channels, see Eq. (4.10), and thus true fidelity can be higher. Presented figure shows that high F phase gate is possible for parameters reachable in the future. It is also a good starting point to find optimal parameters using full numerical two-photon propagation.

It is important to note that in the scope of recent experiments [29, 236] the main limitation of Rydberg-EIT setup is available optical depth per blockade radius: For high densities interaction between Rydberg- and ground- state atoms leads to significant polariton dephasing. The proposed spatially separated geometry [39] does not circumvent this problem. Intuitively, spatial separation a has a similar role to the detuning, i.e., it decreases the imaginary component of the effective interaction V^{eff}. The advantage of the spatially separated setup is that we can have shorter wave-packets because this setup enables larger EIT window, Ω^2/Δ. However, the disadvantages is that scattering to bright polaritons, proportional to Ω/Δ, might not be negligible: The reason is that we are limited by experimentally available C_6 and g, and therefore, in order to achieve desirable ϕ for larger a we need to increase ratio Ω/δ leading to greater losses. Moreover, for intermediate separations $a \sim \xi$ the inhomogeneity of the phase shift, due to the finite range of the interaction, becomes relevant. Summing up, the optimal choice of the setup depends on the value of ϕ we want to achieve and available experimental resources.

5

Quantum theory of Kerr nonlinearity with Rydberg slow light polaritons

In this chapter, we study the propagation of Rydberg slow light polaritons through an atomic medium in the regime where the dispersion relation for the polaritons is well described by the slow light velocity alone [1]. In this regime, the quantum many-body problem can be solved analytically for arbitrary shape of the atomic cloud. We demonstrate the connection of Rydberg polaritons to the behavior of a conventional Kerr nonlinearity for weak interactions and determine the leading quantum corrections for increasing interactions. We propose an experimental setup which allows the measurement of the effective two-body as well as higher-body interaction potentials between slow light polaritons.

5.1 Introduction

Photons interact with their environment much weaker than other quanta and therefore represent excellent carriers of information. On the other hand, a long-standing goal is the realization of a strong and controllable interactions on the level of individual photons. Such interactions would pave the way towards ultralow-power all-optical signal processing [45, 46] which in turn has important applications in quantum information processing and communication [47–50]. A natural mechanism for an interaction is provided by the Kerr nonlinearity of conventional materials [237], but is unfortunately restricted to high field

intensities [52]. On the other hand, the appearance of strong interactions between individual photons has been experimentally realized using Rydberg slow light polaritons [23, 25, 26, 28, 30, 31, 238]. Here, we provide the theoretical framework to connect this regime of strong interactions with the phenomena of a classical Kerr nonlinearity.

Rydberg slow light polaritons have emerged as a highly promising candidates to engineer strong interactions between optical photons with a tremendous recent experimental success [5, 23–31, 238] and several theoretical proposals for the realization of non-classical states of photons [32, 33, 35, 36]. For more details see the introduction and chapter 1. From the theoretical point of view, the effective low energy theory is well understood from a microscopic approach [8, 36], but a full description of the propagation of photons through the medium is limited to extensive numerical simulations and low photon number [**Gorshkov2011a**, 6, 25, 28, 39–43].

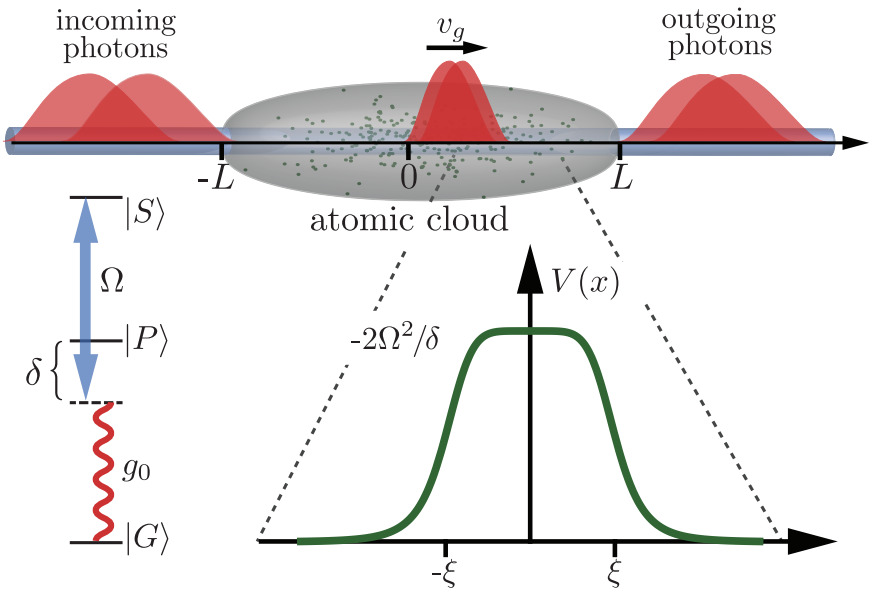

Fig. 5.1: Setup of Rydberg slow light polaritons: each atom consists of three relevant levels, ground state $|G\rangle$, intermediate p-level $|P\rangle$ and Rydberg state $|S\rangle$; the latter are coupled by a strong laser. Incoming photons with a single transverse channel enter the medium and are converted into slow light $v_g < c$ Rydberg polaritons. The interaction between the Rydberg states provides an effective interaction $V(x)$ for the polaritons.

In this chapter, we provide the full input-output formalism of Rydberg polaritons for an intermediate interaction strength where the dispersion relation for the polaritons is well described by the slow light velocity alone, however

allowing for an arbitrary number of incoming photons and an arbitrary shape of the atomic medium. The analysis is performed in the regime with large detuning from the intermediate p-level where losses are strongly suppressed and the effective low-energy theory for the polaritons is well described by an effective interaction potential [8]. We demonstrate that the quantum many-body problem can be solved analytically, and we find the connection of Rydberg polaritons to the behavior of a conventional Kerr nonlinearity for weak interactions. This allows us to determine the leading quantum corrections for such a Kerr nonlinearity. We demonstrate the potential to experimentally determine the effective interaction potential as well as higher-body interactions between the slow light polaritons within a homodyne setup. We expect that our results will play an important role for the generation of strongly-correlated quantum many-body states of photons.

Previous approaches: It is important to point out that previous approaches to describe the quantum propagation of photons in a nonlinear Kerr medium based on a quantization of the phenomenological nonlinear equations provide an inconsistent quantum field theory [239–241] as the interaction is local and the dispersion relation of the photons is linear. This inconsistency was removed by introducing a non-local response in time which leads to a noise term of the same strength as the Kerr nonlinearity [242]. As a consequence, the impossibility to generate a photonic quantum gate based on a large Kerr nonlinearity was concluded [44]. However, the microscopic analysis for Rydberg slow light polaritons shows that such a non-local response in time is absent, but naturally provides a mass term accounting for deviations from the slow light velocity, as well as a finite range of the effective interaction potential describing the blockade phenomena. Here, we demonstrate that the finite range of the interaction potential is sufficient to derive a consistent quantum theory for a Kerr nonlinearity. As a consequence, we conclude that the proposed inability to generate a photonic phase gate by a large Kerr nonlinearity [44] does not apply to Rydberg slow light polaritons.

5.2 Setup

We consider a system of Rydberg slow light polaritons in the dispersive limit with large detuning $|\delta| \gg \gamma, \Omega$ from the intermediate p-level, see Fig. 5.1. Here,

γ describes the decay rate of the p-level, while Ω denotes the Rabi frequency of the coupling laser. Within this regime, losses are strongly suppressed and the intermediate p-level can be adiabatically eliminated [8]. Note, that the decay rates of highly excited Rydberg levels are negligible. We are interested in the propagation of photons along a one-dimensional mode through the medium with frequency close to the condition of electromagnetic induced transparency. In the regime with a low density of Rydberg polaritons, the system is well described by an effective low energy quantum theory [8]. The interaction potential between the polaritons is characterized by a blockade radius ξ and the potential depth $2\hbar\Omega^2/\delta$ at short distances. For a microscopic van der Waals interaction with $C_6\delta < 0$ the effective interaction potential reduces to $V(x) = -(2\hbar\Omega^2/\delta)[1 + (x/\xi)^6]^{-1}$ with the blockade radius $\xi = (|C_6\delta|/2\Omega^2)^{1/6}$, see Fig. 5.1. Note, that for increasing polariton densities additional many-body interactions are expected to appear [4]. In the following, we mainly focus on the two body interactions, but the extension to include many-body interactions is discussed at the end of this chapter.

The kinetic energy for the polaritons at low energies is determined by the slow light velocity of the polaritons and an effective mass term accounting for the curvature in the dispersion relation. The important aspect for the present analysis is the possibility to drop the mass term for moderate interactions between polaritons. The precise condition for the validity of this approximation is discussed below. Then, the Hamiltonian describing the propagation of photons through the spatially inhomogeneous medium with atomic density $n_a(x)$ is given by

$$\begin{aligned} H &= \int \mathrm{d}x \ \left[\beta(x)\psi^\dagger(x)\right](-i\hbar c\partial_x)\left[\beta(x)\psi(x)\right] \\ &+ \frac{1}{2}\int \mathrm{d}x\,\mathrm{d}y\ n(x)n(y)V(x-y)\psi^\dagger(x)\psi^\dagger(y)\psi(y)\psi(x). \end{aligned} \tag{5.1}$$

Here, ψ and $\psi^\dagger$ denote the bosonic field operators annihilating and creating the Rydberg slow light polaritons and satisfy $[\psi(x), \psi^\dagger(x')] = \delta(x-x')$. Furthermore, $\beta(x)$ describes the amplitude of the polariton to be in a photonic state and is related to the slow light velocity $v_g = c\beta(x)^2$, while $n(x) = 1 - \beta(x)^2$ is the probability for the polariton to be in the Rydberg state. These quantities are determined by the atomic density $n_a(x)$ via $\beta(x) = \Omega/\sqrt{\Omega^2 + g_0^2 n_a(x)}$ with g_0 the single atom coupling. Note that outside the atomic medium the operator ψ describes non-interacting photons. The inclusion of higher many-body interactions into the Hamiltonian is straightforward and the influence of a

three-body interaction is discussed at the end of this chapter.

5.3 Exact solution

In the following, it is convenient to introduce a coordinate transformation which removes the reduced velocity v_g of the polaritons inside the media, i.e., we measure distances in the time z/c which is required for the polaritons to reach the position x. The coordinate transformation takes the form $z = \zeta^{-1}(x) = \int_0^x \mathrm{d}y \left(1/\beta(y)^2\right)$, and the Hamiltonian reduces to

$$\begin{aligned} H &= -i\hbar c \int \mathrm{d}z\ \hat{\psi}^\dagger(z)\partial_z\hat{\psi}(z) \\ &\quad + \frac{1}{2}\int \mathrm{d}z\,\mathrm{d}w\,\tilde{n}(z)\tilde{n}(w)\tilde{V}(z,w)\hat{\psi}^\dagger(z)\hat{\psi}^\dagger(w)\hat{\psi}(w)\hat{\psi}(z) \end{aligned} \tag{5.2}$$

with $\tilde{n}(z) = n(\zeta(z))$, $\tilde{V}(z,w) = V(\zeta(z)-\zeta(w))$, and $\hat{\psi}^\dagger(z) = \psi^\dagger(\zeta(z))\beta(\zeta(z))$; the new operators $\hat{\psi}$ still satisfy the bosonic canonical commutation relations.

The quantum many-body theory in Eq. (5.2) is exactly solvable. This remarkable property is most conveniently observed by analyzing the Heisenberg equations for the field operator $\hat{\psi}(z,t)$,

$$i\hbar\partial_t\hat{\psi}(z,t) = -i\hbar c\partial_z\hat{\psi}(z,t) + K(z,t)\hat{\psi}(z,t) \tag{5.3}$$

with the operator $K(z,t)$ accounting for the interaction,

$$K(z,t) = \int \mathrm{d}w\,\tilde{n}(z)\tilde{n}(w)\tilde{V}(z,w)\hat{\psi}^\dagger(w,t)\hat{\psi}(w,t). \tag{5.4}$$

In the following, we denote by $\hat{\psi}_0(z)$ the non-interacting field operator at time $t = 0$. Then, the interacting field operator $\hat{\psi}(z,t)$, satisfying the Heisenberg equation above, reduces to $\hat{\psi}(z,t) = e^{-i\hat{J}(z,t)}\hat{\psi}_0(z-ct)$ with the operator

$$\hat{J}(z,t) = \frac{1}{c\hbar}\int_{z-ct}^{z}\mathrm{d}w\int_{-\infty}^{\infty}\mathrm{d}u\,\tilde{n}(w)\tilde{n}(u)\tilde{V}(u,w)\hat{I}(z-w+u-ct) \tag{5.5}$$

and the polariton density operator $\hat{I}(z) = \hat{\psi}_0^\dagger(z)\hat{\psi}_0(z)$.

5.3.1 Two-photon solution

We start by analyzing the behavior of the *two-photon* solution. It allows us to determine the influence of the involved approximations and to provide a

connection to previous results on two-polariton propagation [8, 28]. For an arbitrary two photon state $|\phi\rangle$, the incoming wave function is defined via

$$\phi^{\text{in}}(x-ct, y-ct) = \lim_{t\to-\infty} \langle 0|\hat{\psi}(z,t)\hat{\psi}(w,t)|\phi\rangle/\sqrt{2}, \tag{5.6}$$

with the coordinates $x = \zeta(z)$ and $y = \zeta(w)$, and the outgoing wave function ϕ^{out} via an analogous expression in the limit $t \to \infty$. Using the above exact solution for the bosonic field operators $\hat{\psi}(z,t)$, we obtain the relation between the incoming and the outgoing photon wave function

$$\phi^{\text{out}}(x,y,t) = e^{-i\varphi(x-y)}\phi^{\text{in}}(x-ct', y-ct') \tag{5.7}$$

where $t' = t - \Delta t$ accounts for the delay of the polaritons inside the medium with $\Delta t = \int_{-\infty}^{\infty} \mathrm{d}y \left(1/\beta(y)^2 - 1\right)/c$. Note, that the outgoing wave function only depends on the reduced coordinate $\tau_1 = x - ct'$ and $\tau_2 = y - ct'$; therefore, in the following, we will use these reduced coordinates to express the outgoing wave function. The phase factor $\varphi(u)$ describes the correlations built up between the photons during the propagation through the medium and takes the form

$$\varphi(u) = \frac{1}{\hbar c}\int_{-\infty}^{\infty} \mathrm{d}w\, \tilde{n}\big(w+u\big)\tilde{n}\big(w\big)\tilde{V}\big(w+u, w\big). \tag{5.8}$$

It is instructive to analyze this phase factor for a specific homogeneous atomic density distribution $n_a(x) = \bar{n}_a\theta(L^2/4 - x^2)$ where θ is a Heaviside step function. The time delay simplifies to $\Delta t = L(1/\tilde{v}_g - 1/c)$, where the slow light velocity $\tilde{v}_g = c\Omega^2/(g^2+\Omega^2)$ and the collective coupling between photon and matter $g = g_0\sqrt{\bar{n}_a}$. In turn, the phase shift acquires the peak value

$$\varphi(0) = \frac{g^4 V(0) L}{(g^2+\Omega^2)\Omega^2\hbar c} = -\frac{g^2}{g^2+\Omega^2}\frac{\kappa\gamma}{\delta} \tag{5.9}$$

with κ the optical depth of the medium. The width of the signal in the phase $\varphi(u)$ is enhanced from the blockade radius by the slow light velocity to $\xi_{\text{out}} = \xi(g^2+\Omega^2)/\Omega^2$. The exact phase shapes for different medium lengths are shown in Fig. 5.2. The determination of $\varphi(u)$ for other physical distributions of atoms is straightforward.

Note, that the interaction provides a spatially dependent phase factor correlating the photons, but is unable to induce a modification in the intensity correlations. A bunching of photons as observed in the experiments by Firstenberg et al. [28] requires the inclusion of the mass term. Here,

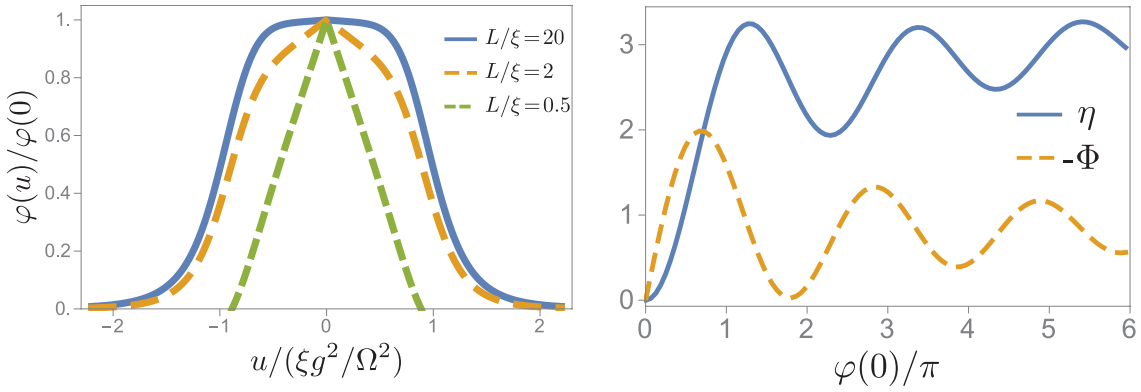

Fig. 5.2: (left) Phase factor $\varphi(u)$ for homogeneous distributions of atoms with different lengths L. For short clouds the condition $\xi \ll L$ is not satisfied and the behavior of $\varphi(u)/\varphi(0)$ is no longer universal, like it is for a long medium. (right) Phase shift and suppression of the electric field for coherent state in the limit $\xi_{\text{out}} \ll l_{\text{coh}}$ as a function of a single photon nonlinearity strength parametrized by $\varphi(0)$. For weak nonlinearities $\varphi(0) \ll 1$ the electric field suppression scales quadratically and the phase shift linearly with the nonlinearity strength. The suppression as well as phase shift oscillate with the increasing strength of interaction.

we estimate the influence of this term, and determine the regime of validity for our approximation to drop it, for details see Appendix A. First, the inclusion of the mass would lead to an additional phase shift estimated by $\varphi_{\text{m}} \sim \hbar\Delta t/(m\xi^2)|\varphi(0)^2 + i\varphi(0)| = |\varphi(0) + i|g^6/(g^2+\Omega^2)^3 L^2/\xi^2$, where we used the expression for the polariton mass $m = \hbar\frac{(g^2+\Omega^2)^3}{2c^2g^2\Delta\Omega^2}$ [8]. In order to drop phenomena like the bunching of photons we require $\varphi_{\text{m}} \ll 1$. Secondly, we would like the phase shift induced by the interaction to dominate the behavior, i.e., $\varphi(0) \gg \varphi_{\text{m}}$. The two conditions are either satisfied for a weak coupling between photon and matter or for a short medium.

The two-photon analysis can be generalized straightforwardly to an N-photon Fock state. Then, the wave function reduces to

$$\frac{\phi^{\text{out}}(\tau_1,\ldots,\tau_N)}{\phi^{\text{in}}(\tau_1,\ldots,\tau_N)} = \exp\left[-i\sum_{i<j}^{N}\varphi(\tau_i-\tau_j)\right],$$

where $\tau_i = x_i - c[t-\Delta t]$. This allows one to derive the outgoing wave function for an arbitrary incoming state. Of special experimental interest however is the behavior of coherent states.

5.4 Coherent incoming state

A general incoming coherent state is characterized by its incoming electric field expectation value $\mathcal{E}(x-ct) = \lim_{t\to-\infty} E(x,t)$ with $E(x,t) = \langle\mathcal{E}|\psi(x,t)\beta(x)|\mathcal{E}\rangle$. Then, the outgoing electric field (see appendix A) behaves as

$$\frac{E^{\text{out}}(\tau)}{\mathcal{E}(\tau)} = \exp\left(\int \mathrm{d}u|\mathcal{E}(u)|^2\left[e^{-i\varphi(u-\tau)}-1\right]\right), \tag{5.10}$$

where $\tau = x - c[t-\Delta t]$. In the limit of a weak non-linearity $\varphi(u) \ll 1$, we can recover the result of a classical Kerr nonlinearity. In this regime, the incoming wave packet has a size l_{coh} much larger than the characteristic size of the interaction $l_{\text{coh}} \gg \xi_{\text{out}}$, and propagates through a long medium $L \gg \xi$. Then, the Eq. (5.10) reduces to $E^{\text{out}}(\tau) = \mathcal{E}(\tau)\exp\left(-i\,\sigma\,|\mathcal{E}(\tau)|^2\right)$ with σ the strength of the Kerr nonlinearity. The latter depends on the shape of the atomic density distribution and reduces for a homogeneous atomic density to

$$\sigma = \int \mathrm{d}u\,\varphi(u) = \frac{2\pi}{3}\frac{g^2}{\Omega^2+g^2}\frac{\kappa\gamma}{\delta}\xi_{\text{out}}. \tag{5.11}$$

However, it is important to stress, that Eq. (5.10) includes also the corrections to the Kerr nonlinearity due to the quantum fluctuations. The corrections can be analyzed by the full evaluation of the factor $i\Phi+\eta = -\int\mathrm{d}u\,(\exp(-i\varphi(u))-1)/\xi_{\text{out}}$, where Φ describes the strength of the Kerr nonlinearity, whereas η accounts for a suppression of the coherences due to quantum fluctuations, see Fig. 5.2. The latter follows from the fact that a coherent state is a superposition of different number states, where each number state picks up a slightly different phase factor. Note, that residual decay processes as well as dephasing can lead to an additional suppression. The observation of the quantum correction therefore requires a precise control of dephasing and a large detuning $|\delta| \gg \gamma$. We would like to stress that these technical noises can be suppressed independently from the strength of the Kerr nonlinearity; in contrast to a system with contact interactions [44].

5.4.1 Correlation functions

The full characterization of the output state and relation to experimentally accessible quantities is most conveniently achieved by the normally ordered

electric field correlations in the reduced coordinates τ_i,

$$G^{\text{out}}_{n,m}(\tau_1,...,\tau_{n+m}) = \left\langle \mathcal{E} \left| \prod_{i=1}^{n} \psi^\dagger(\tau_i) \prod_{j=n+1}^{n+m} \psi(\tau_j) \right| \mathcal{E} \right\rangle .$$

These correlation functions are experimentally accessible in a homodyne detection scheme. The full expression for the correlations of the outgoing fields for an incoming coherent state is presented in Appendix A. In the following, we provide the result for the two point correlation function $G^{\text{out}}_{0,2}$, which reduces to

$$\begin{aligned} G^{\text{out}}_{0,2}(\tau,\tau') &= \mathcal{E}(\tau)\mathcal{E}(\tau') \exp\left[-i\varphi(\tau-\tau')\right] \\ &\quad \times \exp\left(\int \mathrm{d}u \, |\mathcal{E}(u)|^2 \left[e^{-i\varphi(u-\tau)-i\varphi(u-\tau')} - 1 \right] \right). \end{aligned} \tag{5.12}$$

We can distinguish two different contribution: first, we find a strong spatial correlation determined by the phase contribution $\varphi(\tau-\tau')$, which provides direct information about the effective interaction potential between the polaritons. It is this contribution, which allows the access to the effective interaction potential within a homodyne detection scheme. The last factor describes additional phase shift and the suppression due to quantum fluctuations, which are small corrections for $\xi_{\text{out}}|\mathcal{E}(\tau)|^2 \ll 1$.

5.4.2 Wigner function

A full characterization of the outgoing field for an incoming field coherent field $\mathcal{E}$ is provided by the Wigner function $W(q,p)$. In contrast to circuit and cavity QED experiments, where the photons within the resonator are characterized by a single photonic mode [19, 243], our system here corresponds to a multimode setup. Therefore, in terms of the Wigner function, we can only express the reduced density matrix in a specific photonic mode. For this purpose, we define the annihilation operator for an arbitrary spatial mode $u(x)$ as $\hat{a}_u = \int \mathrm{d}x \, u(x)\psi(x)$ and the related quadrature operators as $\hat{q} = (\hat{a}_u + \hat{a}_u^\dagger)/2$, $\hat{p} = (\hat{a}_u - \hat{a}_u^\dagger)/2i$. Then, the Wigner function derives directly from the analytical expression for the correlation functions $G^{\text{out}}_{n,m}$ for the incoming coherent field (see appendix A),

$$W(q,p) = \frac{2}{\pi} \sum_{nm} \frac{(-1)^{n+m}}{n!m!} \mathcal{G}_{nm} \partial^n_{\alpha*} \partial^m_{\alpha} e^{-2|\alpha|^2} \tag{5.13}$$

with $\alpha = q + ip$, and $\mathcal{G}_{nm}$ the overlap of the electric field correlations with the probe photonic mode

$$\mathcal{G}_{nm} = \int \mathrm{d}^{n+m}\tau \, G^{(\mathrm{out})}_{n,m}(\tau_1, ..., \tau_{n+m}) \prod_{i=1}^{n} u(\tau_i)^* \prod_{j=n+1}^{m+n} u(\tau_j).$$

In order to characterize short range correlations between photons we consider a

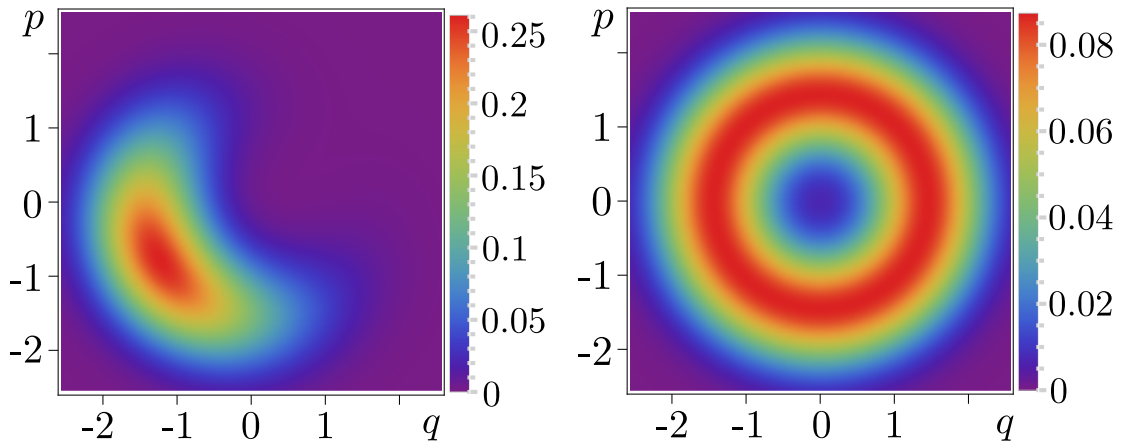

Fig. 5.3: Wigner function describing short range correlations ($l_{\mathrm{probe}} \ll \xi_{\mathrm{out}}$) for long-photons $l_{\mathrm{coh}}/l_{\mathrm{probe}} = 100$ for two different strengths of interaction: $\varphi(0) = \pi/64$ (left) and $\varphi(0) = \pi$ (right).

homodyne detection [244–246] with $u(x)$ being a localized mode having size l_{probe} much shorter than ξ_{out}. The quasi-probability $W(q, p)$ for different strengths of the interaction is shown in Fig. 5.3. For weak interactions $\varphi(0) \ll 1$, the leading correction due to quantum fluctuations to the Gaussian coherent state is a small squeezing. However, for increasing interaction we obtain a strongly mixed state. This behavior is a result of the localized measurement tracing out all positions outside the $u(x)$. Such an operation, acting on our strongly spatially entangled state, leads to the mixed state.

5.4.3 Many-body interactions

A crucial property of our analysis is that it demonstrates the possibility to probe the microscopic interaction potential between the Rydberg polaritons via a homodyne detection scheme for a coherent input state. This method can easily be extended to probe higher body interactions between the polaritons, which are expected to appear for higher polariton densities. Such a n-body

interaction on the microscopic level takes the from

$$H_n = \frac{1}{n!}\int \mathrm{d}\mathbf{x}\, U_n(x_1,\ldots,x_n)\prod_{i=1}^{n} n(x_i)\psi^\dagger(x_i)\psi(x_i) \tag{5.14}$$

with the n-body interaction potential U_n. This term can be straightforwardly included in the exact solution. As an example, we present the results for a three-body interaction, which leads, in analogy to Eq. (5.7), to a phase contribution to the three photon wave-function

$$\phi^{\mathrm{out}}(\tau_1,\tau_2,\tau_3) = e^{-i\varphi_3(\tau_1-\tau_2,\tau_2-\tau_3)}\phi^{\mathrm{in}}(\tau_1,\tau_2,\tau_3).$$

The phase factor $\varphi_3(u,v)$ induced by the three-body interaction takes the form

$$\frac{1}{\hbar c}\int_{-\infty}^{\infty}\mathrm{d}w\;\tilde{n}\big(w+u\big)\tilde{n}\big(w+v\big)\tilde{n}\big(w\big)\tilde{U}_3\big(w+u,w+v,w\big),$$

with $\tilde{U}_3$ defined in analogy to $\tilde{V}$. The corresponding three-body interaction potential can then be experimentally observed in a homodyne detection of the correlations $G^{\mathrm{out}}_{0,3}$.

In general, the quantum field for polaritons is well-defined if at least one of the two conditions, nonzero mass or nonzero range of interactions, is satisfied. Our work concentrated on the case of a finite range of interactions. The system with contact-interaction and nonzero-mass was studied by Gullans et al. [92].

6

Control of Rydberg-mediated few-photon nonlinearities by electrically tuned Förster resonances

In this chapter, we analyze the effects of the electrically tuned Förster resonances on the propagation of slow light Rydberg polaritons in the presence of a stationary Rydberg excitation. The group of S. Hofferberth at the University of Stuttgart experimentally studied this setup with the goal to boost the efficiency of Rydberg-mediated single photon transistors and the non-destructive detection of single Rydberg atoms [5].

Even though a similar problem of a polariton interacting with an impurity via van der Waals interaction has already been studied, see chapter 2, the physics close to the Förster resonance is more complex. For example, the common intuition, that for a vanishing Förster defect the Rydberg blockade should be defined by the resonant dipolar-interactions $\sim r^{-3}$, is incorrect. This is due to the interference between quantum paths for different atomic levels within the EIT scheme. This interference effect also enabled experimentalists to perform high-resolution spectroscopy of two-state Förster resonances, revealing the residual fine structure splitting of high-n Rydberg states and the non-degeneracy of Rydberg Zeeman-substates in finite magnetic and electric fields.

Here, we mostly concentrate on our theoretical contribution. In order to present a coherent story, we will first review relevant experimental details. For

more information see Ref. [5].

Note that in addition to the results presented here, the experimentalists have showed that the $\left|50S_{1/2}, 48S_{1/2}\right\rangle \leftrightarrow \left|49P_{1/2}, 48P_{1/2}\right\rangle$ pair state resonance in ^{87}Rb enables a transistor gain $\mathcal{G} > 100$, as well as a high all-optical detection fidelity of single Rydberg atoms $\mathcal{F} > 0.8$. Moreover, the experimentalists demonstrated for the first time the coherent operation of the Rydberg transistor with $\mathcal{G} > 2$ by reading out the gate photon after scattering source photons. The group of I. Lesanovsky at the University of Nottingham compared the observed readout efficiency to a theoretical model for the projection of the stored spin wave. The comparison yielded to the excellent agreement between theory and experiment and thus successfully identified the main decoherence mechanism of the Rydberg transistor [86, 247].

6.1 Introduction and motivation

As already explained in the introduction and chapter 1, most of the Rydberg quantum optics experiments and proposals employ the van der Waals interaction between Rydberg atoms [148, 149, 248]. A very efficient tool for tuning the interaction are Stark-tuned Förster resonances, where two dipole-coupled pair states are shifted into resonance by a DC [63] or microwave [157, 249] electric field. Förster resonances have been studied by observation of dipole blockade [250], line shape analysis [154], double-resonance spectroscopy [155], excitation statistics [251], and Ramsey spectroscopy [153, 252]. Recently, the anisotropic blockade on Förster resonance [166] as well as quasi-forbidden Förster resonances [253] have been observed, and Förster resonances between different atomic species have been predicted [254]. For Rydberg-mediated single-photon transistors, the near-resonance in zero field for specific pair states has been used to enhance the transistor gain [31], while in experiments on Rydberg atom imaging [88, 89] an increase in Rydberg excitation hopping has been observed on resonance [84].

6.1.1 Setup

The experimental setup based on Refs [30, 31, 38, 89] and the atomic scheme are shown in figure 6.1. First, a gate photon is stored as a Rydberg excitation of the state $\left|S^{(\mathrm{g})}\right\rangle$ inside a cloud of ultracold ^{87}Rb atoms. Afterwards, the existence of this gate excitation is monitored by the transmission of source photons, which are coupled to the source Rydberg state $\left|S^{(\mathrm{s})}\right\rangle$ via electromagnetically induced

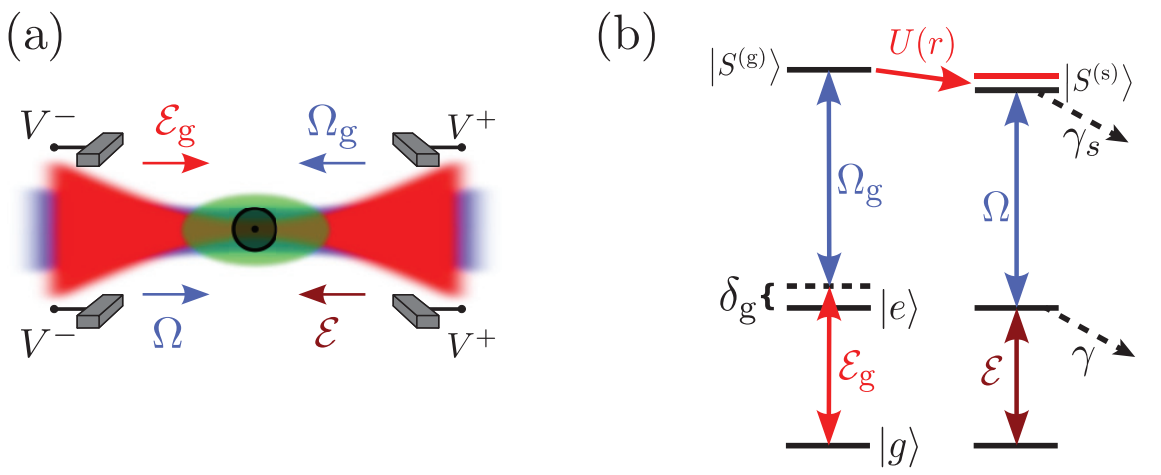

Fig. 6.1: (a) Tightly focused source and gate beams ($w_0 = 6.2\,\mu$m) are overlapped with an optically trapped cloud of 2×10^4 atoms of ^{87}Rb at $3\,\mu$K (cylindrical $1/e$ dimensions $L = 40\,\mu$m, $R = 10\,\mu$m). In-vacuum electrodes, in Löw configuration [255], are used to apply the electric field. (b) Level scheme for gate and source photons coupled to different Rydberg states, where $2\,\Omega$ is the Rabi frequency of the control field and 2γ is the decay rate of $|e\rangle$.

transparency. In case of zero external electric field, the interaction between $\left|S^{(g)}, S^{(s)}\right\rangle$ pair is of van der Waals type. In the experiment a homogeneous electric field was applied along the direction of beam propagation. The electric polarizabilities of S- and P-states differ, which enables shifting the initial pair state into degeneracy with specific $\left|P^{(g)}, P^{(s)}\right\rangle$ pairs. This, in turn, can lead to a resonant dipole-dipole interaction scaling like $\sim r^{-3}$.

This way one can decrease the interaction between source photons compared to the interaction between a source photon and a gate photon, which, in turn can lead to the enhancement of the transistor performance comparing to the previous demonstrations [30, 31].

Resonance structure: In the experiment, two different pairs of states were considered for which observed effects were quantitatively and qualitatively different. First, let us discuss the pair state $\left|S^{(g)}, S^{(s)}\right\rangle = \left|66S_{1/2}, 64S_{1/2}\right\rangle$. Because of the fine structure splitting of the Rydberg P-states, this pair is near resonant with two P-state pairs $\left|65P_{1/2}, 64P_{3/2}\right\rangle$ and $\left|65P_{3/2}, 64P_{1/2}\right\rangle$.

By using an electric field, both $\left|P^{(g)}, P^{(s)}\right\rangle$ pairs can be tuned into resonance. The full pair state Stark map for the magnetic field $B = 1\,$G shows many

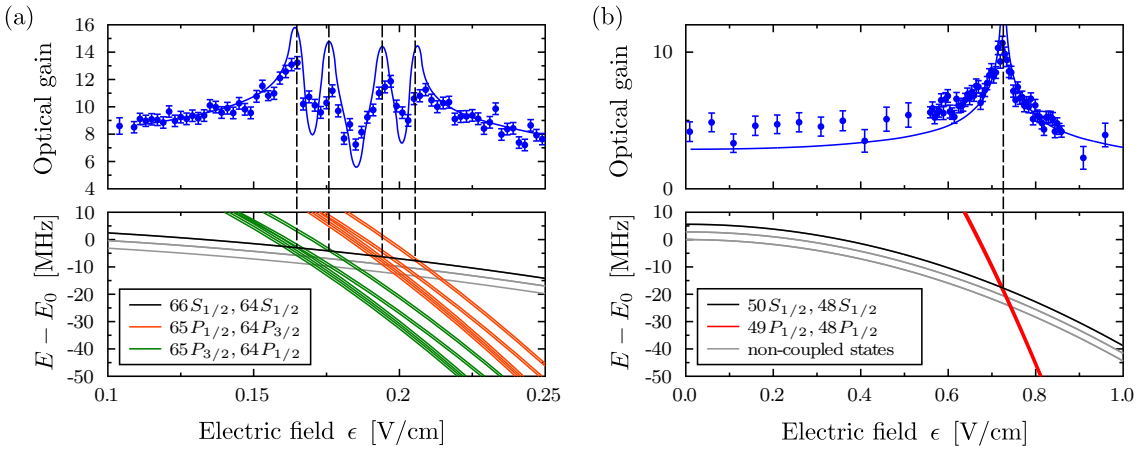

Fig. 6.2: Optical gain: (a) for $\left|S^{(g)}, S^{(s)}\right\rangle = \left|66S_{1/2}, 64S_{1/2}\right\rangle$ and (b) for $\left|S^{(g)}, S^{(s)}\right\rangle = \left|50S_{1/2}, 48S_{1/2}\right\rangle$ as a function of the external electric field. At certain electric fields (vertical dashed lines), the $\left|S^{(g)}, S^{(s)}\right\rangle$ pair state is resonant to pair states of type $\left|P^{(g)}, P^{(s)}\right\rangle$. The enhancement of interaction between $\left|S^{(g)}\right\rangle$ and $\left|S^{(s)}\right\rangle$ manifests in peaking of the transistor gain, visible in the blue data points. In (a), the fine structure of the involved P-states and the m_J-dependence of the Stark-shift results in the observed multi-resonance structure. The blue solid line is a theoretical analysis of the full polariton propagation in the presence of the gate excitation.

closely spaced resonances due to the non-degenerate $(m_J^{(g)}, m_J^{(s)})$ combinations, see figure 6.2. The strength of each individual resonance depends on the angle θ between the interatomic axis and the quantization axis defined by the external fields. This in turn results in a non-spherical blockade volume [149]. In order to quantify these resonances in the experiments we introduce the optical gain

$$\mathcal{G} = \left(\bar{N}_{\text{s,out}}^{\text{no gate}} - \bar{N}_{\text{s,out}}^{\text{with gate}}\right) / \bar{N}_{\text{g,in}}, \tag{6.1}$$

i.e., the number of source photons scattered by a single incident gate photon [31]. The measured optical gain as a function of applied electric field is shown in figure 6.2a). We see that the measured high-resolution spectroscopy revealed four resonances, corresponding to the calculated crossings of different pair state groups.

Note that in between resonances, the coupling of the $\left|S^{(g)}, S^{(s)}\right\rangle$ state to multiple $\left|P^{(g)}, P^{(s)}\right\rangle$ states results in a smaller blockade than in the zero-field case. This interplay between different resonances with positive and negative Förster defects actually decreases the measured gain with respect to the field-free value. This effect does not occur for the Förster resonance $\left|50S_{1/2}, 48S_{1/2}\right\rangle \leftrightarrow$

$\left|49P_{1/2}, 48P_{1/2}\right\rangle$, see figure 6.2(b). For this pair state, there is only one isolated resonance, which leads to the single peak in the optical gain.

6.2 Theoretical description

In order to quantitatively describe the observed resonances, we include the special character of the interaction close to the Förster resonance in the microscopic description of the polariton propagation [8, 25, 34]. For illustration, we consider the $\left|50S_{1/2}, 48S_{1/2}\right\rangle$ pair state and an angle $\theta = 0$, which results in the selection rule $\Delta M_J = \Delta m_J^{(\mathrm{g})} + \Delta m_J^{(\mathrm{s})} = 0$ for the magnetic quantum numbers of the involved states. We then need to include four pair states: $\left\{ \left|50S_{1/2}, 48S_{1/2}\right\rangle, \left|49P_{1/2}, 48P_{1/2}\right\rangle, \left|48P_{1/2}, 49P_{1/2}\right\rangle, \left|48S_{1/2}, 50S_{1/2}\right\rangle \right\}$ with $\left(m_J^{(\mathrm{g})}, m_J^{(\mathrm{s})}\right) = \left(\frac{1}{2}, \frac{1}{2}\right)$. In this basis, the interaction Hamiltonian reduces to

$$H_{\mathrm{dd}}(r) = \frac{1}{r^3} \begin{pmatrix} 0 & C_3 & C_3' & 0 \\ C_3 & 0 & 0 & C_3' \\ C_3' & 0 & 0 & C_3 \\ 0 & C_3' & C_3 & 0 \end{pmatrix} \tag{6.2}$$

with two dipolar coupling parameters C_3, C_3'. Since the interaction is dominated by the Förster resonance, we neglect any residual van der Waals interactions. In general, the Hamiltonian (6.2) gives rise to flip-flop (*hopping*) processes of type $\left|50S_{1/2}, 48S_{1/2}\right\rangle \rightarrow \left\{\left|49P_{1/2}, 48P_{1/2}\right\rangle, \left|48P_{1/2}, 49P_{1/2}\right\rangle\right\} \rightarrow \left|48S_{1/2}, 50S_{1/2}\right\rangle$. However, for our choice of Rydberg states with $|n - n'| > 1$ the dipolar coupling parameters satisfy $C_3 \gg C_3'$, and therefore provide a strong suppression of the hopping. This behavior is in contrast to the results in Ref. [84], where hopping processes strongly influenced the interaction mediated imaging of Rydberg excitations.

6.2.1 Derivation of a photon propagation in the presence of a Rydberg excitation

For the sake of simplicity, we explain our general method explicitly considering the $\left|50S_{1/2}, 48S_{1/2}\right\rangle$ pair state and an angle $\theta = 0$ between the interatomic axis and the quantization axis. Our model system is a one-dimensional gas of atoms, whose electronic levels are given in figure 6.1. The photon field $\hat{\mathcal{E}}(z)$ resonantly couples the ground state $|g\rangle$ with the excited state $|e\rangle$, while 2Ω denotes the

Rabi frequency of the control laser field coupling the $|e\rangle$ state with the Rydberg state $|S^{(s)}\rangle$. Moreover, ω is the probe photon detuning, while γ_s and γ_p describe the decoherence rates of $\left|S^{(s)}\right\rangle$ and $\left|P^{(s)}\right\rangle$ excitations. Following Ref. [8, 25, 34], we introduce operators $\hat{P}^\dagger(z)$ and $\hat{S}^\dagger(z)$ which generate the atomic excitations into the $|e\rangle$ and $\left|S^{(s)}\right\rangle$ states, respectively, at position z. In addition, compared to Ref. [2, 8, 25, 34], we include a more complex atomic level structure of the source and the gate excitations by defining $\hat{\mathcal{P}}^\dagger(z)$, $\hat{\mathcal{Z}}^\dagger(z)$ and $\hat{\mathcal{B}}^\dagger(z)$ which create excitations into $\left|P^{(s)}\right\rangle$, $\left|S^{(g)}\right\rangle$ and $\left|P^{(g)}\right\rangle$ states, respectively. All the operators $\hat{O}(z) \in \left\{\hat{\mathcal{E}}(z), \hat{P}(z), \hat{S}(z), \hat{\mathcal{P}}(z), \hat{\mathcal{Z}}(z), \hat{\mathcal{B}}(z)\right\}$ are bosonic and satisfy the equal time commutation relation, $\left[\hat{O}(z), \hat{O}^\dagger(z')\right] = \delta(z - z')$.

The microscopic Hamiltonian describing the propagation consists of three parts: $\hat{H} = \hat{H}_\mathrm{p} + \hat{H}_\mathrm{ap} + \hat{H}_\mathrm{a}$. The first term describes the photon propagation in the medium and is defined as

$$\hat{H}_\mathrm{p} = -ic \int dz \hat{\mathcal{E}}^\dagger(z) \partial_z \hat{\mathcal{E}}(z),$$

with the speed of light in vacuum c, and we set $\hbar = 1$ throughout this chapter.

The atom-photon coupling is described by

$$\begin{aligned}\hat{H}_\mathrm{ap} = \int dz \Big[& g\hat{\mathcal{E}}(z)\hat{P}^\dagger(z) + \Omega \hat{S}^\dagger(z)\hat{P}(z) + g\hat{P}(z)\hat{\mathcal{E}}^\dagger(z) + \Omega \hat{P}^\dagger(z)\hat{S}(z) \\ & -i\gamma \hat{P}^\dagger(z)\hat{P}(z) - i\gamma_s \hat{S}^\dagger(z)\hat{S}(z) - i\gamma_p \hat{\mathcal{P}}^\dagger(z)\hat{\mathcal{P}}(z)\Big],\end{aligned}$$

where 2γ is the decay rate of $|e\rangle$-state, while $g = g_0\sqrt{n_\mathrm{at}}$ is the collective coupling strength with g_0 being the single atom-photon coupling strength and n_at the atomic density.

The interaction between Rydberg levels is described by

$$\begin{aligned}\hat{H}_\mathrm{a} = \int \mathrm{d}z' \int \mathrm{d}z \Big[& \hat{\mathcal{P}}^\dagger(z)\mathcal{B}^\dagger(z')V(z - z')\hat{\mathcal{Z}}(z')\hat{S}(z) + \\ & \frac{\Delta_D}{2}\hat{\mathcal{P}}^\dagger(z)\hat{\mathcal{B}}^\dagger(z')\hat{\mathcal{B}}(z')\hat{\mathcal{P}}(z) + \mathrm{H.c.}\Big],\end{aligned}$$

where $V(z) = C_3/z^3$ is the dipolar interaction potential and Δ_D the Förster defect. Note, that for the experimental parameters $C_3 \gg C_3'$ and therefore it is sufficient to include only the C_3/z^3 coupling term in the interaction Hamiltonian. In addition, it follows that the hopping of excitations is quenched, and therefore the $\left|S^{(g)}\right\rangle$ excitation is at a fixed position. Then, the description of a single photon propagation requires four components of the wave function: $\mathcal{EZ}(z,t)$, $P\mathcal{Z}(z,t)$, $S\mathcal{Z}(z,t)$ and $\mathcal{PB}(z,t)$, which denote the probability of finding the

source excitation in $\mathcal{E}, |e\rangle, \left|S^{(\mathrm{s})}\right\rangle$ or $\left|P^{(\mathrm{s})}\right\rangle$ state at position z and the gate excitation in $\left|S^{(\mathrm{g})}\right\rangle$ or $\left|P^{(\mathrm{g})}\right\rangle$ state at position z_j. The Schrödinger equation reduces to

$$\begin{aligned}
\partial_t \mathcal{E}\mathcal{Z}(z,t) &= -c\partial_z \mathcal{E}\mathcal{Z}(z,t) - igP\mathcal{Z}(z,t),\\
\partial_t P\mathcal{Z}(z,t) &= -\gamma P\mathcal{Z}(z,t) - ig\mathcal{E}\mathcal{Z}(z,t) - i\Omega S\mathcal{Z}(z,t),\\
\partial_t S\mathcal{Z}(z,t) &= -\gamma_s S\mathcal{Z}(z,t) - iV_j(z)\mathcal{P}\mathcal{B}(z,t) - i\Omega P\mathcal{Z}(z,t),\\
\partial_t \mathcal{P}\mathcal{B}(z,t) &= -\gamma_p \mathcal{P}\mathcal{B}(z,t) - iV_j(z)S\mathcal{Z}(z,t) - i\Delta_D \mathcal{P}\mathcal{B}(z,t),
\end{aligned} \tag{6.3}$$

where $V_j(z) = V(z - z_j)$. We solve the above set of coupled equations via Fourier transform in time, which leads to the equation for the photon field:

$$\left(-ic\partial_z - \frac{g^2\left(V_{\mathrm{ef}}^j(z) - \omega - i\gamma_s\right)}{-i\gamma\omega + (\gamma - i\omega)\gamma_s - \omega^2 + \Omega^2 - V_{\mathrm{ef}}^j(z)(\omega + i\gamma)} - \omega\right)\mathcal{E}\mathcal{Z}(z,\omega) = 0,$$

with

$$V_{\mathrm{ef}}^j(z) = \frac{C_3^2}{\Delta_D - \omega - i\gamma_p}\frac{1}{(z - z_j)^6}. \tag{6.4}$$

It is remarkable that, regardless of Δ_D, our microscopic derivation provides an effective interaction always based on a van der Waals type of interaction.

The equation for the $\mathcal{E}$-field can be generalized to the second pair of states $\left|66S_{1/2}, 64S_{1/2}\right\rangle$ by redefining the expression for $V_{\mathrm{ef}}^j(z)$ to

$$V_{\mathrm{ef}}^j(z) = \sum_\alpha \frac{C_{3,\alpha}^2}{\Delta_D^\alpha - \omega - i\gamma_p}\frac{1}{(z - z_j)^6}, \tag{6.5}$$

where we sum over all relevant pairs of states α, which for $\theta = 0$ are

$$\begin{aligned}
\alpha \in \Big\{ &\left|65P_{1/2}, m_J = \tfrac{1}{2}, 64P_{3/2}, m_J = \tfrac{1}{2}\right\rangle, \left|65P_{1/2}, m_J = -\tfrac{1}{2}, 64P_{3/2}, m_J = \tfrac{3}{2}\right\rangle,\\
&\left|65P_{3/2}, m_j = \tfrac{1}{2}, 64P_{1/2}, m_j = \tfrac{1}{2}\right\rangle, \left|65P_{3/2}, m_j = \tfrac{3}{2}, 64P_{1/2}, m_j = -\tfrac{1}{2}\right\rangle \Big\}.
\end{aligned}$$

6.2.2 Comparison with the experiment

In the experimentally relevant regime with $\omega, \gamma_s, \gamma_p \ll \Omega, \gamma$, the equation describing a single polariton $\mathcal{E}(z,\omega)$ and its interaction with the gate Rydberg excitation $\left|S^{(\mathrm{g})}\right\rangle$ at position r_j simplifies to

$$\left(ic\partial_z + \frac{g^2(\omega - i\gamma_s)}{\Omega^2} + \frac{g^2 V_{\mathrm{ef}}^j(z)}{\Omega^2 - i\gamma V_{\mathrm{ef}}^j(z)}\right)\mathcal{E}(z,\omega) = 0\,, \tag{6.6}$$

with the effective interaction $V_{\mathrm{ef}}^{j}(z)$ given by Eqs (6.4) or (6.5)

For comparison with the experiment, we generalize our calculation to nonzero angles θ between the quantization and interatomic axis as well as to the larger number of states involved for the $\left|66S_{1/2}, 64S_{1/2}\right\rangle$ pair. We then integrate Eq. (6.6) over the cloud shape and average over the stored spin wave. We also take into account the Poissonian statistics of the gate and source photons, the storage efficiency, the fact that the blockade radius is comparable to the beam waist and the finite experimental resolution in electric-field $\Delta\epsilon = \pm 2\frac{\mathrm{mV}}{\mathrm{cm}}$. The comparison, without any free parameters, with experimental results for the gain is shown in Fig. 6.2. We find very good agreement for all electric fields except very close to the resonances. One reason for the discrepancy is the following: Close to the Förster resonance and for distances on the order of r_b between gate and source, the atomic part of the polariton-excitation pair initially in $\left|50S_{1/2}, 48S_{1/2}\right\rangle$ is converted into the superposition of $\left|49P_{1/2}, 48P_{1/2}\right\rangle$ and $\left|50S_{1/2}, 48S_{1/2}\right\rangle$. This results in additional slowing down of the polariton and, consequently, an accumulation of polaritons close to r_b. Then, the assumption to study the propagation of individual polaritons breaks down as the interaction between the polaritons have to be included.

6.3 Outlook

Our polariton propagation theory correctly accounts for the enhanced source-gate interaction and is in excellent agreement with the experiment. It also reveals unexpected and rich properties close to Förster resonances. This regime might enable the study of the transition from two- to many-body interaction and the propagation with excitation hopping [84, 212]. The complexity of the resonances due to the Rydberg level structure provides a wide range of tuning options. The gate-source interaction can be reduced or even switched off completely between individual resonances. Similarly, the angular dependence of the interaction can be greatly varied by the external field. This provides a rich set of new tools for tailoring the interaction of photons coupled to different Rydberg states inside the medium.

7

Dipolar dephasing of Rydberg D-state polaritons

In this chapter, we analyze the effects of the anisotropic Rydberg interaction on D-state slow light Rydberg polaritons. The group of S. Hofferberth at the University of Stuttgart experimentally studied the D-state Rydberg polaritons slowly propagating through a cold atomic sample [7]. They observed the interaction-induced dephasing of Rydberg polaritons at very low photon input rates into the medium. We developed a model combining the propagation of the two-photon wavefunction through the system with nonperturbative calculations of the anisotropic Rydberg-interaction. This way we showed that the observed effect can be attributed to pairwise interaction of individual Rydberg polaritons at distances larger than the Rydberg blockade.

Here, we mostly concentrate on our theoretical contribution. In order to present a coherent story, we will review relevant experimental details. For more information see Ref. [7].

7.1 Introduction

Long-range and spatially anisotropic dipole-dipole (DD) interactions make possible new ways of preparation and exploration of strongly correlated quantum systems [133]. For example, *magnetic* DD interaction leads to the coupling between individual nuclear spins and nitrogen-vacancy centers in diamond [256,

257] and to strong interactions between ultracold gases of dipolar atoms [258, 259]. *Electric* DD interaction is the reason behind the long-range interaction between polar molecules [260], as well as between Rydberg atoms [64, 261]. There have been several proposals to use these interaction in order to study important phenomena such as quantum magnetism [34, 72, 73] and topological phases [262]. In the recent past, the angular dependence of the DD interaction between two Rydberg atoms has been shown experimentally [166].

As we already have stressed multiple times in the introduction and chapter 1, the Rydberg-EIT is an effective way to realize few-photon optical nonlinearities. Here, we will mention a few aspects of Rydberg-EIT, which are relevant in the context of the D-state polaritons. There were many studies of the electric DD interaction between two Rydberg atoms in the perturbative van-der-Waals regime, e.g., see Ref. [148, 149, 263]. In most of the Rydberg-EIT experiments, the Rydberg S-states are used for which the interaction is only weakly angle-dependent [72]. However, some of the recent experiments prepare Rydberg atoms in S- and P-states at the same time [26] or in two S-states with different quantum principal number n [30, 31, 84]. These states are well separated in energy, and interaction between them can lead to novel entanglement schemes for atomic systems [85], as well as to greater flexibility in the control of weak light fields [87, 212].

Here, we study the anisotropic interaction between D-state Rydberg polaritons. Due to the dipolar interactions, the individual Rydberg polaritons decouple from the EIT control field. Importantly, as we will show, this effect can already be relevant for low incoming probe photon rates corresponding to a mean distance between polaritons larger than the blockade radius.

7.2 Experimental setup

The setup consists of an ensemble of three-level atoms. The single-photon probe field $\mathcal{E}$ is on a single-photon resonance, whereas a coupling field Ω is on a two-photon resonance, as illustrated in figure 7.1. The transversal size of the probe field is smaller than the blockade radius and much longer than the length of the medium. Thus, we can consider the photons dynamics within a 1D-approximation and average it over the transversal direction.

First, the experimentalists performed the frequency scan of the probe laser around the EIT resonance. For low rates of incoming photons, they saw very

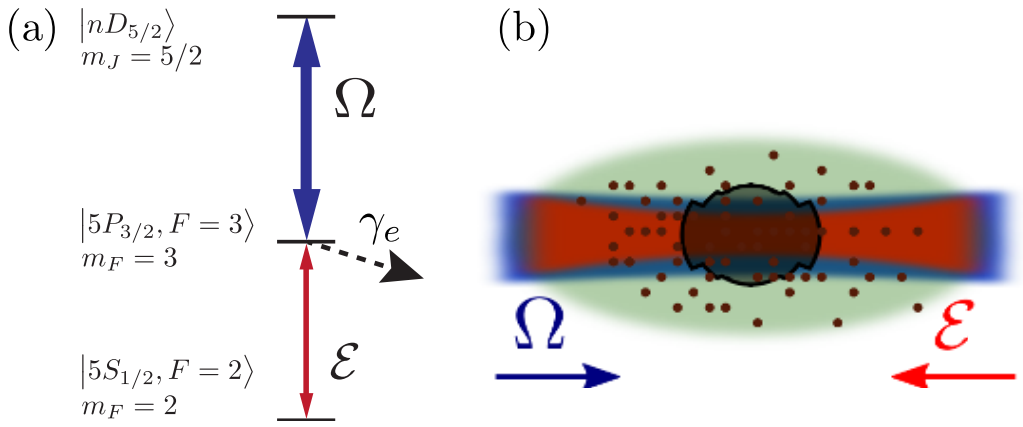

Fig. 7.1: (a) EIT level scheme with weak probe field $\mathcal{E}$ and strong control field Ω. The decay rate γ_e of the intermediate state $|5P_{3/2}\rangle$ is given by $\gamma_e/2\pi = 6.1\,\mathrm{MHz}$. Note that in this chapter the Rabi frequency Ω and decay rate γ_e differ by a factor of 2 compared to the convention used in the rest of this thesis, e.g., $\gamma = \gamma_e/2$. (b) Geometric scheme of our setup consisting of an EIT probe laser with $w_0 \approx 6\,\mu\mathrm{m}$ and of an EIT control laser with $w_0 \approx 12\,\mu\mathrm{m}$, focused onto a thermal cloud of ^{87}Rb atoms with a size of $\sigma_z = 80\,\mu\mathrm{m}$ in the longitudinal direction and a size of $\sigma_r = 25\,\mu\mathrm{m}$ in the transverse direction. The dark grey shadow shows the anisotropic blockade region caused by a $|100D_{5/2}\rangle$ Rydberg excitation. For more details see Ref. [7].

high transmission, whereas for higher rates the transmission dropped. The reason for that is a self-blockade of propagating polaritons and was already demonstrated in the experiments with S-states [24, 25, 75]. Then, they looked into the time dependent transmission on the EIT resonance, see figure 7.2. For low incoming-photon rates R_{in}, when two photons are rarely simultaneously inside the medium, the transmission was nearly constant, whereas for higher rates the decay of transmission over times was faster with increasing rate R_{in} and much stronger than for S-states (the latter observation is based on other measurements for S-states which are not presented in this dissertation).

These observations can be explained by the interaction-induced coupling to degenerate Zeeman sublevels, which leads to polaritons being converted into stationary Rydberg excitations inside the medium. Subsequently, the created impurities shift the Rydberg levels of the surrounding atoms, and therefore other polaritons can not propagate through the cloud on the EIT resonance. The latter part of this mechanism is analogous to the physics behind Rydberg all-optical switch and transistor [29–31].

In order to quantify the dependence of the transmission decay on the photon

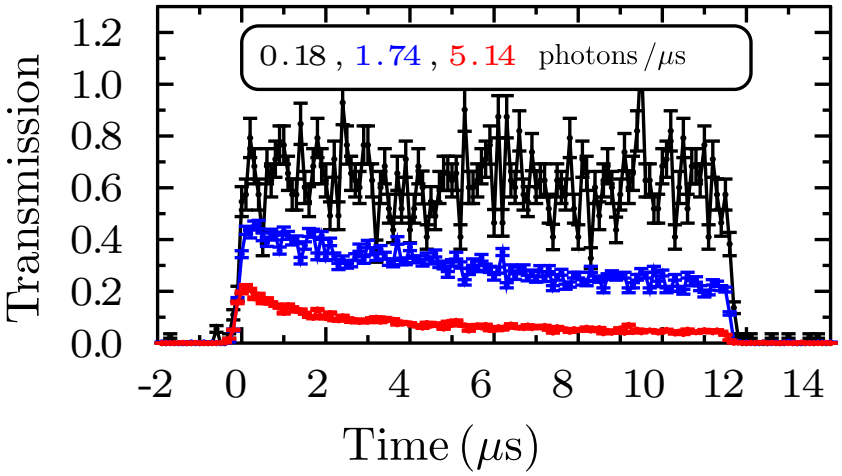

Fig. 7.2: Time-dependent transmission on two-photon resonance for different probe photon input.

rate R_{in}, we introduce an effective optical depth (OD_{eff}) of the medium on the EIT resonance with $\delta = 0$. It is defined as the logarithm of the transmission (figure 7.3(a)) and can be written as

$$OD_{eff} = OD_{dec} + OD_{nl}(R_{in}) + OD_{dph}(R_{in}, t). \tag{7.1}$$

The expression for OD_{eff} accounts for three effects: a decoherence of polaritons due to the thermal motion of atoms (OD_{dec}), a blockade-induced nonlinearity (OD_{nl}), and a dipolar dephasing (OD_{dph}).

Throughout this chapter we will be mostly interested in the last contribution. Neglecting saturation effects for the highest values of R_{in}, we can approximate the increase in OD due to dephasing by a linear function in time. Thus, we write $OD_{dph} = R_{OD} \cdot t$, where we defined R_{OD} depicting the creation rate of optical density by decoupled impurities.

In figure 7.3(b) the extracted rates R_{OD} as a function of R_{in} for different Rabi frequencies Ω of the control field are shown for $n = 88$. For the measurements with higher Rabi frequencies, i.e., $\Omega/2\pi = 16.6\,\mathrm{MHz}$ and $\Omega/2\pi = 26.3\,\mathrm{MHz}$, R_{OD} scales quadratically with R_{in} over experimentally probed rates. In contrast, for lower Rabi frequencies $\Omega/2\pi = 6.1\,\mathrm{MHz}$ and $\Omega/2\pi = 10.8\,\mathrm{MHz}$, we see deviations from the quadratic dependence for R_{in} larger than 1.5 and 2.7, respectively. These deviations coincide with rates corresponding to a mean number of photons in the medium larger than 2 (vertical lines in figure 7.3(b)).

The position of these lines are calculated based on the delay time in the medium given by $\tau_{delay} = \frac{OD \cdot \gamma_e}{\Omega^2}$ and the initial EIT transmission $T_{EIT}(t = 0) < 1$. Note that the quadratic dependence of R_{OD} on R_{in} strongly suggests that the dephasing is a two-body effect.

In the theoretical analysis below we will relate the dephasing to the probability $|\psi_{dd}|^2$ of finding two polaritons in the Rydberg state at the same time. For distances larger than the blockade radius r_b, this probability is given by

$$|\psi_{dd}|^2 = \frac{R_{in}^2}{v_g^2}. \tag{7.2}$$

Motivated by the quadratic dependence, we introduce a rate constant $\mathcal{C}(\Omega)$ which relates R_{OD} and R_{in} in the quadratic regime via the expression $R_{OD} = \mathcal{C}(\Omega) \cdot R_{in}^2$.

The Ω dependence of the experimentally extracted rate constants $\mathcal{C}$ is shown in figure 7.3(c) for three different principal quantum numbers: $n = 80$, $n = 88$, and $n = 100$. In order to compare the outcomes for different principal quantum numbers, we extract the dependence on Ω by a fit of the form

$$\mathcal{C}(\Omega) = a \cdot \Omega^{-k}, \tag{7.3}$$

which leads to $k = 1.67(4)$ for all the different n. However, for the prefactor a we observe a strong scaling with n, which indicates greater dephasing for larger n.

7.3 Pair potentials

In order to explain the observed dephasing, we used the Rydberg pair potentials calculated via the diagonalization of the electrostatic DD interaction Hamiltonian [248]. In figure 7.4(a) and (b), we show pair potentials for $|80D_{5/2}; 80D_{5/2}\rangle$ and $|100D_{5/2}; 100D_{5/2}\rangle$, respectively. The anisotropic DD interaction couples states with different magnetic quantum numbers in the D-pair state manifold which leads to the observed splitting of the manifold in addition to the overall level shift. Next, we consider the coupling of a laser field with a given direction and polarization. We take into account the electric dipole selection rules by calculating the overlap of the coupled pair state in the fixed coordinate system (defined by the direction of light propagation) with the eigenstates in the presence of interaction in the interatomic coordinate system [149].

The colored shade behind the potentials curves depicts the overlap of the $|nD_{5/2}, m_J = 5/2; nD_{5/2}, m_J = 5/2\rangle$ pair state in the fixed coordinate system,

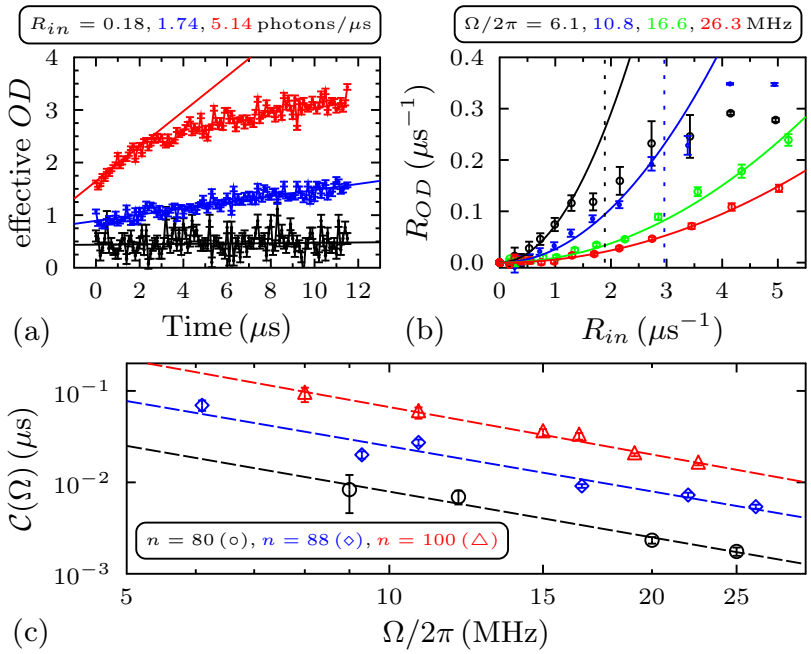

Fig. 7.3: (a) Effective optical density for three different photon rates with fixed $\Omega/2\pi = 8.3\,\mathrm{MHz}$. The solid lines are linear fits to the data from which we extract the rates R_{OD} of additional OD_{eff} due to the creation of impurities. (b) R_{OD} as a function of R_{in} for different Rabi frequencies Ω. Parabolic fits (solid lines) define the rate constants $\mathcal{C}(\Omega)$ for each dataset. The vertical dashed lines depict the mean photon numbers inside the medium exceeding 2 when the quadratic dependence no longer holds. (c) Rate constants $\mathcal{C}$ as a function of Ω. For the different n, we see the same scaling according to Eq. (7.3) with coefficient $k = 1.67(4)$, where dashed lines are numerical fits.

rotated into the interatomic frame via Wigner d-matrices, with the new eigenstates for an angle $\theta = 60°$ between the interatomic axis and the direction of light propagation. This way, a coupled pair state is projected onto multiple new eigenstates. In contrast to the isotropic S-states, the projection for the D-states depends greatly on the angle θ [149]. The anisotropic interaction has two consequences for the physics behind our setup: First, the blockade volume for D-states is no longer spherical and thus it is not enough to use a single C_6 coefficient in order to describe the interaction potential. Secondly, in the presence of the interaction the coupled pair state is not an eigenstate and therefore will evolve in time under the impact of the interaction Hamiltonian.

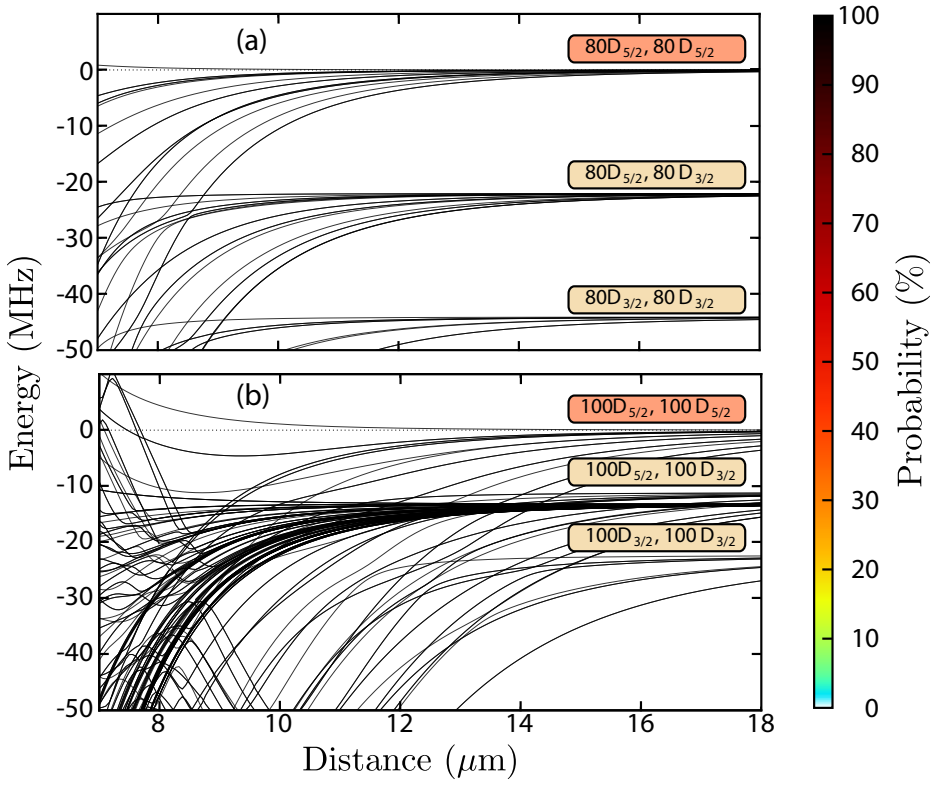

Fig. 7.4: Calculated pair state potentials for (a) $|80D_{5/2}; 80D_{5/2}\rangle$ and (b) $|100D_{5/2}; 100D_{5/2}\rangle$ pair states (grey lines). The color shading represents the projection of the $|m_J = 5/2, m_J = 5/2\rangle$ state (defined with respect to the direction of light propagation) onto the new eigenstates in the presence of interaction for an angle of $\theta = 60°$ between the interatomic axis and the coupling laser beam.

7.4 Theoretical description

In order to incorporate the interaction-induced dynamics with the polariton propagation under EIT, we reduce the full interaction potential to an effective level structure as shown in figure 7.5. In the weak-probe limit it is sufficient to consider only two photons simultaneously inside the medium [8, 25]. Accounting for level shifts and selection rules, we determine the anisotropic blockade distance $r_b(\theta)$ where the laser-coupled pair state is shifted out of the EIT bandwidth (figure 7.6). From this we obtain an effective interaction potential between two slow-light polaritons $V(z, r_\perp)$. This term results in the blockade-induced nonlinearity of the medium.

Outside the blockaded region, where both the overall shift and the splitting of the $D_{5/2}$-Zeeman-manifold are smaller than the EIT bandwidth, we describe

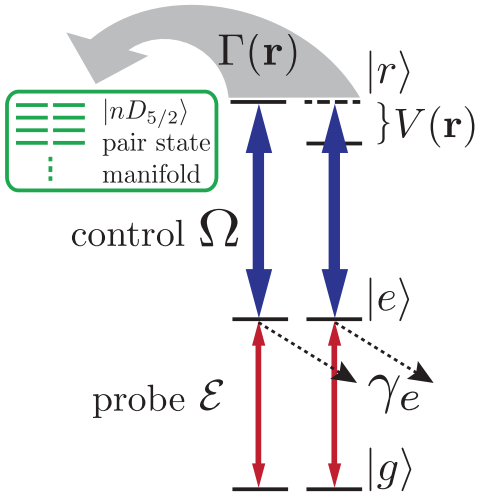

Fig. 7.5: The anisotropic DD interaction between two polaritons is modeled as an effective potential $V(\mathbf{r} = \{z, r_\perp\})$ capturing the interaction-induced blockade effect and a position dependent dephasing rate $\Gamma(\mathbf{r})$ out of the pair-state coupled by the EIT control laser.

the evolution of the coupled pair-state by an effective dephasing rate $\Gamma(z, r_\perp)$ of the Rydberg polaritons into localized Rydberg excitations. Here, $z = z_1 - z_2$ and $r_\perp = r_{\perp,1} - r_{\perp,2}$ are the relative coordinates along and perpendicular to the direction of propagation. In order to obtain $\Gamma(z, r_\perp)$, we calculate from the full interaction potential the time evolution of a stationary Rydberg pair in the initial state (coupled by the fixed control field) at given distance and angle between light propagation direction and interatomic axis. Although this dynamics is fully coherent, the revival of the initial population appears only on time scales long compared to the polariton propagation time due to the large number of states in the D-state manifold. Therefore, the initial time evolution on experimentally relevant time scales is well described by a spatially varying dephasing rate.

The important result is that for D-states the decay $\Gamma(z, r_\perp)$ is large at distances well beyond the blockade volume figure 7.6. In contrast, the same approach results in vanishingly small dephasing rates for S-states.

For the propagation dynamics, we numerically solve the full set of propagation equations for the two-body wave function [25, 28] including the dephasing rate $\Gamma(z, r_\perp)$ as a decay of the amplitude $\psi_{dd}(\mathbf{r}_1, \mathbf{r}_2)$ of two Rydberg excitations. We assume a homogeneous distribution of atoms inside the finite-size medium of length $L = 4\sigma_z$ and include imperfect single-photon transmission due to

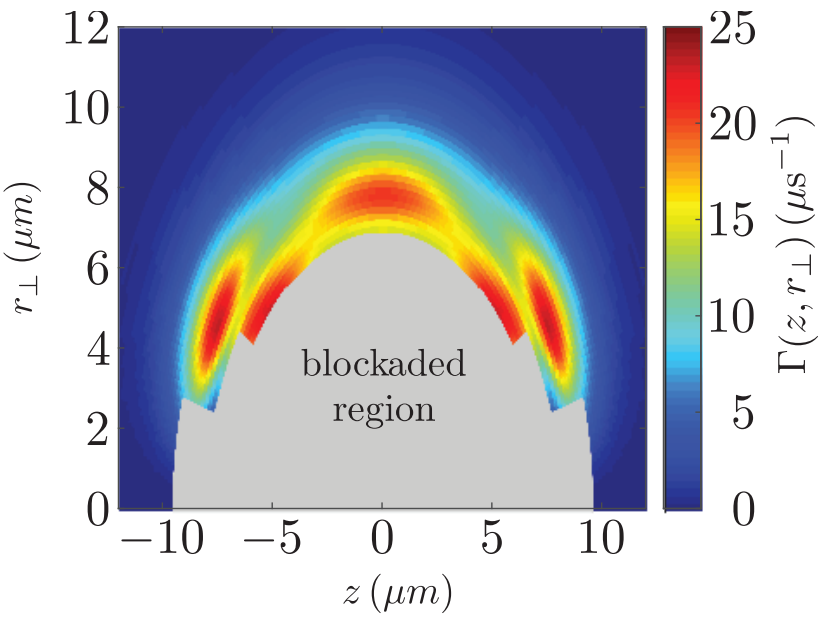

Fig. 7.6: Anisotropic blockaded volume and the dephasing rate outside this region for $n = 80$ and $\Omega/2\pi = 25\,\mathrm{MHz}$.

the decoherence γ_{gr} of the 2-photon transition, which was extracted from experimental data. Neglecting probe-beam diffraction due to the interaction, we solve the polariton dynamics (figure 7.7) for different $r_\perp$ with $V_{1D}(z) = V(z, r_\perp)$ followed by averaging over the $r_\perp$-distribution determined by the Gaussian transverse profile with waist $w_{eff} = 7\mu m$ (corresponding to the waist averaged over length L) of the probe beam.

Then, the rate of events $\mathcal{N}$ that at least one photon is converted into stationary Rydberg excitation is proportional to the amplitude of the two-polariton wavefunction ψ_{dd}:

$$\mathcal{N} \;=\; \int \mathrm{d}^3 r_1 \int \mathrm{d}^3 r_2\, \Gamma(\mathbf{r_1} - \mathbf{r_2}) |\psi_{dd}(\mathbf{r_1}, \mathbf{r_2})|^2. \tag{7.4}$$

We normalize the Rydberg wave function ψ_{dd} with the incoming photon flux as in Eq. (7.2). A single dephasing event increases on average the optical depth within the medium by OD_{im} for the incoming photons. Therefore, the change in transmission by a single dephasing event is $\exp(-OD_{dec} - OD_{sat}(R_{in}))\left(1 - e^{-OD_{im}}\right)$. This reduction appears with the rate $\mathcal{N}$ and therefore the initial time evolution for the averaged transmission behaves as

$$T(t) = e^{-OD_{dec} - OD_{sat}(R_{in})} \exp\left[-\mathcal{N} t \left(1 - e^{-OD_{im}}\right)\right] \tag{7.5}$$

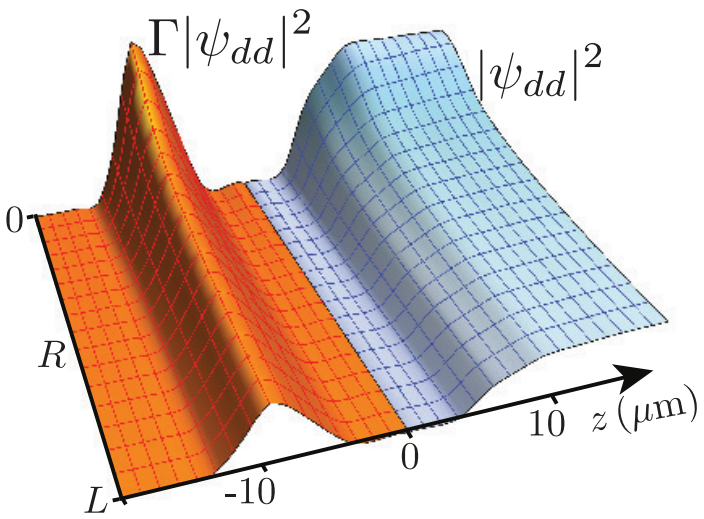

Fig. 7.7: (c) Numerical simulations showing: for $z > 0$, probability distribution associated with two Rydberg excitations $|\psi_{dd}(z, R)|^2$, whereas for $z < 0$, the product $\Gamma(z)|\psi_{dd}(z, R)|^2$, where $R = (z_1+z_2)/2$ is the center-of-mass coordinate. Both quantities are presented in arbitrary units for $r_\perp = 4.2\mu m, \Omega/2\pi = 12\,\mathrm{MHz}, n = 80$ and a probe-beam waist of $w_{eff} = 7\mu m$.

leading to a rate constant $\mathcal{C}(\Omega) = \mathcal{N}\left(1 - e^{-OD_{im}}\right)/R_{in}^2$. Furthermore, we observe that a finite life-time of the Rydberg impurity results in an effective saturation of the transmission. However, the full time evolution for the transmission including higher number of excited Rydberg impurities is extremely challenging and beyond the scope of this work.

Qualitative description of the dephasing: Our calculations provide important insights into the behavior of the dephasing. First, the averaged optical thickness $OD_{im} > 1$ of a dephasing event is sufficient to strongly block the medium. Therefore, the decay mainly follows the probability to absorb at least one impurity. Second, there appears a characteristic distance with the highest probability for the excitation of an impurity Rydberg state. This characteristic distance is given by the competition between the higher dephasing rates at shorter distances and the suppression to find two Rydberg excitations due to the blockade effect, see FIGS 7.6 and 7.7. The latter is strongly affected by the polariton dynamics inside the medium (as has been previously discussed in terms of a diffusive behavior [25]): At the entrance of the two photons into the medium, the probability to find two Rydberg excitations is purely determined by the blockade

due to interactions $\psi_{dd}(z) \sim 1/(1 - \bar{\chi}V_{1D}(z))$ where $\hbar\bar{\chi} = -i(\gamma_e/\Omega^2 + 1/\gamma_e)$ [8]. This dip in the probability broadens during the propagation due to the correction to the linear behavior of the polariton dispersion, while the single polariton losses provide an overall reduction of the amplitude (see figure 7.7). These effects strongly depend on Ω. In addition, photons inside the medium are compressed due to the slow light velocity, which contributes an additional factor Ω^{-4} (see Eq. (7.2)) to the scaling of $\mathcal{C}(\Omega)$ with Ω. Both described effects combined explain the numerical results presented in figure 7.8.

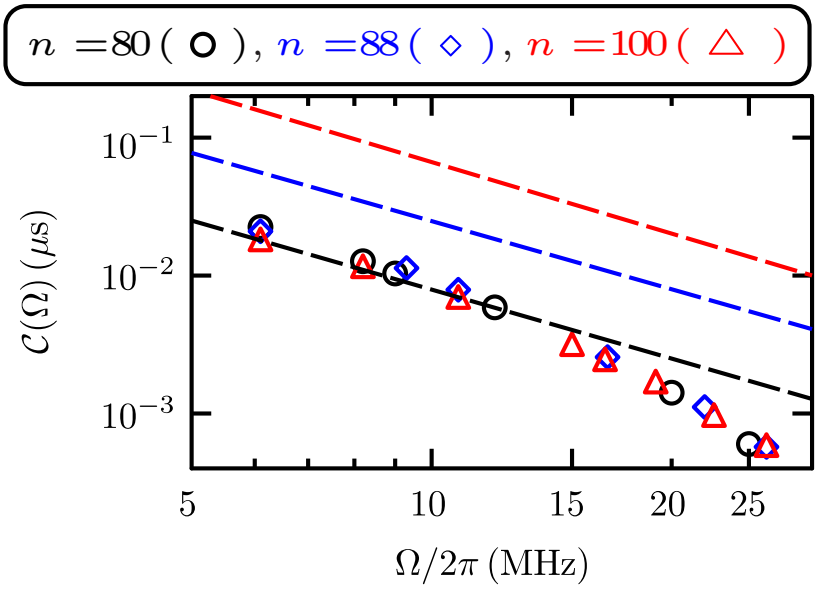

Fig. 7.8: Comparison of $\mathcal{C}(\Omega)$ from numerical simulations (circles) with fits to experimental data from figure 7.3(c) (dashed lines).

Comparison with the experimental results: We find qualitative agreement between theory and experiment without any fitting parameters. While for low n and small values of Ω the agreement is excellent, for larger Ω, we observe a discrepancy and moreover, the theory does not reproduce the strong scaling with the principal quantum number n measured in the experiment. We expect the reason for this discrepancy to be the fact that for large Ω and n, the AC-stark shift and broadening of the Rydberg lines due to the coupling to the $5P_{3/2}$ manifold by the control field become comparable to the splitting between the $nD_{5/2}$ and $nD_{3/2}$ manifold which scales with n^{-3}. In this case, our two-step approach of first calculating the interaction potentials and then incorporating them into the polariton propagation does not capture the full evolution of the system.

7.5 Outlook

Here, we briefly relate our research to other works and describe possible future directions. Our results on the interaction-induced decoupling into stationary Rydberg excitations show that this process can be relevant to all Rydberg experiments employing non-S-states [26] or Förster resonances [31, 84], since the anisotropy of the Rydberg interaction will always result in coupling to additional levels.

In theoretical description, we include the full Rydberg pair state potentials in the numerical two-photon propagation by an effective potential and an anisotropic decay rate. Such a description yields a qualitative agreement with the measurements and therefore makes it a useful tool for taking into account the complicated interaction between Rydberg polariton and excitations.

The fact that experimentalist observed the interaction-induced state-mixing on the few-photon level is a promising result for the proposals based on Rydberg-dressing [72, 73] and engineered polariton-interaction [41] using Rydberg states with orbital angular momentum.

A possible extension of the presented results would be a more detailed study of the anisotropic coupling, e.g., in a storage and retrieval experiments [29, 264], which would enable a control over the number and the position of stored excitations. In this case, it would be also interesting to employ echo techniques [265], which would enable investigation of the coherent spin evolution of interacting Rydberg-polaritons.

A

Supplementary Material to Quantum theory of Kerr nonlinearity with Rydberg polaritons

A.1 Regime of parameters in which mass term is negligible

In this section, we derive a regime of parameters in which we can drop the mass term in the polaritonic dispersion relation. For this purpose, we analyze two polaritons propagating through a cloud of atoms with a constant density. In the relative r and center of mass R coordinates, the Schrödinger equation for the two-body wave function $\phi(R,r)$ takes the form [8]

$$\hbar\omega\phi(R,r) = \left(-i\hbar v_g\partial_R - \frac{\hbar^2}{m}\partial_r^2 + \alpha V(r)\right)\phi(R,r), \tag{A.1}$$

where

$$m = \hbar\frac{(g^2+\Omega^2)^3}{2c^2g^2\Delta\Omega^2}, \qquad V(r) = \frac{2\Omega^2\hbar}{\delta}\frac{1}{1+r^6/\xi^6}, \tag{A.2}$$

$$\alpha = \frac{g^4}{(g^2+\Omega^2)^2}, \qquad v_g = \frac{\Omega^2}{\Omega^2+g^2}c. \tag{A.3}$$

Assuming that the mass term is negligible, we can find the analytical solution of Eq. A.1 of the form

$$\phi_0(R,r) = \phi(0,r)\exp\left(i\frac{\omega}{v_g}R - i\varphi(0)\frac{R}{L}\frac{1}{1+(r/\xi)^6}\right) \tag{A.4}$$

where we used the relation $\varphi(0) = L\alpha V(0)/v_g$, see Eq. (5.9) in Chapter 5. For latter purposes let us define $\varphi_{int}(R,r) = \varphi(0)R/L/(1+(r/\xi)^6)$. Using the above solution, we calculate perturbatively the corrections due to the mass term to the phase shift. For this purpose we express the full solution ϕ using ϕ_0:

$$\phi(R,r) = \phi_0(R,r)e^{-i\vartheta_m(R,r)}, \tag{A.5}$$

where $\vartheta_m(R,r)$ takes into account the impact of the mass term. Next, we insert this Ansatz into Eq. A.1. Exploiting that ϕ_0 is the solution for the unperturbed Hamiltonian, most of the terms cancel and we arrive with the equation for ϑ_m:

$$0 = -iv_g\phi_0(R,r)\partial_R e^{-i\vartheta_m(R,r)} - \frac{\hbar^2}{m}\partial_r^2\phi_0(R,r)e^{-i\vartheta_m(R,r)}. \tag{A.6}$$

This equation can be simplified once we take into account that in the perturbative limit $|\partial_r\vartheta_m(R,r)| \ll |\partial_r\varphi_{\text{int}}(R,r)|$ and $|\partial_r^2\vartheta_m(R,r)| \ll |\partial_r^2\varphi_{\text{int}}(R,r)|$. Moreover, considered photons are much longer than ξ_{out} and, therefore, we drop $\partial_r\phi(0,r)$ and $\partial_r^2\phi(0,r)$ terms. Finally, Eq. A.6 simplifies to

$$\begin{aligned} 0 &= -iv_g\phi_0(R,r)\partial_R e^{-i\vartheta_m(R,r)} \\ &- \frac{\hbar^2}{m}\phi(0,r)e^{-i\vartheta_m(R,r)}e^{i\frac{\omega}{v_g}R}\partial_r^2 \exp\left(-i\varphi(0)\frac{R}{L}\frac{1}{1+(r/\xi)^6}\right). \end{aligned} \tag{A.7}$$

This equation leads to the solution for $\vartheta_m(L,r)$ of the form

$$\vartheta_m(L,r) = -\frac{1}{v_g}\int_0^L \mathrm{d}R\,\frac{\hbar^2}{m}\frac{\partial_r^2 \exp\left(-i\varphi(0)\frac{R}{L}\frac{1}{1+(r/\xi)^6}\right)}{\exp\left(-i\varphi(0)\frac{R}{L}\frac{1}{1+(r/\xi)^6}\right)}. \tag{A.8}$$

In order to estimate $\vartheta_m(R=L,r)$, we consider its value at $r=\xi$, which is equal to

$$\vartheta_m(L,\xi) = 3\left(\varphi(0)+i\right)\frac{L^2}{\xi^2}\frac{g^6}{\left(g^2+\Omega^2\right)^3}, \tag{A.9}$$

and corresponds to the result for φ_m from Chapter 5. We see that the mass term can be dropped if two conditions $\varphi_m \ll 1$ and $\varphi_m/\varphi(0) \ll 1$ are satisfied.

A.2 Correlations of the outgoing fields for an incoming coherent state

Here, we derive the general expression for the correlations $G^{\text{out}}_{n,m}$ of the outgoing fields for an incoming coherent state $|\mathcal{E}\rangle$. We start by inserting the exact solution

for bosonic field operators $\hat{\psi}(z,t) = e^{-i\hat{J}(z,t)}\hat{\psi}_0(z-ct)$ into the definition of $G^{\text{out}}_{n,m}$ from Chapter 5. This leads to

$$G^{\text{out}}_{n,m}(\tau_1,...,\tau_{n+m}) = \left\langle \mathcal{E} \left| \prod_{i=1}^{n} \left(e^{-i\hat{J}(z_i,t)}\hat{\psi}_0(z_i-ct)\right)^{\dagger} \prod_{j=n+1}^{n+m} e^{-i\hat{J}(z_j,t)}\hat{\psi}_0(z_j-ct) \right| \mathcal{E} \right\rangle, \tag{A.10}$$

where $\tau_i = z_i - ct$. Our goal is to transform the product of operators to the normally ordered expression, of which expectation value in a coherent state is trivial. For this purpose, we first use the relation

$$\hat{\psi}_0(z_i-ct)e^{-i\hat{J}(z_j,t)} = e^{-i\hat{J}(z_j,t)}e^{-i\varphi(z_i-z_j)}\hat{\psi}_0(z_i-ct) \tag{A.11}$$

to normally order the ψ_0 operators in the Eq. A.10,

$$\begin{aligned} G^{\text{out}}_{n,m}(\tau_1,...,\tau_{n+m}) = & \\ & \left\langle \mathcal{E} \left| \prod_{k=1}^{n} \hat{\psi}_0^{\dagger}(\tau_k) \prod_{i=1}^{n} e^{i\hat{J}(z_i,t)} \prod_{j=n+1}^{n+m} e^{-i\hat{J}(z_j,t)} \prod_{l=n+1}^{n+m} \hat{\psi}_0(\tau_l) \right| \mathcal{E} \right\rangle \\ & \times \exp\left[i \sum_{k>l=1}^{n} \varphi(\tau_k-\tau_l) \right] \exp\left[-i \sum_{k>l=n+1}^{m+n} \varphi(\tau_k-\tau_l) \right]. \end{aligned} \tag{A.12}$$

Next, we use the fact that in the limit of $t \to \infty$ the expression for $\hat{J}(z_i,t)$ can be written as $\hat{J}(z_i,t) = \int_{\infty}^{-\infty} \mathrm{d}u\, \hat{I}(u)\varphi(u-z_i+ct)$, and that $\hat{J}(z_j,t)$ commutes with $\hat{J}(z_i,t)$, in order to rewrite the product of exponentials appearing in Eq. A.12 in the following way:

$$\begin{aligned} \prod_{i=1}^{n} e^{i\hat{J}(z_i,t)} \prod_{j=n+1}^{n+m} e^{-i\hat{J}(z_j,t)} &= \exp\left(i \sum_{i=1}^{n} \hat{J}(z_i,t) - i \sum_{j=n+1}^{n+m} \hat{J}(z_j,t) \right) \\ &= \exp\left(\int_{-\infty}^{\infty} \mathrm{d}u\, \hat{I}(u) \left[i \sum_{i=1}^{n} \varphi(u-\tau_i) - i \sum_{j=n+1}^{n+m} \varphi(u-\tau_j) \right] \right). \end{aligned} \tag{A.13}$$

The last expression can be transformed to the normally ordered one using the relation [242]:

$$\exp\left(\int \mathrm{d}u\, g(u)\hat{I}(u) \right) = :\exp\left(\int \mathrm{d}u\, \left(e^{g(u)}-1\right)\hat{I}(u) \right): . \tag{A.14}$$

In our case $g(u) = i\sum_{i=1}^{n}\varphi(u-\tau_i) - i\sum_{j=n+1}^{n+m}\varphi(u-\tau_j)$, what leads to

$$\begin{aligned} & \prod_{i=1}^{n} e^{i\hat{J}(z_i,t)} \prod_{j=n+1}^{n+m} e^{-i\hat{J}(z_j,t)} = \\ & :\exp\left(\int_{-\infty}^{\infty} \mathrm{d}u\, \hat{I}(u) \left[\exp\left(i \sum_{i=1}^{n} \varphi(u-\tau_i) - i \sum_{j=n+1}^{n+m} \varphi(u-\tau_j) \right) - 1 \right] \right): . \end{aligned} \tag{A.15}$$

The last equation inserted into the Eq. A.12 provides the final result,

$$G^{\text{out}}_{n,m}(\tau_1,...,\tau_{n+m}) = \tag{A.16}$$
$$\prod_{i=1}^{n}\hat{\mathcal{E}}^*(\tau_i)\prod_{j=n+1}^{n+m}\hat{\mathcal{E}}(\tau_j)\exp\left[i\sum_{k>l=1}^{n}\varphi(\tau_k-\tau_l)\right]\exp\left[-i\sum_{k>l=n+1}^{m+n}\varphi(\tau_k-\tau_l)\right]$$
$$\times\exp\left(\int_{-\infty}^{\infty}\mathrm{d}u\,|\mathcal{E}(u)|^2\left[\exp\left(i\sum_{i=1}^{n}\varphi(u-\tau_i)-i\sum_{j=n+1}^{n+m}\varphi(u-\tau_j)\right)-1\right]\right).$$

Two special cases of these correlations, i.e., $G^{\text{out}}_{0,1}$ and $G^{\text{out}}_{0,2}$ are presented in Chapter 5, see Eqs 5.10 and 5.12, respectively.

A.3 Wigner function from correlation functions

Here, we show how Wigner function $W(q,p)$ can be calculate using the correlation functions $\mathcal{G}_{nm}$. Our starting point is symmetrically ordered characteristic function $\chi(\eta)$ defined as

$$\chi(\eta) = \mathrm{Tr}\left[\rho\exp\left[\eta\hat{a}_u^\dagger-\eta^*\hat{a}_u\right]\right]. \tag{A.17}$$

The function $\chi(n)$ can be expressed using correlation function $\mathcal{G}_{nm}=\left\langle(\hat{a}_u^\dagger)^n\hat{a}_u^m\right\rangle$ as

$$\chi(\eta)=\sum_{nm}\frac{\eta^n(-\eta^*)^m}{n!m!}e^{-|\eta|^2/2}\mathrm{Tr}\left[\rho(\hat{a}_u^\dagger)^n\hat{a}_u^m\right]=\sum_{nm}\frac{\eta^n(-\eta^*)^m}{n!m!}e^{-|\eta|^2/2}\mathcal{G}_{nm}. \tag{A.18}$$

The Wigner function is defined as the Fourier transform of the characteristic function $\chi(\eta)$ [266],

$$W(\alpha) = \frac{1}{\pi^2}\int\mathrm{d}^2\eta\,e^{\eta^*\alpha-\eta\alpha^*}\chi(\eta). \tag{A.19}$$

Finally, we insert $\chi(\eta)$ from Eq. A.18 into the definition A.19 and afterwards transform $W(\alpha)$ to a more concise expression:

$$\begin{aligned}W(\alpha) &= \frac{1}{\pi^2}\sum_{nm}\frac{(-1)^m}{n!m!}\int\mathrm{d}^2\eta\,e^{\eta^*\alpha-\eta\alpha^*}\eta^n(\eta^*)^m e^{-|\eta|^2/2}\mathcal{G}_{nm}\\ &= \frac{1}{\pi^2}\sum_{nm}\frac{(-1)^{n+m}}{n!m!}\mathcal{G}_{nm}\partial^n_{\alpha^*}\partial^m_{\alpha}\int\mathrm{d}^2\eta\,e^{\eta^*\alpha-\eta\alpha^*}e^{-|\eta|^2/2}\\ &= \frac{2}{\pi}\sum_{nm}\frac{(-1)^{n+m}}{n!m!}\mathcal{G}_{nm}\partial^n_{\alpha^*}\partial^m_{\alpha}e^{-2|\alpha|^2},\end{aligned} \tag{A.20}$$

which is the formula presented in Chapter 5.

B

Supplementary Material to Two-photon conditional phase-gate based on Rydberg slow light polaritons

B.1 Poles structure in the regime of $K = 0$

In the regime of $K = 0$ the problem significantly simplifies because two resonance for dark-bright channels (LD and DL pairs), as well as, two resonance for bright-bright channels (LU and UL pairs) do overlap and, therefore, $\alpha_{LD} = \alpha_{DL}$ and $\alpha_{LU} = \alpha_{UL}$. Then, parameters describing poles can be derived analytically but expressions are long. Formulas simplify a lot in the interesting us regime of $g, \Delta \gg \Omega$ and $\omega \leq \omega_c$ to

$$\alpha = \frac{2g^2\Omega^2}{\left(\Delta\omega + 2\Omega^2\right)^2} \tag{B.1}$$

$$\alpha_{LU} = \alpha_{UL} = \frac{g^2\Omega^4}{4\left(\Delta^2 + g^2\right)^3} \tag{B.2}$$

$$\alpha_{LD} = \alpha_{DL} = \frac{\Delta^2 + g^2}{4\Delta^2} \tag{B.3}$$

What corresponds to the expressions for $\zeta_{LU} = \zeta_{UL}$ and $\zeta_{LD} = \zeta_{DL}$ from the main manuscript in the limit of $\omega \ll \omega_c, K = 0$. Expressions taking additionally into account finite K for $\zeta_{LD} = \zeta_{DL}$ are obtained with the help of *far detuned regime* (see next section) and numerics. Regime of $K \to 0$ is useful to show the

weakness of the spatially separated regime proposed in [39]: In the considered there regime of $\Omega \sim \Delta$, the losses to bright channel become relevant.

B.2 Poles structure in far detuned regime

In the far detuned regime the problem simplifies to two channels described, in units of $\omega_c = 2\Omega^2/\Delta$ and $k_c = g^2/\Delta c$, by the following expressions

$$\alpha = \frac{\frac{1}{\sqrt{K^2(\omega+1)^2+1}} + 1}{2(\omega+1)^2}, \tag{B.4}$$

$$\alpha_B = -\frac{\frac{1}{\sqrt{K^2(\omega+1)^2+1}} - 1}{2(\omega+1)^2}, \tag{B.5}$$

$$k_D = \frac{-\sqrt{K^2(\omega+1)^2+1} + 2\omega + 1}{2(\omega+1)}, \tag{B.6}$$

$$k_B = \frac{\sqrt{K^2(\omega+1)^2+1} + 2\omega + 1}{2(\omega+1)}. \tag{B.7}$$

For $\omega \to 0$ it gives us the scaling for the ratio of the pole strengths, *i.e.*, $\lim_{K\to 0} \alpha_B/\alpha = K^2/4$. The pole α_B corresponds to the resonant scattering into bright-dark channel with $\alpha_B \approx \max[\alpha_{DL}, \alpha_{LD}]$ (note that for $K \neq 0$ the relation $\alpha_{LD} = \alpha_{DL}$ presented in the previous section is no longer satisfied).

B.3 Derivation of general expression for fidelity and efficiency based on Fourier components $\mathcal{E}_{\pm}(\omega)$

Here, we describe two photons after passing the medium of the length L. We include the losses due to the propagation, as well as, the interaction between polaritons. We neglect effects related to the entering and leaving the medium. The two photon wave packet for $t \gg L/v_g, x_1 > L$ and $x_2 < 0$, using Eqs (4.11) and (4.12), can be written as

$$\begin{aligned}\mathcal{EE}(x_1,x_2,t) &= \left(\frac{1}{2\pi}\right)^2 \int \mathrm{d}\omega_+ \int \mathrm{d}\omega_- \, \exp\left[i\left(k_+(\omega_+) - ik_-(\omega_-)\right)L\right] \\ &\times \mathcal{E}_+(\omega_+)\exp[i\omega_+(x_1-L)/c - i\omega_+ t]\,\exp[i\varphi(\omega_+,\omega_-)] \\ &\times \mathcal{E}_-(\omega_-)\exp[-i\omega_-(x_2-L)/c - i\omega_- t],\end{aligned} \tag{B.8}$$

whereas in case of noninteracting polaritons the two-photon wave-packet $\mathcal{EE}^{V=0}(x_1, x_2, t)$ is given by similar expression, except that it lacks the term $\varphi(\omega_+, \omega_-)$, *i.e.*,

$$\begin{aligned}\mathcal{EE}^{V=0}(x_1, x_2, t) &= \left(\frac{1}{2\pi}\right)^2 \int \mathrm{d}\tilde{\omega}_+ \int \mathrm{d}\tilde{\omega}_- \, \exp\left[i\left(k_+(\tilde{\omega}_+) - ik_-(\tilde{\omega}_-)\right)L\right] \\ &\times \mathcal{E}_+(\tilde{\omega}_+)\exp[i\tilde{\omega}_+(x_1 - L)/c - i\tilde{\omega}_+ t] \\ &\times \mathcal{E}_-(\tilde{\omega}_-)\exp[-i\tilde{\omega}_-(x_2 - L)/c - i\tilde{\omega}_- t]. \end{aligned} \tag{B.9}$$

In order to calculate the fidelity, given by Eq. (4.1), we calculate the overlap

$$\int \mathrm{d}x_1 \int \mathrm{d}x_2 \, \mathcal{EE}^{V=0}(x_1, x_2, t))^* \mathcal{EE}(x_1, x_2, t). \tag{B.10}$$

To this end, we first integrate over x_1, x_2, which leads to $\delta(\omega_+ - \tilde{\omega}_+)\delta(\omega_- - \tilde{\omega}_-)$. Therefore, time dependent terms in (B.10) cancel each other and the only non-vanishing position-dependent term is

$$\begin{aligned} ik_+(\omega_+)L + (ik_+(\omega_+)L)^* - ik_-(\omega_-)L - (ik_-(\omega_-)L)^* \\ = 2\mathrm{Im}[-k_+(\omega_+) + k_-(\omega_-)]L, \end{aligned} \tag{B.11}$$

which leads to the expression (4.13).

B.4 Expansion of φ in small energies

For $K = 0$ and after the expansion of Eq. (4.9) the exponent φ reads

$$\varphi = \frac{2\pi}{3c} g^2 \xi \Delta^{-5/6} |\Delta|^{-1/6} \left(1 - \frac{7}{6}\frac{\Delta}{2\Omega^2}\omega + \frac{13}{6}\left(\frac{\Delta}{2\Omega^2}\omega\right)^2\right), \tag{B.12}$$

which leads to

$$\sqrt{F}e^{i\phi} = \exp\left[i\phi - \frac{5}{6}\frac{\gamma}{\delta}\phi - \frac{1}{2}\left(7^2\,\phi^2 + i\,91\,\phi\right)\left(\frac{\sigma^\omega|\Delta|}{12\Omega^2}\right)^2\right]. \tag{B.13}$$

For $K \neq 0$ after expansion of Eq. (4.20) the exponent takes the form

$$\begin{aligned}\varphi(\omega_+, \omega_-) &= \frac{2\pi}{3c} g^2 \xi \Delta^{-5/6} |\Delta|^{-1/6} \\ &\times \left(\frac{19\Delta^2(\omega_-^2 + \omega_+^2) + 326\Delta^2\omega_-\omega_+}{288\Omega^4} - \frac{7\Delta\,(\omega_- + \omega_+)}{12\Omega^2} + 1\right). \end{aligned} \tag{B.14}$$

B.5 First order corrections to the scattering of two dark polaritons

In this section we use shorter notation: $V_x^e = V^{\text{eff}}(x), \psi_x = \psi(x)$. We define the wave-function ψ_x as the solution after neglecting other channels:

$$\psi_x = \psi_x^0 + \int \mathrm{d}x'\, G_{x-x'} V_{x'}^e \psi_{x'}. \tag{B.15}$$

We are interested in the first order corrections to this solution when we include the second weaker pole, *i.e.*,

$$\psi_x + \delta\psi_x = \psi_x^0 + \int \mathrm{d}x'\, (G_{x-x'} + \delta G_{x-x'}) V_{x'}^e (\psi_{x'} + \delta\psi_{x'}). \tag{B.16}$$

For first order corrections, we neglect the higher order term, i.e., $\delta G V\, \delta\psi$, and then we arrive with integral equation for $\delta\psi$,

$$\delta\psi_x = \int \mathrm{d}y\, (G_{x-y} V_y^e\, \delta\psi_y + \delta G_{x-y} V_y^e\, \psi_y), \tag{B.17}$$

which we can transform into differential equation by acting on both sides with operator $(k_D + i\partial_x)$

$$(k_D + i\partial_x)\delta\psi_x = \alpha_D V_x^e\, \delta\psi_x + (k_D + i\partial_x) \int \mathrm{d}y\; \delta G_{x-y} V_y^e\, \psi_y. \tag{B.18}$$

Solution of the homogeneous part has the form $\delta\psi^{\text{hom}} = \mathcal{D}\mathcal{A}_x$ where $\mathcal{D}$ is a constant, and $\mathcal{A}_x$ reads

$$\mathcal{A}_x = e^{ik_D x} \exp\left(-i\alpha_D \int \mathrm{d}y\; V_y^e\right). \tag{B.19}$$

The solution of the inhomogeneous first order differential equation (B.18) we get by varying integration constant, $\mathcal{D} \to \mathcal{D}_x$. After plugging $\mathcal{A}_x\mathcal{D}_x$ into Eq. (B.18) we arrive with the equation

$$i\mathcal{A}_x \partial_x \mathcal{D}_x \;=\; (k_D + i\partial_x) \int \mathrm{d}y\; \delta G_{x-y} V_y^e\, \psi_y, \tag{B.20}$$

which can be transformed into

$$\begin{aligned} i\partial_x \mathcal{D}_x &= \mathcal{A}_x^{-1}(k_D + i\partial_x) \int \mathrm{d}y\; \left(-i\alpha_B \theta(x-y) e^{ik_B(x-y)}\right) V_y^e\, \psi_y, \\ -\partial_x \mathcal{D}_x &= \frac{\alpha_B}{\mathcal{A}_x} \int \mathrm{d}y\; \left((k_D - k_B)\theta(x-y) + i\delta(x-y)\right) e^{ik_B(x-y)} V_y^e\, \psi_y. \end{aligned} \tag{B.21}$$

Since $\mathcal{D}(-\infty) = 0$, the solution for $\mathcal{D}_z$ takes the form

$$\mathcal{D}_z \;=\; -\alpha_B \int_{-\infty}^{z} \mathrm{d}x\, \mathcal{A}_x^{-1} \left(\int_{-\infty}^{x} \mathrm{d}y\, (k_D - k_B) e^{ik_B(x-y)} V_y^e\, \psi_y + i V_x^e\, \psi_x \right).$$

The full solution $\delta\psi(z) = \mathcal{D}_z\mathcal{A}_z$ is used for the analytical estimates of the corrections in the next section.

B.6 Estimation of the corrections $\delta\psi$ to the solution ψ

Here, we show a rough estimate of the corrections. Because of the relation $\mathcal{A}_x^{-1}\psi_x = 1$, the last term of Eq. (B.22) can be treated easily without approximations:

$$\lim_{z\gg r_B} -i\alpha_B \int_{-\infty}^{z} \mathrm{d}x\, V_x^e = i\frac{\alpha_B}{\alpha_D}\varphi \tag{B.22}$$

To roughly estimate double integral defining $\delta\psi$, we approximate V_y^e by $v_d\,\theta(r_B - |z|)$ (where v_d is the height of the potential), neglect decay of p-level (*i.e.*, $\Delta \to \delta$), and work in the regime of $g \gg \Omega$. Then $\varphi = \phi = -2\alpha_D\xi v_d$; and the correction for $z > \xi$ takes the form

$$\begin{aligned}\delta\psi &= \frac{\alpha_B v_d e^{-i\xi(2v_d\alpha_D+k_D)}}{k_B+v_d\alpha_D-k_D}\Bigg(-e^{i(k_B(\xi+z)+2\xi v_d\alpha_D)}+e^{i(k_B(z-\xi)+2\xi k_D)} \qquad \text{(B.23)}\\ &- 2i\xi v_d\alpha_D e^{ik_D(\xi+z)} - \frac{v_d\alpha_D\left(e^{ik_D(\xi+z)}-e^{i(2\xi k_B+2\xi v_d\alpha_D+k_D(z-\xi))}\right)}{k_B+v_d\alpha_D-k_D}\Bigg)\end{aligned}$$

which can be rewritten as $\delta\psi(z) = e^{ik_Dz}\delta\psi_D + e^{ik_Bz}\delta\psi_B$ with:

$$\delta\psi_D = \frac{\alpha_B v_d^2\alpha_D e^{-2i\xi(v_d\alpha_D+k_D)}}{(k_B+v_d\alpha_D-k_D)^2} \tag{B.24}$$

$$\times \left(ie^{2i\xi k_D}\left(-2\xi\left(k_B+v_d\alpha_D-k_D\right)+i\right)+e^{2i\xi(k_B+v_d\alpha_D)}\right), \tag{B.25}$$

$$\delta\psi_B = -\frac{2i\alpha_B v_d e^{-i\xi v_d\alpha_D}\sin\left(\xi\left(k_B+v_d\alpha_D-k_D\right)\right)}{k_B+v_d\alpha_D-k_D} \tag{B.26}$$

From figure 4.2 we see that $k_B \approx 2g^2/|\delta|c$. By definition, we know that $v_d\alpha_D = -g^2/\delta c$. In order to fit photons well into EIT-window we use photons with low momenta, *i.e.*, $k_D \ll k_B$. From estimates we see that the sign of detuning δ matters, thus, in order to minimize the scattering into bright polaritons we need $v_d\alpha_D > 0$ and therefore to take $\delta < 0$. In order to estimate scattering processes we also replace $2\xi v_d\alpha_D$ by $-\phi$ (note that ϕ is negative in our case), and k_B by $-\phi/2\xi$, this gives

$$\delta\psi_D = \frac{i\alpha_B\left(-\sin(\phi)+e^{i\phi}\phi\right)}{2\alpha_D}, \tag{B.27}$$

$$\delta\psi_B = \frac{ie^{\frac{i\phi}{2}}\alpha_B\sin(\phi)}{\alpha_D}. \tag{B.28}$$

Whereas for $\phi \ll 1$ those expressions simplify furthermore to

$$\delta\psi_D = -\frac{\phi^2\alpha_B}{2\alpha_D}, \tag{B.29}$$

$$\delta\psi_B = \frac{i\alpha_B\phi}{\alpha_D}. \tag{B.30}$$

Note, that in our problem the total probability flux, but not the total probability density, is conserved. Bright part $\delta\psi_B$ has greater group velocity than dark and therefore leaves the medium earlier. Due to this separation in time of dark and bright components, we use $\delta\psi = \delta\psi_D$ as a measure of the corrections to the solution ψ.

Note, that losses to bright channel, relevant to the He et al. proposal [39], will be even more important for large ϕ. For phase shift $\phi = 0.36$ presented in Ref. [39], the prefactor $\left|-\sin(\phi) + e^{i\phi}\phi\right|$ in Eq. (B.27) is equal to 0.13, whereas for $\phi = \pi/2$ the same prefactor would be approximately 15 times larger. This shows once again that for large phase shift the spatially separated setup has its issues, which were not discussed in [39].

B.7 Optimal parameters for the phase gate

In this section, we describe in detail the calculation behind figure 4.4. First, we sum-up all the effects and estimates for the corrections to the phase gate fidelity F and efficiency Θ. We start with single photon losses due to the propagation, which lead to the efficiency

$$\Theta = \frac{1}{1 + 2\frac{Lg^2}{\delta c}\frac{\delta^2\sigma_\omega^2}{\Omega^4}\frac{\gamma}{\delta}} \approx \exp\left[-2\frac{Lg^2}{\delta c}\left(\frac{\delta\sigma_\omega}{\Omega^2}\right)^2\frac{\gamma}{\delta}\right]. \tag{B.31}$$

The estimate of the effects due to the interaction between dark polaritons (4.21) is given by:

$$\sqrt{F}e^{i\phi} \propto \exp\left[i\phi - \frac{5}{6}\frac{\gamma}{\delta}\phi - \frac{1}{2}\left(7^2\,\phi^2 + i\,19\,\phi\right)\left(\frac{\sigma^\omega|\Delta|}{12\Omega^2}\right)^2\right]. \tag{B.32}$$

The scattering into bright-bright channels is negligible. The scattering into two bright-dark channels for $g \ll |\Delta|$ leads to the wave-function corrections

$$\delta\psi(\omega_+,\omega_-)/\psi(\omega_+,\omega_-) \leq (\Omega^2/|\Delta|^2 + K^2/k_c^2/4)f(\varphi). \tag{B.33}$$

Assuming that corrections are small it leads to the drop of fidelity like $\sqrt{F} \propto 1 - \delta\psi/\psi$, which we have to average over the wavepacket shape. The averaging leads to

$$\sqrt{F} \propto 1 - \left(\frac{\Omega^2}{|\Delta|^2} + \left(\frac{\sigma_\omega |\Delta|}{2\Omega^2} \right)^2 \right) f(\varphi). \tag{B.34}$$

Finally, the transverse size effects are described by $\mathcal{F}(\sigma_\perp/\xi)$ shown in figure 4.3.

Our goal is to maximize the value of $\sqrt{F}$

$$\begin{aligned} \sqrt{F} \;&\approx\; \exp\left[-\frac{5}{6}\frac{\gamma}{\delta}\phi - \frac{1}{2}7^2\,\phi^2 \left(\frac{\sigma^\omega |\Delta|}{12\Omega^2} \right)^2 \right] \\ &\times\; \mathcal{F}(\sigma_\perp, \xi) \left(1 - \left(\frac{\Omega^2}{|\Delta|^2} + \left(\frac{\sigma_\omega |\Delta|}{2\Omega^2} \right)^2 \right) |\varphi| f(\varphi) \right) \end{aligned} \tag{B.35}$$

by finding optimal detuning δ for fixed $\sigma_\perp$, ϕ, C_6 in function of g, L. Then, the value of Rabi frequency Ω is fixed by the constraint on ϕ. Since we work in the regime of small corrections we can approximate $1 - \epsilon \approx \exp[-\epsilon]$. We apply this relation in case of transverse size effects $\mathcal{F}$ and losses to bright channels. Thus, in order to find optimal δ, we can look at the maximum of the following expression in the exponent

$$-\frac{5}{6}\frac{\gamma}{\delta}\phi - \frac{1}{2}7^2\,\phi^2 \left(\frac{\sigma^\omega |\Delta|}{12\Omega^2} \right)^2 + \mathcal{F}(\sigma_\perp, \xi) - \left(\frac{\Omega^2}{|\Delta|^2} + \left(\frac{\sigma_\omega |\Delta|}{2\Omega^2} \right)^2 \right) f(\varphi).$$

This leads to results presented in figure 4.4.

Bibliography

[1] P. Bienias and H. P. Büchler. "Quantum theory of Kerr nonlinearity with Rydberg slow light polaritons" (2016). arXiv: 1604.05125 (cit. on pp. 6, 10, 23, 49, 95).

[2] P. Bienias. "Few-body quantum physics with strongly interacting Rydberg polaritons". To be published in European Phys. J. Special Top. (EPJ ST) Rydberg Gases (2016). arXiv: 1608.01629 (cit. on pp. 5, 10, 49, 112).

[3] P. Bienias and H. P. Büchler. "Performance of two-photon conditional phase-gate based on Rydberg slow light polaritons". In preparation (2016) (cit. on pp. 6, 10, 49).

[4] K. Jachymski, P. Bienias, and H. P. Büchler. "Three-body interaction of Rydberg slow light polaritons". Phys. Lev. Lett. **117** (2016), 053601. arXiv: 1604.03743 (cit. on pp. 23, 49, 98).

[17] H Gorniaczyk, C Tresp, P Bienias, A Paris-Mandoki, W Li, I Mirgorodskiy, H. P. Büchler, I Lesanovsky, and S Hofferberth. "Enhancement of single-photon transistor by Stark-tuned Förster resonances" (2015). arXiv: 1511.09445.

[5] H. Gorniaczyk, C. Tresp, P. Bienias, A. Paris-Mandoki, W. Li, I. Mirgorodskiy, H. P. Büchler, I. Lesanovsky, and S. Hofferberth. "Enhancement of single-photon transistor by Stark-tuned Förster resonances". To be published in Nature Communications (2016). arXiv: 1511.09445 (cit. on pp. 5, 7, 9, 11, 23, 49, 53, 61, 96, 107, 108).

[6] M. F. Maghrebi, M. J. Gullans, P. Bienias, S. Choi, I. Martin, O. Firstenberg, M. D. Lukin, H. P. Büchler, and A. V. Gorshkov. "Coulomb bound states of strongly interacting photons". Phys. Rev. Lett. **115** (2015), 123601. arXiv: 1505.03859 (cit. on pp. 5, 9, 23, 96).

[7] C. Tresp, P. Bienias, S. Weber, H. Gorniaczyk, I. Mirgorodskiy, H. P. Büchler, and S. Hofferberth. "Dipolar Dephasing of Rydberg D -State Polaritons". Phys. Rev. Lett. **115** (2015), 083602. arXiv: 1505.03723 (cit. on pp. 7, 11, 23, 49, 115, 117).

[8] P. Bienias, S. Choi, O. Firstenberg, M. F. Maghrebi, M. Gullans, M. D. Lukin, A. V. Gorshkov, and H. P. Büchler. "Scattering resonances and bound states for strongly interacting Rydberg polaritons". Phys. Rev. A **90** (2014), 053804. arXiv: 1402.7333 (cit. on pp. 6, 10, 23, 49, 59, 67, 84, 86–88, 96–98, 100, 101, 111, 112, 121, 125, 127).

[9] K. Pawłowski, P. Bienias, T. Pfau, and K. Rzążewski. "Correlations of a quasi-two-dimensional dipolar ultracold gas at finite temperatures". Phys. Rev. A **87** (2013), 043620. arXiv: 1304.4792.

[10] P. Bienias, K. Pawłowski, T. Pfau, and K. Rzążewski. "Ground state of a two-component dipolar Fermi gas in a harmonic potential". Phys. Rev. A **88** (2013), 043604. arXiv: 1308.0567.

[11] P. Bienias, K. Pawłowski, M. Gajda, and K. Rzążewski. "Quasicondensation reexamined". J. Phys. Conf. Ser. **414** (2013), 012031. arXiv: 1203.1811v2.

[12] P. Bienias, K. Pawłowski, M. Gajda, and K. Rzążewski. "Statistical properties of one-dimensional attractive Bose gas". Europhys. Lett. **96** (2011), 10011. arXiv: 1103.4017.

[13] T. Karpiuk, P. Deuar, P. Bienias, E. Witkowska, K. Pawłowski, M. Gajda, K. Rzążewski, and M. Brewczyk. "Spontaneous Solitons in the Thermal Equilibrium of a Quasi-1D Bose Gas". Phys. Rev. Lett. **109** (2012), 205302. arXiv: 1205.2363.

[14] P. Bienias, K. Pawłowski, M. Gajda, and K. Rzążewski. "Statistical properties of one-dimensional Bose gas". Phys. Rev. A **83** (2011), 33610. arXiv: 1008.3277.

[15] K. Małek, A. Pollo, T. T. Takeuchi, P. Bienias, M. Shirahata, S. Matsuura, and M. Kawada. "Special feature Star forming galaxies in the AKARI deep field south : identifications and spectral energy distributions". Astron. & Astrophys. **514** (2010). arXiv: 1312.0765.

[16] J. G. T. Jakubczyk, T. Kazimierczuk, A. Golnik, P. Bienias, W. Pacuski, C. Kruse, D. Hommel, Ł. Kłopotowski, T. Wojtowicz. "Optical Study of ZnTe-Based 2D and 0D Photonic Structures Containing CdTe / ZnTe Quantum Dots". Acta Phys. Pol. A **116** (2009), 888.

[18] M. Lewenstein, A. Sanpera, V. Ahufinger, B. Damski, A. Sen De, and U. Sen. "Ultracold atomic gases in optical lattices: mimicking condensed matter physics and beyond". Adv. Phys. **56** (2007), 243. arXiv: 0606771 [cond-mat] (cit. on pp. 5, 9, 35).

[19] S. Haroche and J.-M. Raimond. *Exploring the Quantum Atoms, Cavities, and Photons*. Oxford Univ. Press, 2006 (cit. on pp. 5, 9, 21, 35, 103).

[20] R. P. Feynman. "Simulating physics with computers". Int. J. Theor. Phys. **21** (1982), 467. arXiv: 9508027 [quant-ph] (cit. on pp. 5, 9).

[21] S. Lloyd. "Universal Quantum Simulators". Science **273** (1996), 1073 (cit. on pp. 5, 9).

[22] W. P. Schleich et al. "Quantum technology: from research to application". Appl. Phys. B **122** (2016), 1 (cit. on pp. 5, 9).

[23] A. K. Mohapatra, M. G. Bason, B. Butscher, K. J. Weatherill, and C. S. Adams. "A giant electro-optic effect using polarizable dark states". Nat. Phys. **4** (2008), 890 (cit. on pp. 5, 9, 22, 36, 96).

[24] Y. O. Dudin and A. Kuzmich. "Strongly interacting Rydberg excitations of a cold atomic gas." Science **336** (2012), 887 (cit. on pp. 5, 9, 22, 41, 96, 117).

[25] T. Peyronel, O. Firstenberg, Q.-Y. Liang, S. Hofferberth, A. V. Gorshkov, T. Pohl, M. D. Lukin, and V. Vuletić. "Quantum nonlinear optics with single photons enabled by strongly interacting atoms." Nature **488** (2012), 57 (cit. on pp. 5, 9, 22, 53, 58, 68, 78, 79, 84, 96, 111, 112, 117, 121, 122, 124).

[26] D. Maxwell, D. J. Szwer, D. P. Barato, H. Busche, J. D. Pritchard, A. Gauguet, K. J. Weatherill, M. P. A. Jones, and C. S. Adams. "Storage and Control of Optical Photons Using Rydberg Polaritons". Phys. Rev. Lett. **110** (2013), 103001. arXiv: 1207.6007v3 (cit. on pp. 5, 9, 22, 39, 96, 116, 126).

[27] L Li, Y. O. Dudin, and A Kuzmich. "Entanglement between light and an optical atomic excitation". Nature **498** (2013), 466 (cit. on pp. 5, 9, 96).

[28] O. Firstenberg, T. Peyronel, Q.-Y. Liang, A. V. Gorshkov, M. D. Lukin, and V. Vuletić. "Attractive photons in a quantum nonlinear medium." Nature **502** (2013), 71 (cit. on pp. 5, 9, 22, 23, 53, 68, 75, 78–82, 85, 93, 96, 100, 122).

[29] S. Baur, D. Tiarks, G. Rempe, and S. Dürr. "Single-Photon Switch based on Rydberg Blockade". Phys. Lev. Lett. **112** (2014), 073901. arXiv: 1307.3509v1 (cit. on pp. 5, 9, 22, 61, 94, 96, 117, 126).

[30] H. Gorniaczyk, C. Tresp, J. Schmidt, H. Fedder, and S. Hofferberth. "Single Photon Transistor Mediated by Inter-State Rydberg Interaction". Phys. Rev. Lett. **113** (2014), 053601. arXiv: 1404.2876v2 (cit. on pp. 5, 9, 22, 53, 61, 93, 96, 108, 109, 116, 117).

[31] D. Tiarks, S. Baur, K. Schneider, S. Dürr, and G. Rempe. "Single-Photon Transistor Using a Förster Resonance". Phys. Rev. Lett. **113** (2014), 053602 (cit. on pp. 5, 9, 22, 23, 53, 61, 96, 108–110, 116, 117, 126).

[32] I. Friedler, D. Petrosyan, M. Fleischhauer, and G. Kurizki. "Long-range interactions and entanglement of slow single-photon pulses". Phys. Rev. A **72** (2005), 043803 (cit. on pp. 5, 9, 21, 22, 82–84, 93, 96).

[33] S. Sevinçli, N. Henkel, C. Ates, T. Pohl, S. Sevincli, N. Henkel, C. Ates, and T. Pohl. "Nonlocal nonlinear optics in cold rydberg gases". Phys. Rev. Lett. **107** (2011), 153001 (cit. on pp. 5, 9, 24, 46, 96).

[34] A. V. Gorshkov, S. R. Manmana, G. Chen, J. Ye, E. Demler, M. D. Lukin, and A. M. Rey. "Tunable superfluidity and quantum magnetism with ultracold polar molecules". Phys. Rev. Lett. **107** (2011). arXiv: 1106.1644 (cit. on pp. 5, 9, 111, 112, 116).

[35] A. V. Gorshkov, R. Nath, and T. Pohl. "Dissipative Many-body Quantum Optics in Rydberg Media". Phys. Lev. Lett. **110** (2013), 153601. arXiv: 1211.7060v1 (cit. on pp. 5, 9, 23, 96).

[36] J. Otterbach, M. Moos, D. Muth, and M. Fleischhauer. "Wigner Crystallization of Single Photons in Cold Rydberg Ensembles". Phys. Rev. Lett. **111** (2013), 113001. arXiv: 1304.8096v2 (cit. on pp. 5, 9, 23, 53, 58, 81, 96).

[37] D. Tiarks, S. Schmidt, G. Rempe, and S. Dürr. "Optical π Phase Shift Created with a Single-Photon Pulse" (2015). arXiv: 1512.05740 (cit. on pp. 5, 9, 22, 84).

[38] A. V. Gorshkov, J. Otterbach, M. Fleischhauer, T. Pohl, and M. D. Lukin. "Photon-Photon Interactions via Rydberg Blockade". Phys. Rev. Lett. **107** (2011), 133602. arXiv: 1103.3700 (cit. on pp. 5, 9, 22, 58, 61, 70, 75, 78, 79, 82–84, 86, 89, 108).

[39] B. He, A. V. Sharypov, J. Sheng, C. Simon, and M. Xiao. "Two-Photon Dynamics in Coherent Rydberg Atomic Ensemble". Phys. Rev. Lett. **112** (2014), 133606 (cit. on pp. 5, 9, 22, 84, 85, 94, 96, 132, 136).

[40] M. Moos, M. Höning, R. Unanyan, and M. Fleischhauer. "Many-body physics of Rydberg dark-state polaritons in the strongly interacting regime". Phys. Rev. A **92** (2015), 053846 (cit. on pp. 5, 9, 23, 57, 58, 96).

[41] M. F. Maghrebi, N. Y. Yao, M. Hafezi, T. Pohl, O. Firstenberg, and A. V. Gorshkov. "Fractional quantum Hall states of Rydberg polaritons". Phys. Rev. A **91** (2015), 033838 (cit. on pp. 5, 9, 24, 49, 96, 126).

[42] T. Caneva, M. T. Manzoni, T. Shi, J. S. Douglas, J. I. Cirac, and D. E. Chang. "Quantum dynamics of propagating photons with strong interactions: a generalized input-output formalism". New J. Phys. **17** (2015), 113001. arXiv: 1501.04427 (cit. on pp. 5, 9, 23, 96).

[43] T. Shi, D. E. Chang, and J. I. Cirac. "Multiphoton-scattering theory and generalized master equations". Phys. Rev. A **92** (2015), 053834. arXiv: 1507.08699 (cit. on pp. 5, 9, 23, 96).

[44] J. Shapiro. "Single-photon Kerr nonlinearities do not help quantum computation". Phys. Rev. A **73** (2006), 062305 (cit. on pp. 6, 11, 84, 97, 102).

[45] X. Hu, P. Jiang, C. Ding, H Yang., Q. Gong, H. Yang, and Q. Gong. "Picosecond and low-power all-optical switching based on an organic photonic-bandgap microcavity". Nat. Photon. **2** (2008), 185 (cit. on pp. 21, 95).

[46] D. A. B. Miller. "Are optical transistors the logical next step?" Nat. Photon. **4** (2010), 3 (cit. on pp. 21, 95).

[47] G. J. Milburn. "Quantum optical Fredkin gate". Phys. Rev. Lett. **62** (1989), 2124 (cit. on pp. 21, 95).

[48] H. J. Kimble. "The quantum internet." Nature **453** (2008), 1023 (cit. on pp. 21, 95).

[49] A Muthukrishnan, M. O. Scully, and M. S. Zubairy. "Quantum microscopy using photon correlations". J. Opt. B **6** (2004), S575 (cit. on pp. 21, 95).

[50] V Giovannetti, S Lloyd, and L Maccone. "Advances in quantum metrology". Nat. Photon. **5** (2011), 222 (cit. on pp. 21, 95).

[51] D. E. Chang, V. Vuletić, and M. D. Lukin. "Quantum nonlinear optics — photon by photon". Nat. Photonics **8** (2014), 685 (cit. on pp. 21, 33, 45).

[52] N. Matsuda, R. Shimizu, Y. Mitsumori, H. Kosaka, and K. Edamatsu. "Observation of optical-fibre Kerr nonlinearity at the single-photon level". Nat. Photonics **3** (2009), 95 (cit. on pp. 21, 96).

[53] I. Fushman, D. Englund, A. Faraon, N. Stoltz, P. Petroff, and J. Vuckovic. "Controlled phase shifts with a single quantum dot." Science **320** (2008), 769 (cit. on pp. 21, 83).

[54] A. Rauschenbeutel, G. Nogues, S. Osnaghi, P. Bertet, M. Brune, J. Raimond, and S. Haroche. "Coherent Operation of a Tunable Quantum Phase Gate in Cavity QED". Phys. Rev. Lett. **83** (1999), 5166 (cit. on p. 21).

[55] M. H. Devoret and R. J. Schoelkopf. "Superconducting circuits for quantum information: An outlook". Science **339** (2013), 1169 (cit. on p. 21).

[56] G. Kirchmair, B. Vlastakis, Z. Leghtas, S. E. Nigg, H. Paik, E. Ginossar, M. Mirrahimi, L. Frunzio, S. M. Girvin, and R. J. Schoelkopf. "Observation of quantum state collapse and revival due to the single-photon Kerr effect." Nature **495** (2013), 205. arXiv: 1211.2228 (cit. on p. 21).

[57] M. Fleischhauer, A. Imamoglu, and J. P. Marangos. "Electromagnetically induced transparency: Optics in coherent media". Rev. Mod. Phys. **77** (2005), 633 (cit. on pp. 21, 27, 30, 33, 83).

[58] K. Hammerer, A. S. Sorensen, and E. S. Polzik. "Quantum interface between light and atomic ensembles". Rev. Mod. Phys. **82** (2010), 1041. arXiv: 0807.3358 (cit. on p. 21).

[59] M. Bajcsy, S. Hofferberth, V. Balic, T. Peyronel, M. Hafezi, A. S. Zibrov, V. Vuletic, and M. D. Lukin. "Efficient all-optical switching using slow light within a hollow fiber". Phys. Rev. Lett. **102** (2009), 203902 (cit. on p. 21).

[60] V. Venkataraman, K. Saha, P. Londero, and A. L. Gaeta. "Few-photon all-optical modulation in a photonic band-gap fiber". Phys. Rev. Lett. **107** (2011), 193902 (cit. on p. 21).

[61] H. Tanji-Suzuki, W. Chen, R. Landig, J. Simon, and V. Vuletić. "Vacuum-induced transparency." Science **333** (2011), 1266 (cit. on p. 21).

[62] W. Chen, K. M. Beck, R. Bücker, M. Gullans, M. D. Lukin, H. Tanji-Suzuki, and V. Vuletić. "All-optical switch and transistor gated by one stored photon." Science **341** (2013), 768 (cit. on pp. 21, 41).

[63] M. D. Lukin, M. Fleischhauer, and R. Cote. "Dipole Blockade and Quantum Information Processing in Mesoscopic Atomic Ensembles". Phys. Rev. Lett. **87** (2001), 037901 (cit. on pp. 21, 22, 39, 41, 64, 108).

[64] M. Saffman, T. G. Walker, and K. Mølmer. "Quantum information with Rydberg atoms". Rev. Mod. Phys. **82** (2010), 2313. arXiv: 0909.4777v3 (cit. on pp. 21, 36, 37, 40, 41, 116).

[65] T. Wilk, A. Gaëtan, C. Evellin, J. Wolters, Y. Miroshnychenko, P. Grangier, and A. Browaeys. "Entanglement of Two Individual Neutral Atoms Using Rydberg Blockade". Phys. Rev. Lett. **104** (2010), 010502 (cit. on p. 21).

[66] L. Isenhower, E. Urban, X. L. Zhang, a. T. Gill, T. Henage, T. A. Johnson, T. G. Walker, and M. Saffman. "Demonstration of a Neutral Atom Controlled-NOT Quantum Gate". Phys. Rev. Lett. **104** (2010), 010503 (cit. on p. 21).

[67] H. Weimer, M. Müller, I. Lesanovsky, P. Zoller, and H. P. Büchler. "A Rydberg quantum simulator". Nat. Phys. **6** (2010), 382. arXiv: 0907.1657 (cit. on p. 21).

[68] Y.-Y. Jau, A. M. Hankin, T. Keating, I. H. Deutsch, and G. W. Biedermann. "Entangling atomic spins with a Rydberg-dressed spin-flip blockade". Nat Phys **12** (2016), 71 (cit. on p. 21).

[69] P. Schauss, M. Cheneau, M. Endres, T. Fukuhara, S. Hild, A. Omran, T. Pohl, C. Gross, S. Kuhr, and I. Bloch. "Observation of spatially ordered structures in a two-dimensional Rydberg gas". Nature **491** (2012), 87 (cit. on pp. 21, 41).

[70] P. Schauss, J. Zeiher, T. Fukuhara, S. Hild, M. Cheneau, T. Macrì, T. Pohl, I. Bloch, and C. Gross. "Crystallization in Ising quantum magnets". Science **347** (2015), 1455 (cit. on pp. 21, 41).

[71] T. M. Weber, M. Höning, T. Niederprüm, T. Manthey, O. Thomas, V. Guarrera, M. Fleischhauer, G. Barontini, and H. Ott. "Mesoscopic Rydberg-blockaded ensembles in the superatom regime and beyond". Nat Phys **11** (2015), 157 (cit. on p. 21).

[72] A. W. Glaetzle, M. Dalmonte, R. Nath, C. Gross, I. Bloch, and P. Zoller. "Designing Frustrated Quantum Magnets with Laser-Dressed Rydberg Atoms". Phys. Rev. Lett. **114** (2015), 173002 (cit. on pp. 21, 41, 116, 126).

[73] R. M. W. van Bijnen and T. Pohl. "Quantum Magnetism and Topological Ordering via Rydberg Dressing near Förster Resonances". Phys. Rev. Lett. **114** (2015), 243002 (cit. on pp. 21, 41, 116, 126).

[74] A. K. Mohapatra, T. R. Jackson, and C. S. Adams. "Coherent Optical Detection of Highly Excited Rydberg States Using Electromagnetically Induced Transparency". Phys. Rev. Lett. **98** (2007), 113003 (cit. on pp. 22, 83).

[75] J. D Pritchard, D. Maxwell, A. Gauguet, K. Weatherill, M. Jones, and C. Adams. "Cooperative Atom-Light Interaction in a Blockaded Rydberg Ensemble". Phys. Rev. Lett. **105** (2010), 193603 (cit. on pp. 22, 43, 83, 117).

[76] V. Parigi, E. Bimbard, J. Stanojevic, A. J. Hilliard, F. Nogrette, R. Tualle-Brouri, A. Ourjoumtsev, and P. Grangier. "Observation and Measurement of Interaction-Induced Dispersive Optical Nonlinearities in an Ensemble of Cold Rydberg Atoms". Phys. Rev. Lett. **109** (2012), 233602 (cit. on pp. 22, 83).

[77] W. Li, C. Ates, and I. Lesanovsky. "Nonadiabatic Motional Effects and Dissipative Blockade for Rydberg Atoms Excited from Optical Lattices or Microtraps". Phys. Rev. Lett. **110** (2013), 213005 (cit. on p. 22).

[78] M. Khazali, K. Heshami, and C. Simon. "Photon-photon gate via the interaction between two collective Rydberg excitations". PRA **91** (2015), 030301(R). arXiv: 1407.7510 (cit. on pp. 22, 84, 85).

[79] D Paredes-Barato and C. S. S. Adams. "All-optical quantum information processing using Rydberg gates". Phys. Rev. Lett. **112** (2014), 40501 (cit. on pp. 22, 84).

[80] A. Gaj, A. T. Krupp, J. B. Balewski, R Loew, S. Hofferberth, and T. Pfau. "From molecular spectra to a density shift in dense Rydberg gases." Nat. Commun. **5** (2014), 4546. arXiv: 1404.5761 (cit. on pp. 22, 41).

[81] J. Stanojevic, V. Parigi, E. Bimbard, A. Ourjoumtsev, and P. Grangier. "Dispersive optical nonlinearities in a Rydberg electromagnetically-induced-transparency medium". Phys. Rev. A **88** (2013), 053845 (cit. on p. 22).

[82] A Grankin, E Brion, E Bimbard, R Boddeda, I Usmani, A Ourjoumtsev, and P Grangier. "Quantum statistics of light transmitted through an intracavity Rydberg medium". New J. Phys. **16** (2014), 043020. arXiv: 1312.2621v1 (cit. on p. 22).

[83] S. Das et al. "Photonic controlled-phase gates through Rydberg blockade in optical cavities". Phys. Rev. A **93** (2016), 040303. arXiv: 1506.04300v1 (cit. on pp. 22, 84).

[84] G. Günter, H. Schempp, M. Robert-de Saint-Vincent, V. Gavryusev, S. Helmrich, C. S. Hofmann, S. Whitlock, and M. Weidemüller. "Observing the dynamics of dipole-mediated energy transport by interaction-enhanced imaging." Science **342** (2013), 954 (cit. on pp. 22, 23, 108, 111, 114, 116, 126).

[85] D. Cano and J. Fortágh. "Multiatom entanglement in cold Rydberg mixtures". Phys. Rev. A **89** (2014), 043413 (cit. on pp. 22, 45, 116).

[86] W. Li and I. Lesanovsky. "Coherence in a cold-atom photon switch". Phys. Rev. A **92** (2015), 043828 (cit. on pp. 22, 108).

[87] Y.-M. Liu, X.-D. Tian, D. Yan, Y. Zhang, C.-L. Cui, and J.-H. Wu. "Nonlinear modifications of photon correlations via controlled single and double Rydberg blockade". Phys. Rev. A **91** (2015), 043802 (cit. on pp. 22, 116).

[88] B. Olmos, W. Li, S. Hofferberth, and I. Lesanovsky. "Amplifying single impurities immersed in a gas of ultracold atoms". Phys. Rev. A **84** (2011), 041607 (cit. on pp. 23, 108).

[89] G. Günter, M. Robert-de Saint-Vincent, H. Schempp, C. S. Hofmann, S. Whitlock, and M. Weidemüller. "Interaction Enhanced Imaging of Individual Rydberg Atoms in Dense Gases". Phys. Rev. Lett. **108** (2012), 013002 (cit. on pp. 23, 108).

[90] J. Honer, R. Löw, H. Weimer, T. Pfau, and H. P. Büchler. "Artificial Atoms Can Do More Than Atoms: Deterministic Single Photon Subtraction from Arbitrary Light Fields". Phys. Rev. Lett. **107** (2011), 093601. arXiv: 1103.1319v1 (cit. on p. 23).

[91] C. Tresp, C. Zimmer, I. Mirgorodskiy, H. Gorniaczyk, A. Paris-Mandoki, and S. Hofferberth. "Single-photon absorber based on strongly interacting Rydberg atoms" (2016). arXiv: 1605.04456 (cit. on p. 23).

[92] M. J. Gullans, Y. Wang, J. D. Thompson, Q. Y. Liang, V. Vuletic, M. D. Lukin, and A. V. Gorshkov. "Effective Field Theory for Rydberg Polaritons" (2016). arXiv: 1605.05651 (cit. on pp. 23, 105).

[93] A. Sommer, H. P. Büchler, and J. Simon. "Quantum Crystals and Laughlin Droplets of Cavity Rydberg Polaritons" (2015). arXiv: 1506.00341v1 (cit. on p. 24).

[94] J. Ningyuan, A. Georgakopoulos, A. Ryou, N. Schine, A. Sommer, and J. Simon. "Observation and characterization of cavity Rydberg polaritons". Phys. Rev. A **93** (2016), 41802 (cit. on p. 24).

[95] R. W. Boyd. *Nonlinear Optics*. 2008, 613 (cit. on pp. 25, 26).

[96] J Pritchard, K Weatherill, and C Adams. "Nonlinear Optics Using Cold Rydberg Atoms". Annu. Rev. Cold Atoms Mol. Vol. 1 (2013), 301 (cit. on pp. 26, 41).

[97] S. E. Harris, J. E. Field, and A Imamoglu. "Nonlinear optical processes using electromagnetically induced transparency". Phys. Rev. Lett. **64** (1990), 1107 (cit. on p. 27).

[98] K.-J. Boller, A. Imamoğlu, and S. E. Harris. "Observation of electromagnetically induced transparency". Phys. Rev. Lett. **66** (1991), 2593 (cit. on pp. 27, 33).

[99] M. D. Lukin. "Colloquium : Trapping and manipulating photon states". **75** (2003) (cit. on pp. 27, 33).

[100] M. O. Scully and M. S. Zubairy. *Quantum Optics*. 1997 (cit. on p. 27).

[101] C. L. G. Alzar, M. a. G. Martinez, and P. Nussenzveig. "Classical Analog of Electromagnetically Induced Transparency". Am. J. Phys. **37** (2001), 6. arXiv: 0107061 [quant-ph] (cit. on p. 29).

[102] J. Gea-Banacloche, Y.-q. Li, S.-z. Jin, and M. Xiao. "Electromagnetically induced transparency in ladder-type inhomogeneously broadened media: Theory and experiment". Phys. Rev. A **51** (1995) (cit. on p. 30).

[103] O. Firstenberg, C. S. Adams, and S. Hofferberth. "Nonlinear quantum optics mediated by Rydberg interactions" (2016). arXiv: 1602.06117 (cit. on pp. 30, 41).

[104] E. Arimondo. "Coherent population trapping in laser spectroscopy". Prog. Opt. **35** (1996), 257 (cit. on p. 33).

[105] L. V. Hau, S. E. Harris, Z. Dutton, and C. H. Behroozi. "Light speed reduction to 17 metres per second in an ultracold atomic gas". **397** (1999), 594 (cit. on p. 33).

[106] M. S. Bigelow, N. N. Lepeshkin, and R. W. Boyd. "Observation of ultraslow light propagation in a ruby crystal at room temperature." Phys. Rev. Lett. **90** (2003), 113903 (cit. on p. 33).

[107] M. S. Bigelow, N. N. Lepeshkin, and R. W. Boyd. "Superluminal and slow light propagation in a room-temperature solid." Science **301** (2003), 200 (cit. on p. 33).

[108] T. Wang, R. Rajapakse, and S. F. Yelin. "Electromagnetically induced transparency and slow light with n-doped GaAs". Opt. Commun. **272** (2007), 154 (cit. on p. 33).

[109] M Bajcsy, a. S. Zibrov, and M. D. Lukin. "Stationary pulses of light in an atomic medium." Nature **426** (2003), 638 (cit. on p. 33).

[110] F. Zimmer, A. André, M. D. Lukin, and M. Fleischhauer. "Coherent control of stationary light pulses". Opt. Commun. **264** (2006), 441 (cit. on p. 33).

[111] a André and M. D. Lukin. "Manipulating light pulses via dynamically controlled photonic band gap." Phys. Rev. Lett. **89** (2002), 143602. arXiv: 0205072 [quant-ph] (cit. on p. 33).

[112] M. D. Eisaman, A. André, F. Massou, M. Fleischhauer, A. S. Zibrov, and M. D. Lukin. "Electromagnetically induced transparency with tunable single-photon pulses." Nature **438** (2005), 837 (cit. on p. 33).

[113] D. Höckel and O. Benson. "Electromagnetically induced transparency in cesium vapor with probe pulses on the single-photon level". Phys. Rev. Lett. **105** (2010), 153605. arXiv: 0807.3358 (cit. on p. 33).

[114] M. Mücke, E. Figueroa, J. Bochmann, C. Hahn, K. Murr, S. Ritter, C. J. Villas-Boas, and G. Rempe. "Electromagnetically induced transparency with single atoms in a cavity." Nature **465** (2010), 755 (cit. on p. 33).

[115] T. Kampschulte, W. Alt, S. Brakhane, M. Eckstein, R. Reimann, A. Widera, and D. Meschede. "Optical control of the refractive index of a single atom". Phys. Rev. Lett. **105** (2010). arXiv: 1004.5348 (cit. on p. 33).

[116] L. Slodička, G. Hétet, S. Gerber, M. Hennrich, and R. Blatt. "Electromagnetically Induced Transparency from a Single Atom in Free Space". Phys. Rev. Lett. **105** (2010), 153604. arXiv: 1005.3289v1 (cit. on p. 33).

[117] M Fleischhauer and M. Lukin. "Dark-state polaritons in electromagnetically induced transparency". Phys. Rev. Lett. **84** (2000), 5094 (cit. on pp. 33, 34).

[118] M. Fleischhauer and M. Lukin. "Quantum memory for photons: Dark-state polaritons". Phys. Rev. A **65** (2002), 022314 (cit. on pp. 33, 34).

[119] A. Gorshkov, A. André, M. Lukin, and A. Sørensen. "Photon storage in Λ-type optically dense atomic media. II. Free-space model". Phys. Rev. A **76** (2007), 033805 (cit. on p. 33).

[120] D. F. Phillips, A. Fleischhauer, a. Mair, R. L. Walsworth, and M. D. Lukin. "Storage of Light in Atomic Vapor". Phys. Rev. Lett. **86** (2001), 783. arXiv: 0012138 [quant-ph] (cit. on p. 33).

[121] C. Liu, Z. Dutton, C. H. Behroozi, and L. V. Hau. "Observation of coherent optical information storage in an atomic medium using halted light pulses". Nature **409** (2001), 490 (cit. on p. 33).

[122] A. V. Turukhin, V. S. Sudarshanam, M. S. Shahriar, J. A. Musser, B. S. Ham, and P. R. Hemmer. "Observation of Ultraslow and Stored Light Pulses in a Solid". Phys. Rev. Lett. **88** (2001), 023602 (cit. on p. 33).

[123] I. Novikova, A. V. Gorshkov, D. F. Phillips, A. S. Sørensen, M. D. Lukin, and R. L. Walsworth. "Optimal control of light pulse storage and retrieval". Phys. Rev. Lett. **98** (2007), 243602. arXiv: 0702266v1 [arXiv:quant-ph] (cit. on p. 33).

[124] U. Schnorrberger, J. D. Thompson, S. Trotzky, R. Pugatch, N. Davidson, S. Kuhr, and I. Bloch. "Electromagnetically Induced Transparency and Light Storage in an Atomic Mott Insulator". Phys. Rev. Lett. **103** (2009), 033003 (cit. on p. 33).

[125] H. P. Specht. "A single-atom quantum memory". Nature **473** (2011), 190 (cit. on p. 33).

[126] T. Chanelière, D. Matsukevich, S. Jenkins, S. Lan, T. Kennedy, and A. Kuzmich. "Storage and retrieval of single photons transmitted between remote quantum memories." Nature **438** (2005), 833. arXiv: 0511014 [quant-ph] (cit. on p. 33).

[127] C.-S. Chuu, T. Strassel, B. Zhao, M. Koch, Y.-A. Chen, S. Chen, Z.-S. Yuan, J. Schmiedmayer, and J.-W. Pan. "Quantum Memory with Optically Trapped Atoms". Phys. Rev. Lett. **101** (2008), 120501. arXiv: 0808.2687v1 (cit. on p. 33).

[128] M. Himsworth, P. Nisbet, J. Dilley, G. Langfahl-Klabes, and A. Kuhn. "EIT-based quantum memory for single photons from cavity-QED". Appl. Phys. B Lasers Opt. **103** (2011), 579. arXiv: 1011.4755 (cit. on p. 33).

[129] N. Sangouard, C. Simon, H. De Riedmatten, and N. Gisin. "Quantum repeaters based on atomic ensembles and linear optics". Rev. Mod. Phys. **83** (2011), 33. arXiv: 0807.3358v5 (cit. on p. 33).

[130] L. M. Duan, M. D. Lukin, J. I. Cirac, and P Zoller. "Long-distance quantum communication with atomic ensembles and linear optics." Nature **414** (2001), 413 (cit. on p. 33).

[131] I. Bloch, W. Zwerger, and J. Dalibard. "Many-body physics with ultracold gases". Rev. Mod. Phys. **80** (2008), 885 (cit. on p. 35).

[132] R. Blatt and C. F. Roos. "Quantum simulations with trapped ions". Nat. Phys. **8** (2012), 277 (cit. on p. 35).

[133] T. Lahaye, C. Menotti, L. Santos, M. Lewenstein, and T. Pfau. "The physics of dipolar bosonic quantum gases". Reports Prog. Phys. **72** (2009), 126401. arXiv: 0905.0386v1 (cit. on pp. 35, 115).

[134] M. A. Baranov, M. Dalmonte, G. Pupillo, and P. Zoller. "Condensed matter theory of dipolar quantum gases". Chem. Rev. **112** (2012), 5012. arXiv: 1207.1914 (cit. on p. 35).

[135] K. Baumann, C. Guerlin, F. Brennecke, and T. Esslinger. "Dicke quantum phase transition with a superfluid gas in an optical cavity." Nature **464** (2010), 1301 (cit. on p. 35).

[136] T. F. Gallagher. *Rydberg Atoms*. Cambridge Monographs on Atomic, Molecular and Chemical Physics. Cambridge University Press, 2005 (cit. on pp. 35, 36).

[137] R. Löw, H. Weimer, J. Nipper, J. B. Balewski, B. Butscher, H. P. Büchler, and T. Pfau. "An experimental and theoretical guide to strongly interacting Rydberg gases". J. Phys. B At. Mol. Opt. Phys. **45** (2012), 113001 (cit. on p. 36).

[138] J. Lim, H.-g. Lee, and J. Ahn. "Review of cold Rydberg atoms and their applications". J. Korean Phys. Soc. **63** (2013), 867 (cit. on p. 36).

[139] J. B. Balewski, A. T. Krupp, A. Gaj, D. Peter, H. P. Büchler, R. Löw, S. Hofferberth, and T. Pfau. "Coupling a single electron to a Bose-Einstein condensate". Nature **502** (2013), 664. arXiv: 1306.5181v1 (cit. on pp. 36, 41).

[140] A. Osterwalder and F. Merkt. "Using high Rydberg states as electric field sensors". Phys. Rev. Lett. **82** (1999), 1831 (cit. on p. 36).

[141] A. Tauschinsky, R. M. T. Thijssen, S. Whitlock, H. B. van Linden van den Heuvell, and R. J. C. Spreeuw. "Spatially resolved excitation of Rydberg atoms and surface effects on an atom chip". Phys. Rev. A **81** (2010), 063411 (cit. on p. 36).

[142] R. P. Abel, C. Carr, U. Krohn, and C. S. Adams. "Electrometry near a dielectric surface using Rydberg electromagnetically induced transparency". Phys. Rev. A **84** (2011), 023408. arXiv: 1106.3495 (cit. on p. 36).

[143] S. Müller, J. Billy, E. A. L. Henn, H. Kadau, A. Griesmaier, M. Jona-Lasinio, L. Santos, and T. Pfau. "Stability of a dipolar Bose-Einstein condensate in a one-dimensional lattice". Phys. Rev. A **84** (2011), 053601 (cit. on p. 36).

[144] V. Y. F. Leung, A. Tauschinsky, N. J. Van Druten, and R. J. C. Spreeuw. "Microtrap arrays on magnetic film atom chips for quantum information science". Quantum Inf. Process. **10** (2011), 955. arXiv: 1104.3067 (cit. on p. 36).

[145] J. A. Sedlacek, A. Schwettmann, H. Kubler, and J. P. Shaffer. "Atom-based vector microwave electrometry using rubidium rydberg atoms in a vapor cell". Phys. Rev. Lett. **111** (2013), 063001. arXiv: 1304.4299 (cit. on p. 36).

[146] J. M. Raimond, M. Brune, and S. Haroche. "Colloquium: Manipulating quantum entanglement with atoms and photons in a cavity". Rev. Mod. Phys. **73** (2001), 565 (cit. on p. 36).

[147] C. Boisseau, I. Simbotin, and R. Côté. "Macrodimers: ultralong range Rydberg molecules." Phys. Rev. Lett. **88** (2002), 133004. arXiv: 0201022 [physics] (cit. on p. 36).

[148] K. Singer, J. Stanojevic, M. Weidemüller, and R. Côté. "Long-range interactions between alkali Rydberg atom pairs correlated to the ns–ns, np–np and nd–nd asymptotes". J. Phys. B At. Mol. Opt. Phys. **38** (2005), S295 (cit. on pp. 36, 108, 116).

[149] T. G. Walker and M. Saffman. "Consequences of Zeeman degeneracy for the van der Waals blockade between Rydberg atoms". Phys. Rev. A **77** (2008), 032723 (cit. on pp. 36, 38, 108, 110, 116, 119, 120).

[150] K. Singer, J. Stanojevic, M. Weidemüller, and R. Côté. "Long-range interactions between alkali Rydberg atom pairs correlated to the n s– n s, n p– n p and n d– n d asymptotes". J. Phys. B At. Mol. Opt. Phys. **38** (2005), S295 (cit. on p. 36).

[151] D. Peter. "Quantum states with topological properties via dipolar interactions". PhD thesis. University of Stuttgart, 2015 (cit. on p. 37).

[152] E. Altiere, D. P. Fahey, M. W. Noel, R. J. Smith, and T. J. Carroll. "Dipole-dipole interaction between rubidium Rydberg atoms". Phys. Rev. A **84** (2011), 053431 (cit. on p. 39).

[153] J. Nipper, J. Balewski, A. Krupp, S. Hofferberth, R. Löw, and T. Pfau. "Atomic Pair-State Interferometer: Controlling and Measuring an Interaction-Induced Phase Shift in Rydberg-Atom Pairs". Phys. Rev. X **2** (2012), 031011 (cit. on pp. 39, 108).

[154] I. I. Ryabtsev, D. B. Tretyakov, I. I. Beterov, and V. M. Entin. "Observation of the Stark-Tuned Förster Resonance between Two Rydberg Atoms". Phys. Rev. Lett. **104** (2010), 073003. arXiv: 0909.3239 (cit. on pp. 39, 108).

[155] A. Reinhard, K. C. Younge, T. C. Liebisch, B. Knuffman, P. R. Berman, and G. Raithel. "Double-resonance spectroscopy of interacting Rydberg-atom systems". Phys. Rev. Lett. **100** (2008), 233201 (cit. on pp. 39, 108).

[156] K Afrousheh, P Bohlouli-Zanjani, J. A. Petrus, and J. D. D. Martin. "Determination of the Rb ng-series quantum defect by electric-field-induced resonant energy transfer between cold Rydberg atoms". Phys. Rev. A **74** (2006), 062712 (cit. on p. 39).

[157] K. Afrousheh, P. Bohlouli-Zanjani, D. Vagale, A. Mugford, M. Fedorov, and J. D. D. Martin. "Spectroscopic observation of resonant electric dipole-dipole interactions between cold Rydberg atoms". Phys. Rev. Lett. **93** (2004), 233001. arXiv: 0411076 [physics] (cit. on pp. 39, 108).

[158] A. Tauschinsky, C. S. E. Van Ditzhuijzen, L. D. Noordam, and H. B. V. L. Van Den Heuvell. "Radio-frequency-driven dipole-dipole interactions in spatially separated volumes". Phys. Rev. A **78** (2008), 063409. arXiv: 0808.1648 (cit. on p. 39).

[159] D. B. Tretyakov, I. I. Beterov, V. M. Entin, E. A. Yakshina, I. I. Ryabtsev, S. F. Dyubko, E. A. Alekseev, N. L. Pogrebnyak, N. N. Bezuglov, and E Arimondo. "Effect of photoions on the line shape of the Förster resonance lines and microwave transitions in cold rubidium Rydberg atoms". J. Exp. Theor. Phys. **114** (2012), 14 (cit. on p. 39).

[160] G Günter, H Schempp, M Robert-de Saint-Vincent, V Gavryusev, S Helmrich, C. S. Hofmann, S Whitlock, and M Weidemüller. "Observing the dynamics of dipole-mediated energy transport by interaction-enhanced imaging." Science **342** (2013), 954 (cit. on p. 39).

[161] J. Nipper. "Interacting Rydberg atoms: Coherent control at Förster resonances and polar homonuclear molecules". Ph.D. thesis. University of Stuttgart, 2012 (cit. on p. 39).

[162] M. Şener, J. Strümpfer, J. Hsin, D. Chandler, S. Scheuring, C. N. Hunter, and K. Schulten. "Förster energy transfer theory as reflected in the structures of photosynthetic light-harvesting systems." Chemphyschem **12** (2011), 518 (cit. on p. 39).

[163] L. Beguin, A. Vernier, R. Chicireanu, T. Lahaye, A. Browaeys, H. Labuhn, and L. Béguin. "Direct Measurement of the van der Waals Interaction between Two Rydberg Atoms". Phys. Rev. Lett. **110** (2013), 263201. arXiv: 1302.4262v1 (cit. on p. 39).

[164] D. Barredo, S. Ravets, H. Labuhn, L. Béguin, A. Vernier, F. Nogrette, T. Lahaye, and A. Browaeys. "Demonstration of a Strong Rydberg Blockade in Three-Atom Systems with Anisotropic Interactions". Phys. Rev. Lett. **112** (2014), 183002 (cit. on p. 39).

[165] S. Ravets, H. Labuhn, D. Barredo, L. Béguin, T. Lahaye, and A. Browaeys. "Coherent dipole-dipole coupling between two single atoms at a Förster resonance". Nat. Phys. **10** (2014), 914. arXiv: 1405.7804 (cit. on p. 39).

[166] S. Ravets, H. Labuhn, D. Barredo, T. Lahaye, and A. Browaeys. "Measurement of the angular dependence of the dipole-dipole interaction between two individual Rydberg atoms at a Förster resonance". Phys. Rev. A **92** (2015), 020701. arXiv: 1504.00301v1 (cit. on pp. 39, 108, 116).

[167] D. Jaksch, J. I. Cirac, P. Zoller, S. Rolston, R Cote, M. D. M. Lukin, and R. Côté. "Fast quantum gates for neutral atoms". Phys. Rev. Lett. **85** (2000), 2208 (cit. on p. 39).

[168] V. Vuletic. "Quantum networks: When superatoms talk photons". Nat. Phys. **2** (2006), 801 (cit. on p. 40).

[169] T. Keating, K. Goyal, Y. Y. Jau, G. W. Biedermann, A. J. Landahl, and I. H. Deutsch. "Adiabatic quantum computation with rydberg-dressed atoms". Phys. Rev. A **87** (2013), 052314. arXiv: 1209.4112 (cit. on p. 41).

[170] H. Weimer, M. Müller, I. Lesanovsky, P. Zoller, and H. P. Büchler. "A Rydberg quantum simulator". Nat. Phys. **6** (2010), 382 (cit. on p. 41).

[171] M. Saffman and T. Walker. "Creating single-atom and single-photon sources from entangled atomic ensembles". Phys. Rev. A **66** (2002), 065403 (cit. on p. 41).

[172] M. Ebert, A. Gill, M. Gibbons, X. Zhang, M. Saffman, and T. G. Walker. "Atomic fock state preparation using Rydberg blockade". Phys. Rev. Lett. **112** (2014), 043602. arXiv: 1310.7561v1 (cit. on p. 41).

[173] A. Gaëtan, Y. Miroshnychenko, T. Wilk, A. Chotia, M. Viteau, D. Comparat, P. Pillet, A. Browaeys, and P. Grangier. "Observation of collective excitation of two individual atoms in the Rydberg blockade regime". en. Nat. Phys. **5** (2009), 115 (cit. on p. 41).

[174] E. Urban, T. a. Johnson, T. Henage, L. Isenhower, D. D. Yavuz, T. G. Walker, and M. Saffman. "Observation of Rydberg blockade between two atoms". Nat. Phys. **5** (2009), 110 (cit. on p. 41).

[175] F. Nogrette, H. Labuhn, S. Ravets, D. Barredo, L. Béguin, A. Vernier, T. Lahaye, and A. Browaeys. "Single-Atom Trapping in Holographic 2D Arrays of Microtraps with Arbitrary Geometries". Phys. Rev. X **4** (2014), 021034 (cit. on p. 41).

[176] M. Ebert, M. Kwon, T. G. Walker, and M. Saffman. "Coherence and Rydberg Blockade of Atomic Ensemble Qubits". Phys. Rev. Lett. **115** (2015), 093601. arXiv: 1501.04083 (cit. on p. 41).

[177] J. Zeiher, P. Schauss, S. Hild, T. Macrì, I. Bloch, and C. Gross. "Microscopic Characterization of Scalable Coherent Rydberg Superatoms". Phys. Rev. X **5** (2015), 031015 (cit. on p. 41).

[178] C. Greene, A. Dickinson, and H. Sadeghpour. "Creation of polar and nonpolar ultra-long-range rydberg molecules". Phys. Rev. Lett. **85** (2000), 2458 (cit. on p. 41).

[179] V. Bendkowsky, B. Butscher, J. Nipper, J. P. Shaffer, R. Löw, and T. Pfau. "Observation of ultralong-range Rydberg molecules." Nature **458** (2009), 1005 (cit. on p. 41).

[180] V. Bendkowsky, B. Butscher, J. Nipper, J. Balewski, J. Shaffer, R. Löw, T. Pfau, W. Li, J. Stanojevic, T. Pohl, and J. Rost. "Rydberg Trimers and Excited Dimers Bound by Internal Quantum Reflection". Phys. Rev. Lett. **105** (2010), 163201 (cit. on p. 41).

[181] W Li, T Pohl, J. M. Rost, S. T. Rittenhouse, H. R. Sadeghpour, J Nipper, B Butscher, J. B. Balewski, V Bendkowsky, R Löw, and T Pfau. "A homonuclear molecule with a permanent electric dipole moment." Science **334** (2011), 1110 (cit. on p. 41).

[182] C. Murray and T. Pohl. "Chapter Seven – Quantum and Nonlinear Optics in Strongly Interacting Atomic Ensembles". *Adv. At. Mol. Opt. Phys.* **65**. 2016, 321 (cit. on p. 41).

[183] M. K. Tey. "Strong interaction between light and a single trapped atom without the need for a cavity". Nat. Phys. **4** (2008), 924 (cit. on p. 41).

[184] G. Zumofen, N. M. Mojarad, V. Sandoghdar, and M. Agio. "Perfect reflection of light by an oscillating dipole". Phys. Rev. Lett. **101** (2008), 180404. arXiv: 0805.3231 (cit. on p. 41).

[185] J. Hwang, M. Pototschnig, R. Lettow, G. Zumofen, A. Renn, S. Götzinger, and V. Sandoghdar. "A single-molecule optical transistor". *Conf. Proc. - Lasers Electro-Optics Soc. Annu. Meet.* 2009, 286 (cit. on p. 41).

[186] S. A. Aljunid, G. Maslennikov, Y. Wang, H. L. Dao, V. Scarani, and C. Kurtsiefer. "Excitation of a single atom with exponentially rising light pulses". Phys. Rev. Lett. **111** (2013), 103001. arXiv: 1304.3761v1 (cit. on p. 41).

[187] K. M. Birnbaum, A Boca, R Miller, a. D. Boozer, T. E. Northup, and H. J. Kimble. "Photon blockade in an optical cavity with one trapped atom." Nature **436** (2013), 87 (cit. on p. 41).

[188] T. Wilk, S. C. Webster, A. Kuhn, and G. Rempe. "Single-Atom Single-Photon Quantum Interface". Science **317** (2007), 488 (cit. on p. 41).

[189] B. Dayan, A. S. Parkins, T. Aoki, E. P. Ostby, K. J. Vahala, and H. J. Kimble. "A photon turnstile dynamically regulated by one atom." Science **319** (2008), 1062 (cit. on p. 41).

[190] N. Henkel, R. Nath, and T. Pohl. "Three-dimensional Roton-Excitations and Supersolid formation in Rydberg-excited Bose-Einstein Condensates". Phys. Rev. Lett. **195302** (2010), 195302. arXiv: 1001.3250 (cit. on p. 44).

[191] J. Honer, H. Weimer, T. Pfau, and H. Büchler. "Collective Many-Body Interaction in Rydberg Dressed Atoms". Phys. Rev. Lett. **105** (2010), 1 (cit. on p. 44).

[192] G. Pupillo, A. Micheli, M. Boninsegni, I. Lesanovsky, and P. Zoller. "Strongly Correlated Gases of Rydberg-Dressed Atoms: Quantum and Classical Dynamics". Phys. Rev. Lett. **104** (2010), 223002 (cit. on p. 44).

[193] J. D. Pritchard, C. S. Adams, and K Mølmer. "Correlated Photon Emission from Multiatom Rydberg Dark States". Phys. Rev. Lett. **108** (2012), 43601 (cit. on p. 45).

[194] S. Xu and S. Fan. "Input-output formalism for few-photon transport: A systematic treatment beyond two photons". Phys. Rev. A **91** (2015), 043845 (cit. on p. 45).

[195] L. D. Carr. "Negative Temperatures?" Science **339** (2013), 42 (cit. on p. 45).

[196] D. Petrosyan. "Two-dimensional crystals of Rydberg excitations in a resonantly driven lattice gas". Phys. Rev. A **88** (2013), 043431. arXiv: 1306.0320v2 (cit. on p. 45).

[197] D. D. B. Rao and K. Mølmer. "Deterministic entanglement of Rydberg ensembles by engineered dissipation". Phys. Rev. A **90** (2014), 062319. arXiv: 1407.1228v1 (cit. on p. 45).

[198] D. Møller, L. Madsen, and K. Mølmer. "Quantum Gates and Multiparticle Entanglement by Rydberg Excitation Blockade and Adiabatic Passage". Phys. Rev. Lett. **100** (2008), 170504 (cit. on p. 45).

[199] M. Müller, I. Lesanovsky, H. Weimer, H. P. Büchler, P. Zoller, M Muller, I. Lesanovsky, H. Weimer, H. P. Buchler, and P. Zoller. "Mesoscopic Rydberg Gate Based on Electromagnetically Induced Transparency". Phys. Rev. Lett. **102** (2009), 170502 (cit. on p. 45).

[200] D. D. B. Rao and K. Mølmer. "Dark entangled steady states of interacting rydberg atoms". Phys. Rev. Lett. **111** (2013), 033606. arXiv: 1304.4466v2 (cit. on p. 45).

[201] D. D. B. Rao and K. Mølmer. "Robust Rydberg-interaction gates with adiabatic passage". Phys. Rev. A **89** (2014), 30301 (cit. on p. 45).

[202] V. R. Overbeck and H. Weimer. "Time evolution of open quantum many-body systems". Phys. Rev. A **93** (2016), 012106. arXiv: 1510.01339 (cit. on p. 46).

[203] H. Weimer. "Variational principle for steady states of dissipative quantum many-body systems". Phys. Rev. Lett. **114** (2015). arXiv: 1409.8307 (cit. on p. 46).

[204] H. Weimer. "Variational analysis of driven-dissipative Rydberg gases". Phys. Rev. A **91** (2015), 1. arXiv: 1501.07284 (cit. on p. 46).

[205] H. Schempp, G. Günter, C. S. Hofmann, C. Giese, S. D. Saliba, B. D. Depaola, T. Amthor, M. Weidemüller, S. Sevinçli, and T. Pohl. "Coherent population trapping with controlled interparticle interactions". Phys. Rev. Lett. **104** (2010). arXiv: 0912.4099 (cit. on p. 46).

[206] C Ates, T Pohl, T Pattard, and J. M. Rost. "Strong interaction effects on the atom counting statistics of ultracold Rydberg gases". J. Phys. B At. Mol. Opt. Phys. **39** (2006), L233 (cit. on p. 46).

[207] C. Ates, T. Pohl, T. Pattard, and J. Rost. "Antiblockade in Rydberg Excitation of an Ultracold Lattice Gas". Phys. Rev. Lett. **98** (2007), 023002 (cit. on p. 46).

[208] C. Ates, T. Pohl, T. Pattard, and J. M. Rost. "Many-body theory of excitation dynamics in an ultracold Rydberg gas". Phys. Rev. A **76** (2007), 013413. arXiv: 0705.4040 (cit. on p. 46).

[209] M. Bonitz. *Quantum Kinetic Theory*. 2nd ed. Springer International Publishing, 2016, XVIII, 406 (cit. on p. 46).

[210] Claude Cohen-Tannoudji, J. Dupont-Roc, and G. Grynberg. *Atom-Photon Interactions*. New York: Wiley, 2004 (cit. on p. 55).

[211] A. A. Abrikosov, L. P. Gorkov, and I. E. Dzyaloshinski. *Methods of quantum field theory in statistical physics*. New York, N.Y.: Dover, 1963 (cit. on pp. 59, 61, 69, 71).

[212] W. Li, D. Viscor, S. Hofferberth, and I. Lesanovsky. "Electromagnetically induced transparency in an entangled medium". Phys. Rev. Lett. **112** (2014), 243601. arXiv: 1404.0311v1 (cit. on pp. 61, 114, 116).

[213] C. Chin, R. Grimm, P. Julienne, and E. Tiesinga. "Feshbach resonances in ultracold gases". Rev. Mod. Phys. **82** (2010), 1225 (cit. on pp. 67, 70, 75).

[214] G. E. Astrakharchik, J. Boronat, J. Casulleras, and S. Giorgini. "Beyond the Tonks-Girardeau Gas: Strongly Correlated Regime in Quasi-One-Dimensional Bose Gases". Phys. Rev. Lett. **95** (2005), 190407 (cit. on p. 81).

[215] S. Chen, L. Guan, X. Yin, Y. Hao, and X.-W. Guan. "Transition from a Tonks-Girardeau gas to a super-Tonks-Girardeau gas as an exact many-body dynamics problem". Phys. Rev. A **81** (2010), 031609 (cit. on p. 81).

[216] M. D. Girardeau and G. E. Astrakharchik. "Wave functions of the super-Tonks-Girardeau gas and the trapped one-dimensional hard-sphere Bose gas". Phys. Rev. A **81** (2010), 061601 (cit. on p. 81).

[217] E. Haller, M. Gustavsson, M. J. Mark, J. G. Danzl, R. Hart, G. Pupillo, and H.-C. Nägerl. "Realization of an excited, strongly correlated quantum gas phase." Science **325** (2009), 1224 (cit. on p. 81).

[218] S. Sala, P.-I. Schneider, and A. Saenz. "Inelastic Confinement-Induced Resonances in Low-Dimensional Quantum Systems". Phys. Rev. Lett. **109** (2012), 073201. arXiv: 1104.1561 (cit. on p. 81).

[219] M. A. Nielsen and I. L. Chuang. *Quantum computation and quantum information*. 2000, 676 (cit. on p. 83).

[220] Q. a. Turchette, C. J. Hood, W. Lange, H. Mabuchi, and H. J. Kimble. "Measurement of conditional phase shifts for quantum logic". Phys. Rev. Lett. **75** (1995), 4710. arXiv: 9511008 [quant-ph] (cit. on p. 83).

[221] J. Volz, M. Scheucher, C. Junge, and A. Rauschenbeutel. "Nonlinear [pi] phase shift for single fibre-guided photons interacting with a single resonator-enhanced atom". Nat Phot. **8** (2014), 965. arXiv: 1403.1860 (cit. on p. 83).

[222] A. Reiserer, N. Kalb, G. Rempe, and S. Ritter. "A quantum gate between a flying optical photon and a single trapped atom." Nature **508** (2014), 237. arXiv: 1404.2453 (cit. on p. 83).

[223] H.-Y. Lo, Y.-C. Chen, P.-C. Su, H.-C. Chen, J.-X. Chen, Y.-C. Chen, I. a. Yu, and Y.-F. Chen. "Electromagnetically-induced-transparency-based cross-phase-modulation at attojoule levels". Phys. Rev. A **83** (2011), 041804 (cit. on p. 83).

[224] B. W. Shiau, M. C. Wu, C. C. Lin, and Y. C. Chen. "Low-light-level cross-phase modulation with double slow light pulses". Phys. Rev. Lett. **106** (2011), 193006 (cit. on p. 83).

[225] A. Feizpour, M. Hallaji, G. Dmochowski, and A. M. Steinberg. "Observation of the nonlinear phase shift due to single post-selected photons". Nat. Phys. **11** (2015), 905. arXiv: 1508.05211 (cit. on p. 83).

[226] K. Nemoto and W. J. Munro. "Nearly deterministic linear optical controlled-NOT gate". Phys. Rev. Lett. **93** (2004), 250502. arXiv: 0408118 [quant-ph] (cit. on p. 83).

[227] M. Mašalas and M. Fleischhauer. "Scattering of dark-state polaritons in optical lattices and quantum phase gate for photons". Phys. Rev. A **69** (2004), 061801 (cit. on p. 84).

[228] A. André, M. Bajcsy, A. Zibrov, and M. Lukin. "Nonlinear Optics with Stationary Pulses of Light". Phys. Rev. Lett. **94** (2005), 063902 (cit. on p. 84).

[229] E. Shahmoon, G. Kurizki, M. Fleischhauer, and D. Petrosyan. "Strongly interacting photons in hollow-core waveguides". Phys. Rev. A **83** (2011), 033806 (cit. on p. 84).

[230] K. Marzlin, Z. Wang, S. Moiseev, and B. Sanders. "Uniform cross-phase modulation for nonclassical radiation pulses". JOSA B **27** (2010), 36. arXiv: 1001.1893 (cit. on p. 84).

[231] J. H. Shapiro and M. Razavi. "Continuous-time cross-phase modulation and quantum computation". New J. Phys. **9** (2007), 16 (cit. on p. 84).

[232] J. Gea-Banacloche. "Impossibility of large phase shifts via the giant Kerr effect with single-photon wave packets". Phys. Rev. A **81** (2010), 043823 (cit. on pp. 84, 85).

[233] B. He and A. Scherer. "Continuous-mode effects and photon-photon phase gate performance". *Phys. Rev. A*. **85**. 2012, 033814 (cit. on p. 85).

[234] C. Simon et al. "Quantum memories". Eur. Phys. J. D **58** (2010), 1. arXiv: 1003.1107 (cit. on p. 85).

[235] B. He, A. MacRae, Y. Han, A. I. Lvovsky, and C. Simon. "Transverse multimode effects on the performance of photon-photon gates". Phys. Rev. A **83** (2011), 022312. arXiv: 1006.3584 (cit. on p. 93).

[236] a. Gaj, a. T. Krupp, P. Ilzhöfer, R. Löw, S. Hofferberth, and T. Pfau. "Hybridization of Rydberg Electron Orbitals by Molecule Formation". Phys. Rev. Lett. **115** (2015), 023001 (cit. on p. 94).

[237] R. W. Boyd. *Nonlinear Optics*. Academic Press, 2003 (cit. on p. 95).

[238] C. S. Hofmann, G. Günter, H. Schempp, M. Robert-de Saint-Vincent, M. Gärttner, J. Evers, S. Whitlock, and M. Weidemüller. "Sub-Poissonian Statistics of Rydberg-Interacting Dark-State Polaritons". Phys. Rev. Lett. **110** (2013), 203601 (cit. on p. 96).

[239] K. J. Blow, R. Loudon, and S. J. D. Phoenix. "Exact solution for quantum self-phase modulation". J. Opt. Soc. Am. B **8** (1991), 1750 (cit. on p. 97).

[240] F. X. Kartner, L. Joneckis, and H. A. Haus. "Classical and quantum dynamics of a pulse in a dispersionless non-linear fibre". Quantum Opt. J. Eur. Opt. Soc. Part B **4** (1992), 379 (cit. on p. 97).

[241] L. G. Joneckis and J. H. Shapiro. "Quantum propagation in a Kerr medium: lossless, dispersionless fiber". J. Opt. Soc. Am. B **10** (1993), 1102 (cit. on p. 97).

[242] L. Boivin, F. Kärtner, and H. Haus. "Analytical Solution to the Quantum Field Theory of Self-Phase Modulation with a Finite Response Time". Phys. Rev. Lett. **73** (1994), 240 (cit. on pp. 97, 129).

[243] A. Wallraff, D. I. Schuster, A. Blais, L. Frunzio, R.-S. Huang, J. Majer, S. Kumar, S. M. Girvin, and R. J. Schoelkopf. "Strong coupling of a single photon to a superconducting qubit using circuit quantum electrodynamics." Nature **431** (2004), 162. arXiv: 0407325 [cond-mat] (cit. on p. 103).

[244] S. Deléglise, I. Dotsenko, C. Sayrin, J. Bernu, M. Brune, J.-M. Raimond, and S. Haroche. "Reconstruction of non-classical cavity field states with snapshots of their decoherence." Nature **455** (2008), 510 (cit. on p. 104).

[245] A. I. Lvovsky and M. G. Raymer. "Continuous-variable optical quantum-state tomography". Rev. Mod. Phys. **81** (2009), 299. arXiv: 0511044 [quant-ph] (cit. on p. 104).

[246] E. Bimbard, R. Boddeda, N. Vitrant, A. Grankin, V. Parigi, J. Stanojevic, A. Ourjoumtsev, and P. Grangier. "Homodyne Tomography of a Single Photon Retrieved on Demand from a Cavity-Enhanced Cold Atom Memory". Phys. Rev. Lett. **112** (2014), 033601 (cit. on p. 104).

[247] C. R. Murray, A. V. Gorshkov, and T. Pohl. "Many-body decoherence dynamics and optimised operation of a single-photon switch" (2016). arXiv: 1511.09445 (cit. on p. 108).

[248] A. Schwettmann, J. Crawford, K. Overstreet, and J. J. Shaffer. "Cold Cs Rydberg-gas interactions". Phys. Rev. A **74** (2006), 020701 (cit. on pp. 108, 119).

[249] P. Bohlouli-Zanjani, J. A. Petrus, and J. D. D. Martin. "Enhancement of rydberg atom interactions using ac stark shifts". Phys. Rev. Lett. **98** (2007). arXiv: 0612233 [physics] (cit. on p. 108).

[250] T. Vogt, M. Viteau, J. Zhao, A. Chotia, D. Comparat, and P. Pillet. "Dipole blockade at Förster resonances in high resolution laser excitation of rydberg states of cesium atoms". Phys. Rev. Lett. **97** (2006), 083003. arXiv: 0603038v2 [physics] (cit. on p. 108).

[251] A Reinhard, K. C. Younge, and G Raithel. "Effect of Förster resonances on the excitation statistics of many-body Rydberg systems". Phys. Rev. A **78** (2008), 060702 (cit. on p. 108).

[252] J. Nipper, J. B. Balewski, A. T. Krupp, B. Butscher, R. Löw, and T. Pfau. "Highly resolved measurements of stark-tuned Förster resonances between Rydberg atoms". Phys. Rev. Lett. **108** (2012), 113001. arXiv: 1201.6210 (cit. on p. 108).

[253] B. Pelle, R. Faoro, J. Billy, E. Arimondo, P. Pillet, and P. Cheinet. "Quasiforbidden two-body Förster resonances in a cold Cs Rydberg gas". Phys. Rev. A **93** (2016), 023417. arXiv: 1510.05350 (cit. on p. 108).

[254] I. I. Beterov and M. Saffman. "Rydberg blockade, Förster resonances, and quantum state measurements with different atomic species". Phys. Rev. A **92** (2015), 042710. arXiv: 1508.07111 (cit. on p. 108).

[255] R. Löw, H. Weimer, J. Nipper, J. B. Balewski, B. Butscher, H. P. Büchler, and T. Pfau. "An experimental and theoretical guide to strongly interacting Rydberg gases". J. Phys. B At. Mol. Opt. Phys. **45** (2012), 113001 (cit. on p. 109).

[256] M. V. G. Dutt, L Childress, L Jiang, E Togan, J Maze, F Jelezko, a. S. Zibrov, P. R. Hemmer, and M. D. Lukin. "Quantum register based on individual electronic and nuclear spin qubits in diamond." Science **316** (2007), 1312 (cit. on p. 115).

[257] P. Neumann, N. Mizuochi, F. Rempp, P. Hemmer, H. Watanabe, S. Yamasaki, V. Jacques, T. Gaebel, F. Jelezko, and J. Wrachtrup. "Multipartite entanglement among single spins in diamond." Science **320** (2008), 1326 (cit. on p. 115).

[258] T. Lahaye, T. Koch, B. Frohlich, M. Fattori, J. Metz, A. Griesmaier, S. Giovanazzi, and T. Pfau. "Strong dipolar effects in a quantum ferrofluid". Nature **448** (2007), 672 (cit. on p. 116).

[259] K. Aikawa, S. Baier, A. Frisch, M. Mark, C. Ravensbergen, and F. Ferlaino. "Observation of Fermi surface deformation in a dipolar gas: a quantum nematic phase in the ultracold regime". Science **345** (2014), 1484. arXiv: 1405.2154 (cit. on p. 116).

[260] B. Yan, S. a. Moses, B. Gadway, J. P. Covey, K. R. a. Hazzard, A. M. Rey, D. S. Jin, and J. Ye. "Observation of dipolar spin-exchange interactions with lattice-confined polar molecules." Nature **501** (2013), 521. arXiv: 1305.5598v1 (cit. on p. 116).

[261] D. Comparat and P. Pillet. "Dipole blockade in a cold Rydberg atomic sample". J. Opt. Soc. Am. B **27** (2010), 208. arXiv: 1006.0742 (cit. on p. 116).

[262] N. Y. Yao, C. R. Laumann, A. V. Gorshkov, S. D. Bennett, E. Demler, P. Zoller, and M. D. Lukin. "Topological Flat Bands from Dipolar Spin Systems". Phys. Rev. Lett. **109** (2012), 266804. arXiv: 1207.4479 (cit. on p. 116).

[263] B. Vermersch, A. W. Glaetzle, and P. Zoller. "Magic distances in the blockade mechanism of Rydberg p and d". Phys. Rev. A **91** (2015), 023411 (cit. on p. 116).

[264] Y. O. Dudin, L. Li, F. Bariani, and A. Kuzmich. "Observation of coherent many-body Rabi oscillations". Nat. Phys. **8** (2012), 790. arXiv: 1205.7061v1 (cit. on p. 126).

[265] R. Kimmich. *NMR Tomography, Diffusometry, Relaxometry*. Springer, 2001 (cit. on p. 126).

[266] D. F. Walls and G. J. Milburn. *Quantum Optics*. Springer-Verlag, 2008 (cit. on p. 130).